NOVEL STRATEGIES FOR CARDIAC DRUG DELIVERY

A Dissertation
Presented to
The Academic Faculty

by

Jay Christopher Sy

In Partial Fulfillment
of the Requirements for the Degree
Doctor of Philosophy in the
Wallace H. Coulter Department of Biomedical Engineering

Georgia Institute of Technology
May 2011

NOVEL STRATEGIES FOR CARDIAC DRUG DELIVERY

Approved by:

Dr. Michael E. Davis, Advisor Department of Biomedical Engineering Georgia Institute of Technology & Emory University	Dr. Niren Murthy, Advisor Department of Biomedical Engineering Georgia Institute of Technology & Emory University
Dr. Elliot Chaikof Department of Surgery Harvard School of Medicine	Dr. Kathy K. Griendling Division of Cardiology Emory University School of Medicine
Dr. Hanjoong Jo Department of Biomedical Engineering Georgia Institute of Technology & Emory University	Dr. W. Robert Taylor Department of Biomedical Engineering Georgia Institute of Technology & Emory University

Date Approved: March 21, 2011

To my first teachers,

Cesar and Mona Sy,

and all the other teachers that have come after them

ACKNOWLEDGEMENTS

First and foremost, I would like to acknowledge everyone that I may have inadvertently left out. The work described in this dissertation was supported by hundreds of people in many different ways. Thank you to everyone who helped me along the way.

I would like to thank my advisors, Michael Davis and Niren Murthy. They've provided me with the opportunity to bridge their two labs and develop projects starting from chemical synthesis and ending with *in vivo* testing. Mike and Niren managed to strike the balance between letting me spin my wheels a little bit (or sometimes a lot) to learn from my mistakes and nudging me (or cracking the whip) when I needed the motivation. I remember the meeting we had in the Tech food court five years ago; who would have thought that such an informal meeting would have lead to this dissertation.

My dissertation was funded by fellowships granted by the Department of Homeland Security and National Science Foundation. In addition to keeping me fed slightly better than the average graduate student, these fellowships gave me additional freedom to pursue projects that interested me. I'm not sure I could have convinced Mike and Niren to take me as a joint student without my own funding. The DHS fellowship gave me a unique opportunity to spend a summer at Sandia National Labs in Livermore, CA to work on a microfluidics project completely beyond the scope of my dissertation.

My committee – Elliot Chaikof, Hanjoong Jo, Kathy Griendling, and Bob Taylor – has been a guiding influence that did not hesitate to provide strong scientific criticism. I am grateful for all the points of view conveyed by my committee. There were times when my committee brought me back to the biology, after I had swept myself away in the materials science and chemistry aspects, to make sure the project made sense in the context of the problem. Thank you for making sure that my science was sound. I look forward to interacting with each and every one of you as my career progresses.

To all my teachers and advisors from the past, thank you for molding me into the scholar I am today. I have been fortunate to attend great school after great school. A special thanks to Prasad Shastri and Bill Graham who set me on the biomaterials path nearly ten years ago. Prasad put me through a challenge of will power by making me press hundreds of polymer pellets for degradation studies for an entire summer. I must have impressed him with my astute skill of handling a hydraulic press because he let me hang around his lab at Children's Hospital of Philadelphia and Vanderbilt for the next three years. Although, I probably broke more polymer pellets trying to get them out of the mold than we actually ended up using in the study. I look forward to having our paths cross many, many times in the future.

Dr. Graham, rest in peace, I aspire to be a tenth the teacher you were. Spring of 2003 was by far the most intellectually stimulating during my undergraduate years; having you teach both intro to materials science and quantum physics truly made my semester. I also owe Dr. Graham my gratitude for allowing me to serve as his TA for two semesters. That small teaching experience, along with the research experience in Prasad's lab set my mind to pursue a career in academia. Penn and the greater materials science community lost a great educator when you passed in 2009. You are missed.

Thank you to all my lab mates, past and present. We shared all the small victories of the successful experiments; more often than not, we also shared the defeat of an experiment gone awry. All of you were there to put in your words of encouragement, pick me up, and get me going again with a new plan of attack or new piece of sage advice. I fear I'll leave someone out if I start listing names, but I'll give it a shot. In the Davis lab: Milton Brown, Gokul Seshadri/Iyer (I still haven't figured out which you prefer!), Katie Maiellaro Rafferty, Archana Boopathy, Theresa Oh, Inthu Somasuntharam, Karl Pendergrass, Kristen French, Bernadette Cabigas, Pauline Che, and last but not least, the hundreds of rats and mice that participated in our studies. In the Murthy lab: Scott Wilson, Stephen Yang, Mike Heffernan, Chen-Yu Kao, Kousik Kundu, Madhuri Dasari, Yash Kolambkar, Sungmun Lee, Dongwoon Lee, Xinghai Ning, Warren Gray, Siraj Khaja, Jason Lee, Khalilah Reddie, and Abhinav Acharya. I hope I got everyone!

Thank you, Gokul and Milton. The three of us were the original Davis Lab. I'll treasure all the lunch and coffee breaks we took as we avoided doing work. Thank you to the postdocs that have passed through – Susan, Katie, and Bernadette. Katie, your tireless work ethic inspired not just me, but the entire lab. To the younger guys – Archana, Inthu, and Warren – I know I've been tough on you guys. Gokul and I are passing the torch to you guys soon and we know you'll be able to handle all the young ruffians that will come after you. Thank you for your patience as you gave me the opportunity to work on my mentoring skills. I will always carry certain memories of the Davis lab, like the time we lost a mouse in the centrifuge, when I was working with a Lego-man headlamp as others were running DHE assays, or all the venting sessions we shared.

To the older students in Niren's lab – particularly Mike, Stephen, and Scott – thank you for showing me the ropes. We all made the transition from our different (non-chemistry) skill sets to being productive members. Your experience and guidance have made my own journey much less perilous. Kousik, thank you for the hours of conversation shared in our office. I hope you learned as much from me as I did from you and thank you for always answering my small chemistry questions. Madhuri, you were instrumental in the Hoechst project. I could always count on your help, with a smile, nonetheless.

To all the friends I have made along the way. The cohort of 2006, intramural sports teams, and everyone else; you guys have been there for me when I had questions about an assay and kept me sane outside of lab. Thank you to some of the older students – Brock, Tim, Rich, Scott– for setting a great example both scientifically and how to enjoy life outside of lab. A special thanks to my housemates – Chris, Mel, Ivan, Lauren, and Seth – who made sure I had ample distraction when I wasn't in lab. Rich and Brent, thank you for organizing all the IM sports teams. I don't know how you guys came up with some of those team names, but keep up the tradition. Ed, thanks for expressing milligrams of VEGF for me; but even more importantly, thanks for having lunch at Eats with me before we started graduate school. It was a fitting introduction to the friendliness and hospitality of the graduate student community at Tech. I'd be remiss if I didn't mention of a few other people by name – Andres & Erin, Casey & Randy, Jeremy, Ashley & Chris, Amber & Nick, Gina, Ryan and Laveeta, Ian, Chris Lee, Taymour. I was flipping through pictures before writing this and realized all the different ways we managed to distract ourselves (game nights, pot lucks, Hawks games). It's hard to pin down a single reason to be thankful to have met all of you guys.

To all the people working behind the scenes, you have my deepest gratitude. Thank you to Beth, Sally, and Shannon in the Academic office who made sure I dotted my Is and crossed my Ts. It was truly a pleasure working with you on recruiting and other department events. Thank you to Leita, Risha, and Lisa in the BME office at Emory; I bugged you my fair share of times with paperwork or mooching office supplies. A big thanks to the IBB staff, Meg, Allen, Floyd, Collie, Steve, James, and Alyceson. IBB is a great place because of your hard work and dedication. I belonged to a number of departments and organizations during my graduate career and felt at home in each and every one.

To my friends outside the GT/Emory community, you guys have supported me in so many different ways that I could write a whole chapter. Thank you, Sue, Minnar, Justin, Austin, Chediak, O'Grady, Wu, Joe, and Bez.

All this could not have been possible without the support of my family. My parents, to whom this dissertation is dedicated, have given me every opportunity I could have ever wanted. In addition to the love and support that they have always showed me, they always asked if I needed money, even if I was doing pretty well on my fellowships (by grad student standards). Thank you for giving me this special chance to make you proud. My brothers, Bill and Kev, and I couldn't be in any more different in our choices of career paths. Yet put the three of us in the same room with a video game system and you'll see us revert back to the kids we were in Saudi. Thanks, Bill and Kev, for keeping us young (even if we have to settle for playing each other over XBox live).

And last, but not least, to Rachel. Especially over the final stretch, you've put up with my work schedule and you are the joy I get to come home to at the end of the day. Thank you for getting Emma, our wonderful dog, who has forced us to leave lab and enjoy Atlanta's weather during out countless walks and meet our neighbors at Freedom

Bark, our unofficial dog park. A lot of people that I thanked in this section may make the comment that I disappeared after our first year in graduate school. You can blame Rachel for that; when we started dating, I knew I found a match that would not just help me get through this journey, but make it one in which I have no regrets as long as she is by my side.

Had we a hundred lives to live,
we could afford to be conventional
In one of them.

Rex McGuinn
(1951-2002)

TABLE OF CONTENTS

LIST OF FIGURES

LIST OF ABBREVIATIONS

AHA	American Heart Association
Ang II	angiotensin II
ANOVA	analysis of variance
ATP	adenosine triphosphate
CM	cardiac myocyte
CVD	cardiovascular disease
DAPI	4’,6-diamidino-2-phenylindole dihydrochloride
DCM	dicholoromethane/methylene chloride
DHE	dihydroethidium
DNA	deoxyribonucleic acid
DNase	deoxyribonuclease
DOGS-NTA	1,2-dioleoyl-sn-glycero-3-[(N-(5-amino-1-carboxypentyl) iminodiacetic acid)succinyl]
DTPA	diethylenetriamine penta-acetic acid
EC	endothelial cell
ELISA	enzyme-linked immunosorbent assay
EPR	enhanced permeability and retention
Fb	fibroblast
FDA	Food and Drug Administration
Fv	variable fragment
GPC	gel permeation chromatography
GSH-PO	glutathione peroxidase
His-GFP	His-tagged Green Fluorescent Protein
His-tag	(6x) Histidine tag

His-VEGF	His-tagged vascular endothelial growth factor
Ho	Hoechst
HoSOD	Hoechst-superoxide dismutase
HoVEGF	Hoechst-vascular endothelial growth factor
HPLC	high pressure/performance liquid chromatography
HUVEC	human umbilical vein endothelial cells
IC50	half maximal inhibition concentration
IFN-γ	interferon gamma
IL-1β	interleukin-1 beta
IL-6	interleukin-6
IMAC	immobilized metal affinity chromatography
IR786	2-[2-[2-Chloro-3-[(1,3-dihydro-1,3,3-trimethyl-2H-indol-2-ylidene)ethylidene]-1-cyclohexen-1-yl]ethenyl]-1,3,3-trimethylindolium
IR-surgery	ischemia-reperfusion surgery
logP	logarithm base ten of octanol-water partition coefficient (P)
LV	left ventricle
MALDI-TOF	matrix assisted laser desorption and ionization - time of flight
MAPK	mitogen activated protein kinase
MI	myocardial infarction
MRI	magnetic resonance imaging
MTT	3-[4,5-dimethylthiazol-2-yl]-2,5-diphenyltetrazolium bromide
NHS	N-hydroxysuccinimide
NOX	β-nicotinamide adenine dinucleotide phosphate oxidase

NTA-Ni	nitrilotriacetic acid-nickel
PBS	phosphate buffered saline
PCADK	poly(cyclohexane-1,4-diyl acetone dimethylene ketal)
PEG	poly(ethylene glycol)
PET	positron emission tomography
PK	empty polyketal microparticle
PK-p38i	SB239063-loaded polyketal microparticle
PLGA	poly(lactic-co-glycolic acid)
PMN	polymorphonuclear leukocyte
ROS	reactive oxygen species
RV	right ventricle
SEM	scanning electron/standard error of the mean
SFM	serum free media
siRNA	small interfering ribonucleic acid
SOD	superoxide dismutase
TGF-β	transforming growth factor beta
TNF-α	tumor necrosis factor alpha
TTC	triphenyltetrazolium chloride
VE-Cadherin	vascular endothelial cadherin
VEGF	vascular endothelial growth factor
VEGFR2	vascular endothelial growth factor receptor 2/ KDR/Flk1/CD309

SUMMARY

The American Heart Association (AHA) estimates that at least one American will die from a coronary event every minute, costing over $150 billion in 2008 alone. Regenerating the myocardium of patients that survive the initial infarction has proven to be an elusive goal. A variety of factors – including the loss of contractile cells, inflammatory response following infarction, cardiac hypertrophy, and lack of suitable cues for progenitor cells – causes fibrosis in the heart and loss of cardiac function. This dissertation examines three drug delivery strategies aimed at improving conditions for cardiac regeneration: polyketal microspheres as non-inflammatory drug delivery vehicles; surface functionalization of microparticles with nitrilotriacetic acid-nickel (NTA-Ni) for non-covalent tethering of proteins; and using Hoechst-inspired ligands for targeting extracellular DNA in necrotic tissue.

The non-acidic degradation products of poly(cyclohexane-1,4-diyl acetone dimethylene ketal) (PCADK) make it a prime candidate for treating inflammatory disease. We tested the *in vitro* and *in vitro* biocompatibility of the polymer and found that it did not significantly recruit or activate inflammatory cells and had comparable pro-inflammatory cytokine levels compared to saline injection. We formulated microparticles containing SB239063, a p38 mitogen associated protein kinase (MAPK) inhibitor, and found that we were able to improve cardiac function in a rat model of myocardial infarction with PCADK microparticles, but not with size- and loading-matched poly(lactic-co-glycolic acid) (PLGA) microparticles suggesting that the polymer chemistry played a role in preventing fibrosis.

NTA-Ni complexes are traditionally used in immobilized metal affinity chromatography (IMAC) purification of Histidine-tagged recombinant proteins. The surface of polymer microparticles was functionalized with NTA-Ni complexes, which can be used as a non-covalent tethering mechanism for therapeutic proteins and targeting ligands. Utilizing immobilized metal chelates prevents protein denaturation by eliminating exposure of proteins to organic solvent and maintains high loading efficiency, even when using dilute protein solutions. Bioactive growth factors can be released from the microparticles and modest cell surface targeting was achieved using vascular endothelial growth factor (VEGF) and vascular-endothelial cadherin (VE-Cadherin) as model protein systems.

Traditional drug targeting schemes rely on antibody-antigen interactions. This strategy inherently limits the lower bound of the size, and therefore diffusivity, of a drug delivery vehicle. Furthermore, this strategy relies on identifying protein antigens with tissue-specific expression or upregulation. Instead, studies focused on examining the potential for targeting another biomarker for tissue damage post-myocardial infarction, extracellular deoxyribonucleic acid (DNA) generated in necrotic cell death. Using Hoechst as an inspiration, a variety of conjugates were synthesized that can be used for protein delivery and imaging necrotic tissue after infarction.

CHAPTER 1

INTRODUCTION

Heart disease is a growing problem across the world, resulting in enormous patient and financial burdens. Lifestyle changes that combat obesity, such as increasing physical activity and maintaining a healthy diet, are among the most effective treatments. However, increasingly sedentary lifestyles and poor patient compliance have slowed progress in combating cardiovascular disease (CVD). Furthermore, treating patients that already show signs of CVD will rely on drug discovery and development of new technologies to effectively deliver these compounds.

1.1 Motivation

The AHA estimated that over a million Americans suffered a myocardial infarction (MI) in 2010 [1]. Improved therapies such as percutaneous coronary intervention and antithrombotic drugs have reduced the mortality rate of MI. While it is increasingly likely that patients survive the initial infarction, progressive cardiac dysfunction remains an issue due to loss of contractile heart muscle and reduced cardiac output. For patients with severe cardiac dysfunction, the only definitive cure is heart transplantation. While this treatment can extend a patient’s life by years, there are inherent issues, including donor availability and requisite immunosuppression. Additional strategies are needed to rescue and regenerate the patient’s own myocardium.

The loss of cardiac function stems from the inadequate healing response of heart tissue post-MI. The body replaces the damaged heart tissue by hypertrophy of surviving cardiac myocytes and generation of a non-contractile scar, which leads to adverse cardiac remodeling in response to the changes in cardiac load and eventual heart failure. Old dogma concluded that the heart was a terminally differentiated organ with no regenerative capacity. However, recent findings have overturned this and have identified cells and cues that are central to the regenerative response [2-4]. The biology behind achieving cardiac regeneration is a rapidly evolving area of research with potential treatments – ranging from cell therapy [5] to soluble factors [4] – being explored worldwide. Though studies show promise in some instances, one common shortcoming is the lack of suitable delivery vehicles for the treatment, which can drastically improve the efficacy of existing therapies. This dissertation focuses on the design of new drug delivery vehicles given the constraints of the post-MI environment.

1.2 Research Objectives

Delivering regenerative cues to the heart post-MI requires strict spatiotemporal control in order to be effective. Given the phases of cardiac dysfunction, discussed in Chapter 2, delivering a particular drug at the wrong time or location can have no effect or in the worst case scenario, produce deleterious side effects. Drug delivery vehicles can give researchers spatiotemporal control over the drug concentration in a tissue and can thus boost a therapeutic's efficacy. The main objective of this project was to design and synthesize candidate drug delivery vehicles that are appropriate for treating cardiac dysfunction.

Degradable polymers are routinely used in a variety of drug delivery systems [6]. A therapeutic of interest can be encapsulated in a polymer matrix, which serves as a depot for sustained delivery. The polymer matrix can then be fabricated into a number of forms, including microspheres, for implantation into the body. As the polymer degrades, the therapeutic is released into the surrounding tissue thereby maintaining a therapeutically relevant concentration of the drug. The most commonly used degradable polymer family, polyesters, are based on a hydrolyzable linkage that generates acidic degradation products. While suitable for certain applications, these acidic products have the potential to produce or exacerbate inflammation [7, 8]. The polyketal class of degradable polymer is based on a linkage that produces neutral degradation products (acetone and a diol). These products do not affect pH and may have beneficial properties for treating inflammatory diseases. The first specific aim examines the biocompatibility of PCADK microspheres in the heart. Furthermore, a p38 MAPK inhibitor was encapsulated in PCADK microspheres and tested in a rat model of MI.

Synthetic, hydrophobic polymers are ideal for encapsulating traditional small molecule pharmaceuticals. Traditional drugs are generally hydrophobic and have high solubility in polymer matrices, allowing high loading efficiencies and predictable release kinetics. However, therapeutic proteins are becoming increasingly important for treating patients and have different physicochemical properties. Protein activity relies strongly on the secondary and tertiary structures of the molecule, which are largely dictated by hydrophobic/hydrophilic interactions. As a result, there is a high risk of protein denaturation when proteins are removed from aqueous solutions and come in contact with organic solvents that are typically used to process synthetic polymers. As a result, complex processing techniques are required to microencapsulate proteins into polymer matrices in high, bioactive amounts. The second specific aim will examine techniques to non-covalently tether proteins to the surface of microparticles using simple immobilized metal affinity strategies.

Another major focus in the development of drug delivery vehicles is the ability to target therapeutics to a particular tissue. Targeted therapeutics can be delivered systemically at lower doses, and due to enrichment at the organ of interest, beneficial concentrations of a drug can be maintained. This is particularly advantageous where access to the organ of interest is limited, such as the heart. Tissues have been traditionally targeted by identifying particular proteins that are highly expressed or upregulated in the diseased state. These proteins then serve as antigens for high affinity interactions with antibody-conjugated drug delivery vehicles. Antibody-based systems are typically larger (<50 nm in diameter) and have trouble diffusing far from capillaries. Furthermore, identification of candidate target proteins can be difficult for particular diseases where organ specific expression is not prevalent. The final specific aim will investigate the feasibility of using extracellular DNA generated during necrosis as a targeting platform. Small molecule dyes for DNA are routinely used for quantification and histology in lab and high affinity interactions. Molecules inspired by these DNA binding dyes can potentially aid in reducing the size of the drug delivery vehicle while achieving similar levels of targeting. The final specific aim will examine using Hoechst conjugates to bind extracellular DNA in the necrotic core of the infarct as a mechanism to target therapeutics to the heart.

1.3 Specific Aims

The central hypothesis of this dissertation asserts that judicious design of drug delivery vehicles can improve the efficacy of therapeutics in the failing heart. The underlying chemistry must be well suited to overcome the specific challenges presented by the environment of the myocardium after infarction. This dissertation focuses on the evaluation of three novel drug delivery strategies for treating cardiac dysfunction.

Specific Aim 1: Evaluate the biocompatibility and efficacy of PCADK microspheres for delivering anti-inflammatory drugs

We hypothesized that PCADK microparticles can more effectively deliver anti-inflammatory drugs to the heart compared to commonly used polyesters due to the fact that neutral degradation products of polyketals and improved biocompatibility. In this study, the response to PCADK microspheres was measured and the ability of PCADK formulations to release anti-inflammatory drugs in the heart after MI was assessed.

Specific Aim 2: Development of metal-affinity based protein delivery and targeting for microspheres.

We hypothesized that non-covalent tethering of histidine-tagged (His-tag) proteins can be achieved by incorporating NTA-Ni complexes on the surface of microparticles. This functional handle allows us to use the surface of microparticles to immobilize therapeutic proteins as well as targeting ligands. More importantly, this strategy eliminates exposure to organic solvent thus improving bioactivity and loss of protein.

Specific Aim 3: Assess the feasibility of targeting the infarct via extracellular DNA released by necrotic cells using small molecule conjugates

We hypothesized that the DNA-binding dye Hoechst 33258 (Hoechst) can be used to target necrotic regions of the heart following intravenous injection. DNA does not usually persist in the extracellular space in healthy individuals. However, extracellular DNA is connected to some pathological conditions, including necrotic cell death, which is prevalent acutely following MI. Hoechst has long been used as a fluorescent marker of DNA in histological and cytological applications due to its high binding affinity for DNA. A variety of Hoechst-conjugates have been synthesized in order to assess the presence of extracellular DNA and potential for targeting therapeutic proteins to the infarct.

CHAPTER 2

BACKGROUND

2.1 Myocardial infarction and the progression of cardiac dysfunction

Myocardial infarction (MI), or more colloquially known as “heart attack,” is loosely defined as loss of blood flow to a region of the heart, and subsequent death of cardiac tissue. Treatments developed over the past thirty years, such as percutaneous transluminal coronary intervention and antithrombotic drugs, have made survival of the initial obstruction of a coronary artery more likely. However, even after reperfusion of the heart, nearly one in ten will die due to lethal reperfusion injury and nearly one in four will suffer from cardiac dysfunction [9]. The heart does not have a sufficient, endogenous healing response following infarction and a number of factors converge to prevent regeneration.

Temporal aspects of cardiac dysfunction and the role of inflammation

The onset of myocardial infarction occurs with the occlusion of a coronary artery. Blockage of a major artery in the heart halts flow of oxygen and other nutrients to downstream tissue and causes the accumulation of metabolic waste. The downstream myocardium rapidly depletes available adenosine triphosphate (ATP), and if flow is not restored, cardiac myocytes begin to die through a number of pathways. In clinical settings, one of the key goals for treating patients expressing symptoms of MI is minimizing the amount of time to administration of thrombolytic drugs or angioplasty. These treatments aim to restore blood flow to the heart through biochemical or mechanical routes. Rapid reperfusion is crucial, as the amount of cardiac tissue initially lost is dependent on the duration of occlusion.

While reperfusion is important for salvaging the heart, restoration of flow is a double-edged sword; decreasing the duration of occlusion decreases infarct size, but reperfusion can cause additional cell death through several mechanisms [10-15]. Reoxygenation of cardiac tissue can increase oxidative stress due to the generation of reactive oxygen species (ROS). This can reduce the bioavailability of nitric oxide radicals, which has downstream effects of promoting neutrophil accumulation and reduced superoxide inhibition. Oxidative stress is further compounded by the recruitment of inflammatory cells into the infarct, which is effectively treated as a wound [16].

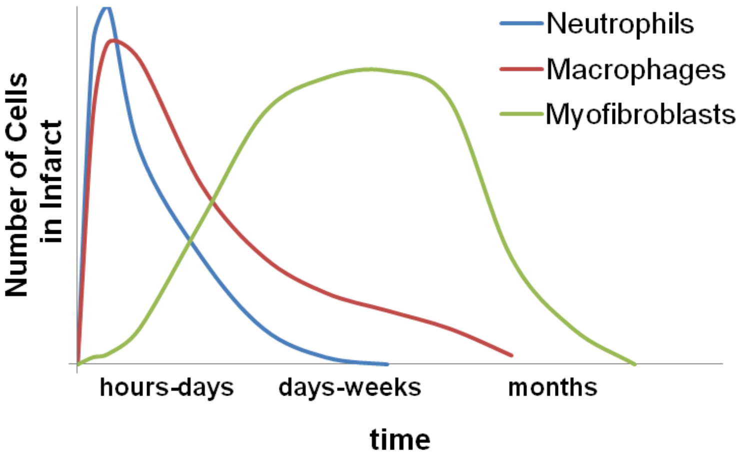

Figure 2.1. Inflammatory phases in the heart post-MI. Infarct healing follows a classical wound healing trajectory that is also seen in responses to implanted biomaterials. Inflammatory cells are recruited to the infarct at different times following MI. Neutrophils are the primary early responders and persist hours to days following injury. Macrophages respond with a slight delay but persist longer than neutrophils. Macrophages and neutrophils are responsible for clearing the infarction of dead cells and other debris. By three to seven days, voids left by dead cardiac myocytes are filled by granulation tissue, which is composed of neovasculature, fibroblasts, and macrophages. Myofibroblasts respond days to weeks days following injury and begin to synthesize extracellular matrix (i.e. collagen) in response to the loss of mechanical integrity in the infarct. The granulation tissue eventually matures into a collagenous scar. Adapted from Frangogiannis, *Antioxid. Redox Signal.* (2006) [17].

The role of inflammation in cardiac dysfunction has been well characterized in experimental models of MI. It is generally believed that the cell death during ischemia activates the complement cascade, which triggers additional components of the inflammatory response [18]. Amongst other cytokines, tumor necrosis factor alpha (TNF-α) has been implicated in the response of heart tissue following acute MI [19-23]. TNF-α may set off the cytokine cascade that leads to apoptosis of cardiac myocytes and increase in ROS in the myocardium. The generation of ROS and amplification of the inflammatory response have feed forward effects that destroy viable cardiac myocytes [11, 24], further compromising cardiac function. Studies that systematically reduced inflammatory cytokines or specific ROS have had success in small animal models but human clinical trials have seen mixed results [25, 26].

One of the central radical oxidants involved in cardiac dysfunction is superoxide. Superoxide is typically generated by neutrophils and other phagocytic cells by β-nicotinamide adenine dinucleotide phosphate (NADPH) oxidase, but can also be produced by cardiac myocytes, fibroblasts, and endothelial cells in the heart under certain stimuli (e.g. angiotensin II, TNF-α). Under healthy conditions, this production of superoxide is balanced by the scavenging properties of superoxide dismutase (SOD), which converts superoxide to hydrogen peroxide. Hydrogen peroxide is broken down further into water and oxygen by catalase and glutathione peroxidase. However, studies have shown that SOD expression is decreased following MI [27]. This can cause a pathological condition where increased superoxide reacts to form other harmful radicals such as peroxynitrite and hydroxy radicals (dotted line pathways, **Figure 2.2**). Various studies have shown that increasing levels of SOD following MI has beneficial effects on cardiac functions [28, 29], but delivery remains difficult due to the short circulation half life of SOD [30].

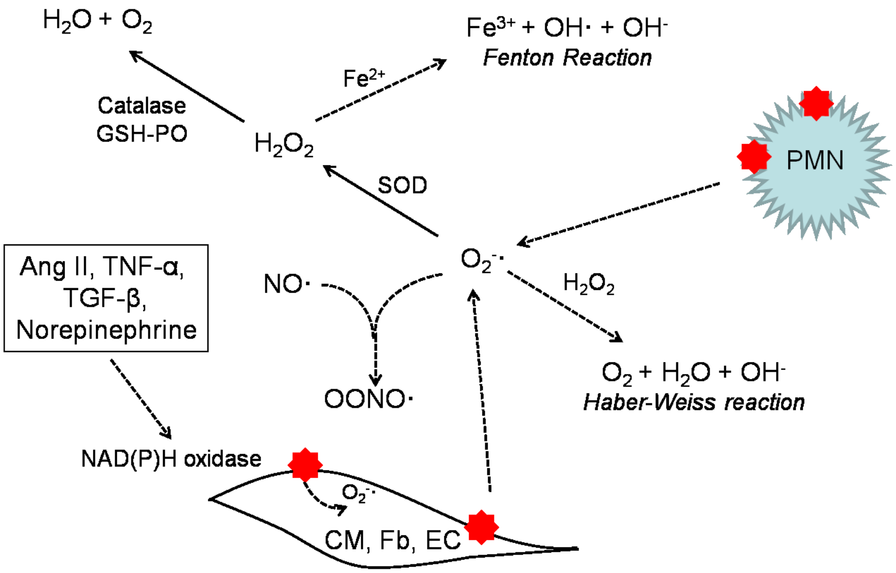

Figure 2.2. Reactive oxygen species pathways in heart failure. Superoxide plays a central role in the generation of free radicals. Superoxide is produced by inflammatory cells or cardiac cells that have been stimulated by a variety of different factors. Superoxide can then react with other compounds to produce additional radical oxidants such as peroxynitrite or the hydroxy radical. The antioxidant enzymes superoxide dismutase, catalase, and glutathione-peroxidase are crucial in regulating the redox environment in healthy tissue. (GSH-PO – glutathione peroxidase, SOD – superoxide dismutase, PMN – polymorphonuclear leukocytes, Ang II – angiotensin II, TNF-α – tumor necrosis factor alpha, TGF-β – transforming growth factor beta, NAD(P)H – reduced nicotineamide adenine dinucleotide phosphate, CM – cardiac myocyte, Fb – fibroblast, EC – endothelial cell) Adapted from Sorescu and Griendling, *CHF* (2002) [24].

Spatial organization of the infarct and modes of cell death

Cell death can occur through a number of different pathways, depending on the stimuli that initiate cell death as well as the amount of ATP available to the cell. Most cell death in the healthy human body occurs through programmed cell death or apoptosis. This is a highly organized death pathway activated by a variety of well defined cell signaling events. The general hallmarks of apoptosis involve DNA laddering, controlled recycling of cellular components, and eventual degeneration into apoptotic bodies (with intact cell membranes) that are cleared by inflammatory cells. On the other end of the spectrum is necrosis, an energy independent process. Necrosis is marked by disruption of cell membrane integrity, which leads to the leakage of intracellular components into the interstitial spaces between cells. These fragments can recruit large numbers of inflammatory cells, which eventually clear necrotic debris. Autophagy lies between apoptosis and necrosis in the spectrum of cell death and is characterized by fusion of organelles with lysosomes and enlargement of membrane bound vesicles. This process frees nutrients for other cellular processes. The prevalence of autophagy, as well as effect on cardiac dysfunction, is still under debate [31].

In general, the pattern of cell death in the infarct corresponds to the gradient of ATP and oxygen depletion (**Figure 2.3**). As distance increases from the arterial occlusion, more ATP and oxygen are available to cells due to collateral circulation. The area directly downstream of the occlusion experiences anoxic conditions, resulting in a necrotic core. In humans, these necrotic lesions are macroscopic entities that can be seen by the unaided eye [32]. The infarct core is generally considered to be unsalvageable. The border zone contains significant numbers of cardiac myocytes that have undergone cellular damage, but are still viable immediately after infarction. However, due to the hostile microenvironment in the infarct, many of these cells undergo apoptotic cell death. Autophagy may also play a significant role in cell death in the border zone, but this has yet to be fully determined. Remote myocardium that is not directly downstream of the occlusion does not suffer from much cell death acutely post-infarction. However, soluble factors and other cues may cause delayed apoptotic cell death concurrent with the oxidative stress following reperfusion.

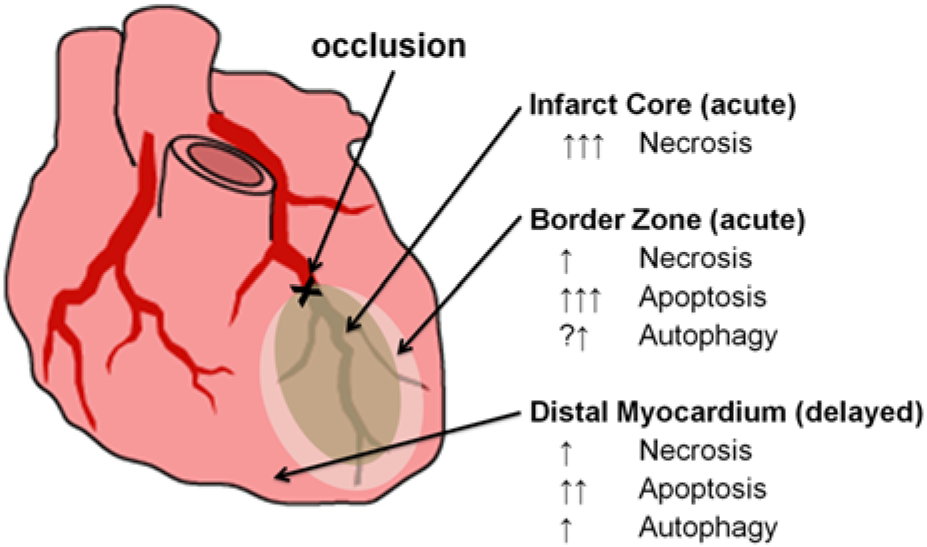

Figure 2.3. Types of cell death involved in myocardial infarction. The extent of ATP depletion generally dictates the cell death pathway, and therefore, the regions of cell death are typically defined by the distance from the occlusion. The most severe area of ATP depletion occurs at the core of the infarct and primarily drives necrotic cell death in the acute stage. As distance increases from the core into the border zone, apoptosis overtakes necrosis as the primary mode of cell death. While still controversial, it is believed that a small level of autophagy may occur in this region. Distal areas of the myocardium are generally not affected acutely by the infarction (i.e. do not experience loss of oxygenation/depletion of ATP), but can experience delayed cell death, primarily through apoptotic pathways, due to soluble signaling factors. Adapted from Mani, *Heart Fail Rev* (2008) [31].

2.2 Cardiac drug delivery vehicles

Systemic, intravenous, or intracoronary delivery of small molecules and proteins remain popular forms of drug delivery for treating MI due to minimal invasiveness. These delivery methods require frequent dosing to achieve therapeutic concentrations in the infarct zone for significant periods of time. This pulsatile concentration profile and high systemic concentration greatly increases the chances for potential side effects and toxicity. More localized delivery of therapeutics may be achieved by specialized surgical tools for direct intramyocardial injection [33]. This approach is effective for cell therapy, where the "therapeutic" ultimately engrafts in the site of injection. However, for pharmaceutical interventions (i.e. soluble drugs) localized injections are quickly washed into bloodstream, both diluting the therapeutic and negating any local delivery effects. Two alternative delivery strategies that circumvent these issues are systemically delivered targeted drug delivery vehicles and locally delivered sustained release formulations.

Controlled release formulations

A variety of diseases have been treated using controlled release systems. The general principal behind controlled release is that a reservoir of sequestered drug is implanted in the body. Through a combination of diffusion, degradation, or more sophisticated release mechanisms, the drug is slowly administered to the affected area [34-36]. This gradual release of drug bypasses the need for repeated dosing and tailoring the rate of release versus the rate of drug metabolism can achieve a desired therapeutic concentration. Degradable polymers are often used in controlled release applications.

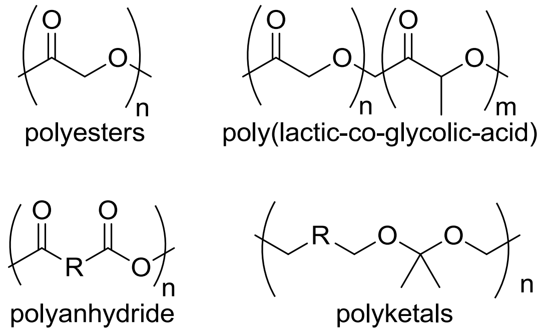

Figure 2.4. Degradable polymers used in drug delivery. Polyesters are FDA-approved for a number of medical applications. PLGA is used in commercial formulations as well as in other medical devices such as degradable sutures and screws. Polyanhydrides are another class of FDA-approved degradable polymer used in drug delivery. Polyanhydrides have rapid hydrolysis kinetics, which give them surface eroding properties. Polyketals are a new class of degradable polymers hypothesized to have improved tissue biocompatibility due to neutral degradation properties.

Biodegradable, hydrophobic polymers have been widely used in sustained release formulations both in the clinic and in research laboratories. Synthetic polymers are often better characterized than naturally derived materials and can survive a variety of processing techniques. The most common class of biodegradable polymers used in medicine is polyesters, such as PLGA. These polymers rely on the water-cleavable ester linkage and degrade into low molecular weight carboxylic acids which can be metabolized or cleared by the body and are among the few biodegradable polymers approved by the Food and Drug Administration (FDA) in the United States. Following the approval of PLGA as a suture material by the FDA, researchers have explored using biodegradable polymer microspheres as controlled release vehicles for drugs. Several microsphere formulations, including Lupron Depot (Abbott Labs) and Zoladex (Astra Zeneca), are currently on the market for the treatment of prostate cancer, breast cancer, endometriosis, and other disorders. These formulations rely on the principle of controlled release of an encapsulated drug from a biodegradable polymer matrix. Release of the drug occurs through a combination of hydrolysis of the polymer matrix and diffusion of the drug out of the microsphere. The net result is that therapeutic concentrations of the drug can be maintained for a longer time with fewer administrations. This concept is particularly important for drugs with short circulation half lives or for those that are potentially toxic at high concentrations. These formulations have the benefit of not relying on patient compliance for maintaining therapeutic levels of the drug in the bloodstream.

Polyanhydrides, another FDA-approved class of biodegradable polymers, are used in the formulation of Gliadel (Eisai) for the treatment of brain tumors. These polymers degrade into acidic products by base-catalyzed hydrolysis. The role of these acids in inciting an inflammatory response has been debated in the literature [19, 46-51]. Delivery vehicles fabricated for these polymers may not be suitable for use in inflammatory diseases where the vehicle itself may exacerbate the condition, suggesting that new polymer chemistries need to be explored for treating inflammatory disease.

Reports of cardiac-specific drug delivery vehicles are scarce. While not widely used for drug delivery directly to the myocardium, PLGA has been used for other cardiovascular applications such as stent coating [36, 37] and cardiac tissue engineering [38]. PLGA and the related polymer poly(glycolic acid) has been widely used in tissue engineering, particularly as a controlled release platform to temporally control growth factor release for neovascularization of constructs [39]. There has been one report of a potential myocardial application of PLGA to deliver heat shock protein-27 in a controlled manner [40]. In this study, the treatment was performed on cultured cardiomyocytes only, though it was able to rescue these cells from apoptosis.

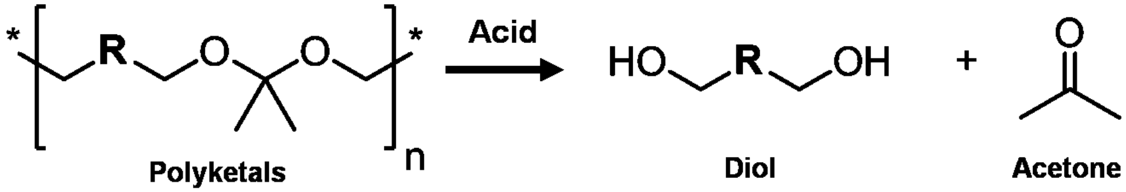

Figure 2.5. Polyketals degrade into neutral degradation products. Polyketals are characterized by the acid catalyzed ketal linkage (-O-C-O-), which degrades into a diol and acetone. This is unique amongst other degradable polymer systems since these byproducts do not affect pH.

Our laboratory has focused on the use of a new class of biodegradable polymers called polyketals [41]. Polyketal technology is central for Specific Aim 1 and is discussed in depth in Chapter 3. Polymers based on the ketal linkage provide key advantages over the more widely used polyesters. The ketal linkage is an acid-sensitive, hydrolyzable bond that degrades to produce acetone and a diol (**Figure 2.5**) and can be tuned to degrade over time spans ranging from days to months [42, 43]. The two main advantages with using polyketals over more established degradable polymers lies in biocompatibility of the degradation products. Polyketals have the unique property of degrading into neutral compounds rather than acidic byproducts. As a result, degradation of polyketals *in vivo* does not affect the local pH in the surrounding tissue, which may happen with polyester degradation [44-47]. This is a potential advantage when treating diseases where inflammation plays a large role and specific examples are given in Chapters 3 and 6.

Protein Delivery Systems

Hydrophobic, biodegradable polymers, such as PLGA and polyketals, have been widely used to deliver drugs to diseased tissues. There is currently great interest in using these polymers for the delivery of proteins, however protein-based therapeutics present unique challenges for drug delivery vehicle design. Microencapsulation of traditional pharmaceuticals (small molecules) has been straightforward in hydrophobic biodegradable polymers due to good drug solubility in organic solvents and stability over a wide range of temperatures. However, the secondary and tertiary structures of proteins strongly dictate bioactivity and are sensitive to processing conditions such as temperature and exposure to organic solvent. These properties have made it more difficult to microencapsulate proteins and limited the widespread use of protein delivery via microparticles .

A common procedure used to encapsulate proteins in hydrophobic polymer microparticle systems employs a double emulsion, solvent evaporation procedure [37-40]. In this process, the protein is typically dissolved at a high concentration in aqueous medium and emulsified into an oil phase that includes the polymer matrix. This first emulsion is then homogenized in a second water phase, forming the second emulsion that gives rise to the microparticle shape. Polymers such as PLGA and PCADK, have been used successfully to deliver proteins *in vivo*, but the techniques used to encapsulate the proteins are not optimal. During the drying process, the protein is exposed to organic solvent, which frequently damages its structure/activity. The protein can also diffuse out of the microparticle while organic solvent evaporates, reducing encapsulation efficiency. Approaches such as solid/oil/water emulsions have attempted to address these issues, but they require additional processing steps and use hydrophilic polymer carriers, such as poly(ethylene glycol) (PEG) and sodium alginate, to protect proteins from denaturation [41, 42].

Another broad class of drug delivery particles is based on naturally derived hydrogels. Extracellular matrix proteins – such as collagen, gelatin, and fibrin – have been used as matrices for sustained release of therapeutic compounds, particularly hydrophilic compounds. These materials are often supplemented with synthetic hydrogels, such as poly(ethylene glycol), in order to improve mechanical properties or impart specific functionalities [43, 44]. However, these materials are typically delivered as an injectable hydrogel or tissue engineered patch for cell delivery or tissue engineering. Hydrogels have been formulated as microparticle drug delivery vehicles. Gelatin microparticles have been used to encapsulate angiogenic and anti-fibrotic factors. These include plasmid DNA, proteins such as basic fibroblast growth factor, and chemical agonists [45-47]. While potentially biocompatible, there are concerns regarding the ability to control degradation profiles, especially with potential upregulation of gelatinases and other proteases following MI [48].

In an effort to avoid denaturation due to organic solvents, alternative protein delivery systems have focused on hydrophilic materials to achieve sustained delivery of proteins. Most of these approaches use crosslinked biologically derived polymers, such a gelatin or alginate, or synthetic polymers, such as PEG, to form a matrix around polymers, thus reducing diffusivity. A variety of crosslinking strategies, including covalent [49-51], ionic/electrostatic [52], and mechanical [53] strategies have been used to form drug delivery vehicles with these polymers.

Immobilized metal affinity chromatography (IMAC) techniques have been used to purify recombinant proteins for over thirty years and are well suited for protein delivery since they rely on non-covalent, reversible interactions with proteins [54, 55]. IMAC works by immobilizing chelating chemical groups on a substrate, which in turn chelates a bivalent metal ion (typically Ni^{+2}, Cu^{+2}, or Co^{+2}). The use of nitrilotriacetic acid (NTA) for IMAC was reported in 1987 by Hochuli, et al. and has become one of the more widely used chemistry in commercially available products [55]. The bond strength for these types of interactions have been estimated to be in the 200-400 pN range by using single molecule AFM studies [56]. Studies have been performed varying the number of histidine residues on the protein as well as the valency of NTA on the capture substrate in order to tune dissociation constants and thus provide a pathway for changing release kinetics [57, 58]. This metal complex binds sequential histidine residues on proteins and interacts with a high affinity ranging from 13 mM to 1.2 nM depending on NTA valency and other factors [59, 60].

Recently, NTA chemistry has been employed for a variety of new applications outside chromatography. Polystyrene microparticles have been modified with NTA for flow cytometric analysis of proteins [61]. NTA has also been used in lipid bilayers to examine protein interactions; 1,2-dioleoyl-sn-glycero-3- [N (5-amino-1-carboxypentyl) iminodiacetic acid] succinyl (DOGS-NTA), a lipid conjugate of NTA, was used to create two dimensional protein crystals and study protein-protein interactions on supported lipid bilayers [62-64]. Despite these new applications, NTA has seen limited use for drug delivery purposes. Researchers have functionalized liposomes with DOGS-NTA for capturing and presenting His-tagged proteins [65-68]. In addition, poly(ethylene glycol) (PEG) hydrogels have been functionalized with NTA in order to retard the release rates of proteins encapsulated in the hydrogels [43, 69, 70]. Similar affinity-based strategies have been attempted using heparin interactions. Previous work with PLGA microparticles and other materials have functionalized surfaces with heparin [46, 71]. This approach relies on heparin binding domains found on many growth factors. The affinity between heparin and various growth factors allows for local retention and sustained delivery, but the heparin binding domain is significantly larger than the His-tag and may not be as useful *in vivo* due to numerous proteins that naturally contain these domains.

Targeted Drug Delivery Vehicles

One goal in drug delivery is the targeted delivery of therapeutics. Ideally, one would be able to administer a formulation to a patient either orally or through intravenous injection and have the drug home to a specific tissue or region of the body. This strategy reduces the risk of systemic effects of a drug as well as lowers the necessary dose of the drug. This approach has been pursued in the field of cancer treatment due to the toxicity/systemic effects of the associated drugs and attractive targeting characteristics of tumors. The traditional approach for targeted drug delivery is to identify proteins that are either unique to a particular disease or specifically upregulated in a given condition [72, 73]. Cancer is an excellent model for targeted drug delivery since tumors generally have "leaky" vasculature as well as very specific cell surface markers [73]. Leaky vasculature permits enhanced permeability and retention (EPR) of delivery vehicles (typically nano- or micro-particles) into the tissue of interest. The actual targeting agents employed can vary from study to study, but the many studies use antibodies specific to the protein target of interest [65, 74, 75].

Targeting the myocardium has primarily focused on using liposomal and antibody-based approaches. Antibodies directed against intracellular proteins exposed following infarction and inflammatory proteins that are upregulated following MI have been the focus of infarct-specific delivery [76-78]. However, some research suggests that the infarcted heart inherently has an EPR property similar to that seen in tumors which may passively enhance accumulation of nanoparticles in the infarct [79]. While these liposomal formulations require modifications for serum stability [80], they offer the advantages of excellent size control at the submicron scale and the unique potential to "plug and seal" membranes [81]. This phenomenon was hypothesized by a group that used liposomal formulations to deliver adenosine triphosphate (ATP) [82] to rabbit models of MI, which reduced the volume of at-risk myocardium as measured by nitroblue tetrazolium. Other groups have utilized the mechano-acoustic properties of liposomes in order to achieve on-demand release of encapsulated therapeutics. Liposomes can be acoustically disrupted by ultrasound, a common imaging modality for cardiovascular applications, resulting in localized delivery [83]. A variety of compounds have been delivered to the heart including gene therapy constructs for VEGF, ATP, and coenzyme Q10 [83-86].

2.3 Necrosis, extracellular DNA, and DNA-binding compounds

As described previously, necrosis plays a central role in myocardial infarction and the progression of cardiac dysfunction. MI represents one of the few pathological conditions where extracellular DNA is present in high concentrations. It is estimated that ~10^{11}-10^{12} cells die naturally every day. This accounts for 1-10 grams of DNA being cleared or recycled by the body. Under most circumstances, the cell death progresses through apoptosis and the DNA is laddered into180n base pair fragments by deoxyribonuclease (DNase) II. While there are reports of apoptotic cells shedding DNA, most is contained within the apoptotic body and cleared by inflammatory cells [87]. DNA produced by necrosis, by comparison, is cleaved by DNase I into 20-80 kilobase pair fragments and the entire genome is released into the interstitial space or circulation due to loss of membrane integrity [88]. Experimental measurements done in rats suggest that DNA circulating in the blood is cleared rapidly. Hisazumi, et al. injected radiolabeled DNA into rats and found that less than 90% of the DNA was still present in the plasma after 10 minutes [89]. Nearly 99% was cleared in thirty minutes. Most of the radiolabel (60%) was detected in the liver, suggesting hepatic clearance pathways.

Certain pathological conditions can increase the occurrence of extracellular DNA. One prime example is cancer. Large tumor masses often develop necrotic cores, as the rate of cancerous cell division outpaces development of blood vessels to perfuse the center of the tumor. There have also been reports of increased circulating DNA in the blood of patients with metastatic tumors [90], but the sources remain unclear. Other conditions that have been documented to increase levels of extracellular DNA include traumatic injuries [91], cystic fibrosis [92], lupus [93], bacterial biofilms [94], and pregnancy [95].

Hoechst compounds have a long history of being used as fluorescent markers of DNA for use in histology and flow cytometry due to its large increase in fluorescence upon binding to nucleic acids [96-98]. Hoechst dyes are minor grove binding agents that have a high affinity for regions of DNA rich in AT-sequences [99, 100]. Due to their unique minor groove binding properties, some studies have been conducted using Hoechst derivates as potential antitumor or antibiotic agents, as they can inhibit DNA helicase activity [101]. In fact, Hoechst compounds were tested in human clinical trials for use in pancreatic cancer [102, 103]. Ultimately, the compounds were not approved due to lack of efficacy, but the compounds were tolerated at the up to 26 mg/m^2 daily doses. Hoechst dyes are also cell permeable, a characteristic which has been leveraged for use in tracking angiogenesis in tumors and other animal models [104-107].

CHAPTER 3

SUSTAINED P38 INHIBITION WITH DEGRADABLE PCADK MICROPARTICLES

3.1 Introduction

Due to neutral degradation products, polyketals are strong candidates for use in treating inflammatory diseases. The polyketals are a unique class of degradable polymers in that they do not produce degradation products that can affect pH. Most synthetic polymers used in drug delivery applications, such as polyesters and polyanhydrides, are based on linkages that produce acidic degradation products. In cases where inflammation plays a central role, these changes in pH may have detrimental effects on the healing process or even affect therapeutic molecules [108]. This chapter highlights the use of PCADK microspheres as a drug delivery vehicle for a small molecule inhibitor of the p38 MAPK pathway.

The development of suitable drug-delivery vehicles that can improve cardiac dysfunction following MI remains a major challenge in the field of biomaterials. Following acute MI, an excessive inflammatory response is initiated in the myocardium, causing chronic elevation of inflammatory cytokines and reactive oxygen species, resulting in cardiac dysfunction [10, 109-111]. A large number of clinically approved small molecule inhibitors have been identified that can suppress inflammation and have great potential for improving cardiac dysfunction. However, delivery remains a challenge, as many of these drugs require large doses and daily injections for efficacy and cause toxicity at these high doses [112-114]. Drug delivery vehicles that can sustain effective doses of therapeutics within the myocardium for weeks have the potential to slow or halt the progression of cardiac dysfunction [115]. Although biomaterials have been developed for use in the heart, these materials have been designed to deliver protein therapeutics and cells, and are typically based on hydrophilic polymers that form hydrogels. However, hydrophilic molecules are not well suited for the controlled release of hydrophobic drugs, such as small molecule inhibitors, because of their large pore sizes and low loading efficiency for compounds with high logP (logarithm of octanol/water partition coefficient; higher values represent more hydrophobic compounds) values [116, 117]. Hydrophobic polyester-based microparticles have long been used to deliver hydrophobic drugs [118]; however, their use in cardiac drug delivery has not been fully investigated and the acidic degradation products pose some concern.

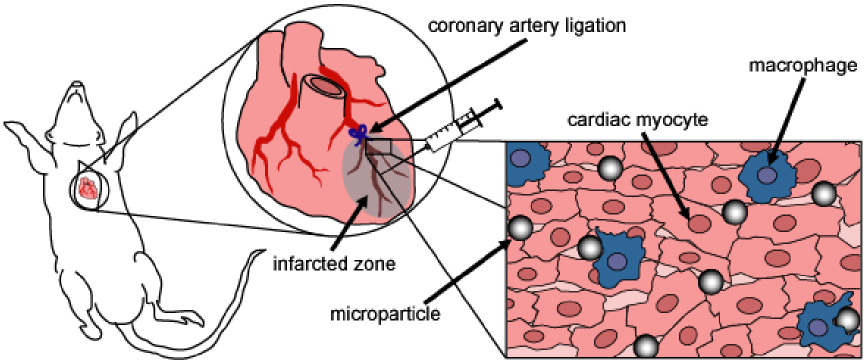

Figure 3.1. Sustained cardiac delivery via PCADK microparticles. Rats underwent permanent occlusion of the left anterior descending coronary artery (LAD) and received a direct intramyocardial injection of microparticles. These microparticles were fabricated to have diameters in the 15-20 µm range so that they lodged in the myocardium rather than being cleared in the circulation. Encapsulated compound was released over the course of weeks as they hydrolyzed or were degraded by macrophages.

Prior to this work, the biocompatibility of PCADK and its ability to deliver drugs to the heart was not fully characterized. Biocompatibility was assessed by analyzing inflammatory pathways of cultured macrophages in response to PCADK microspheres. In addition, *in vivo* experiments were conducted in order to assess the cytokine and inflammatory response of muscle tissue in response to high doses of PCADK microspheres. Upon establishing biocompatibility of the delivery vehicle, new microparticles were fabricated containing SB239063, an inhibitor of the p38 MAPK pathway. The p38 pathway has been shown to play a central role in cardiac dysfunction in both the activation of macrophages and the induction of apoptosis in cardiac myocytes [119-124]. The SB239063-loaded PCADK microparticles (PK-$p38_i$) were directly injected into the hearts of rats that had undergone permanent left anterior descending coronary artery (LAD) ligation (**Figure 3.1**). These microparticles released SB23063 as they were engaged and degraded by macrophages and other inflammatory cells.

3.2 Results

Microparticle Characterization

PCADK was synthesized as described in Appendix A with an average molecular weight of 6 kDa and polydispersity index of 1.9, as measured by gel permeation chromatography (GPC). Microparticles were fabricated using a single-emulsion/solvent evaporation protocol as described in the appendix. Since microparticle size could play a large role in the retention of microparticles in the heart tissue, control over size was determined by fabricating four batches of microparticles with different homogenization speeds (8500, 11500, 20000, and 30000 RPM). In all cases, the polymer concentration was held constant at 100 mg/ml in dichloromethane (DCM). Particles were then washed and dried, and examined using scanning electron microscopy (SEM) in order to determine microparticle diameter. The size versus homogenization speed curve showed that we could generate between 0.8-18 μm diameter microparticles (**Figure 3.2**). Subsequent microparticles were fabricated using the slowest homogenization speed (8500 RPM) in order to produce batched of microparticles that ranged in diameter from 15-20 μm.

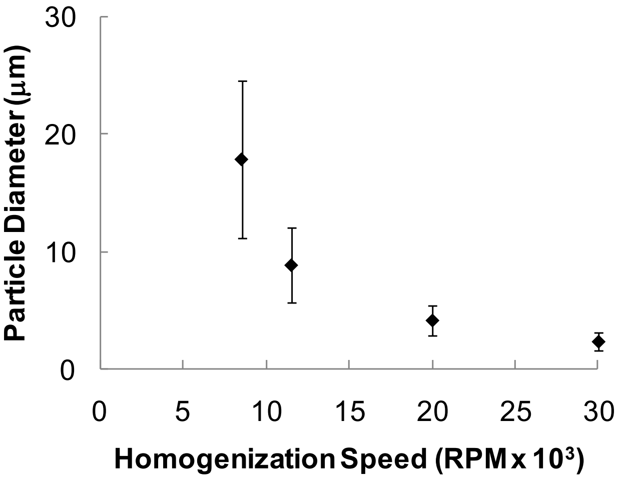

Figure 3.2. Size versus homogenization speed relationship for PCADK microparticles. Microparticle diameters were strongly dependent on the homogenization speed used to create the oil-in-water emulsion. Microparticle diameter was determined via SEM images. (mean ± std. dev., three fields of view counted, total microparticles measured per group ≤200)

Microparticles containing SB239063 were formulated to have a maximal loading of 10 μg SB239063/mg microparticle. Achieved loading efficiencies were on the order of 45%. As a control, PLGA microparticles were also fabricated containing SB239063 and had similar loading efficiencies and diameters (**Figure 3.3**).

In vitro release kinetics of SB239063 from PCADK microparticles were determined at pH 4.5 and 7.4 (**Figure 3.4**). These pH values represent phagolysosomal and blood ranges, which should be indicative of release kinetics *in vivo*. Microparticles were tested in either 100 mM acetic acid adjusted to pH 4.5, or phosphate buffered saline (PBS) adjusted to pH 7.4. Microparticles were suspended in buffer and constantly agitated at 37ºC over the course of three weeks. Tests with PCADK microparticles containing no inhibitor were also conducted in order to have a time-matched blank. Concentrations were determined spectrophotometrically at a wavelength of 320 nm. Release studies at pH 4.5 showed a higher initial burst release, with 41% of inhibitor released after three days. By comparison, pH 7.4 samples only released 17% of encapsulated inhibitor over the same time period.

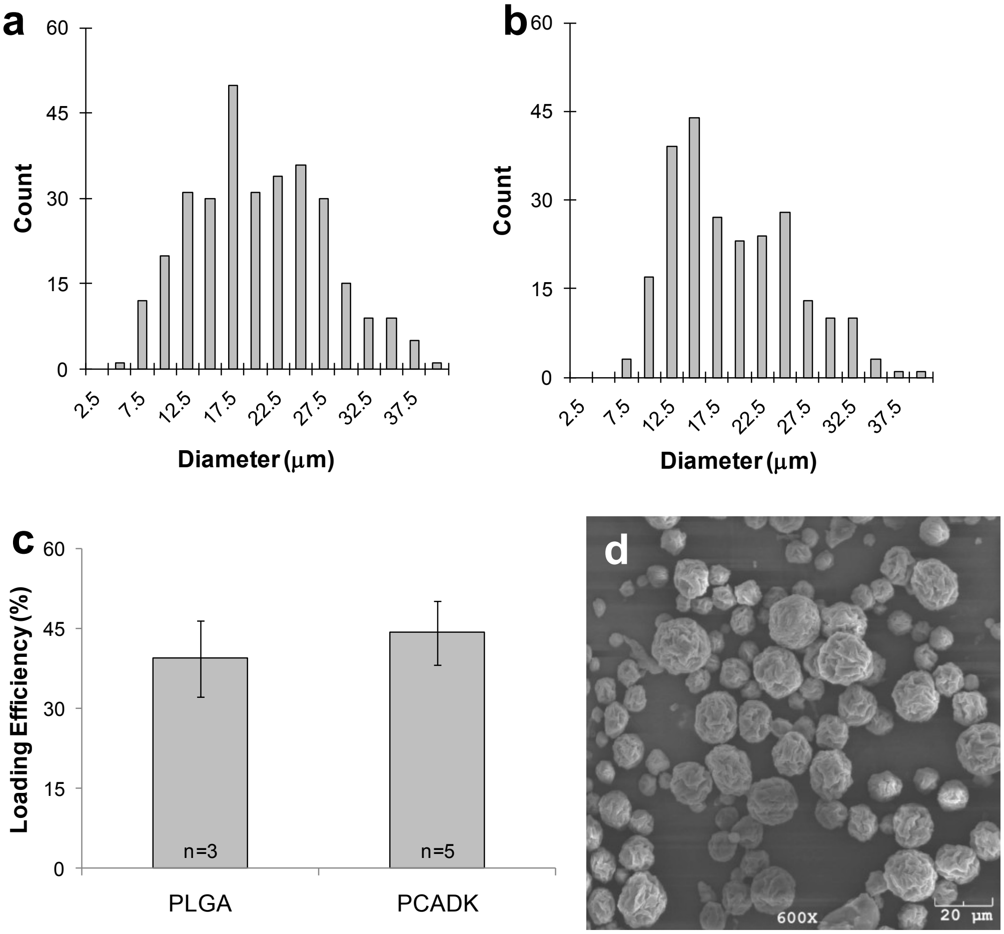

Figure 3.3. PLGA and PCADK microparticles are size- and loading-matched. SB239063 was encapsulated in PLGA and PCADK microparticles. Identical protocols were used to fabricated the microparticles and produced similar sized and loaded microspheres. (a-b) The mean diameters were 19.3 and 17.9 µm for PLGA (a) and PCADK (b) microparticles, respectively. (c) PLGA microparticles contained 3.4 µg/mg SB239063, which was slightly lower than the 4.5 µg/mg attained with PCADK microparticles. (mean±SEM, n≤3) (d) Representative scanning electron micrograph of PCADK microparticles. (scale: 20 µm)

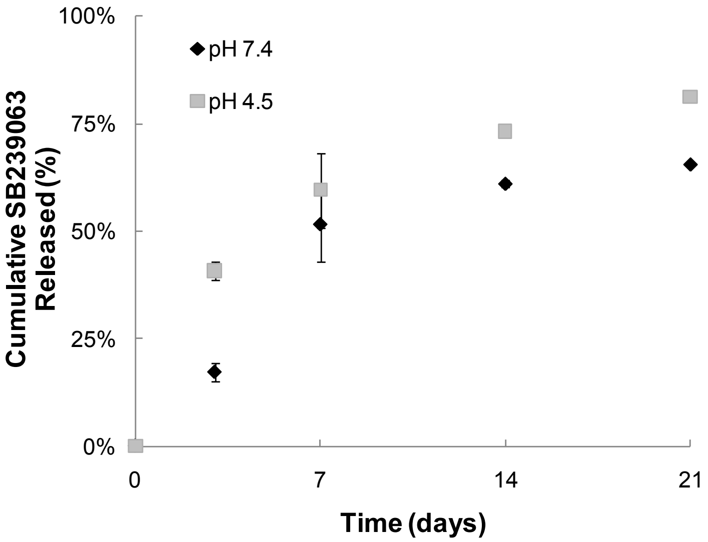

Figure 3.4. ***In Vitro*** **release kinetics of SB239063.** The release of SB239063 from PCADK microparticles was tracked over a period of three weeks at physiological (7.4) and lysosomal (4.5) pHs. Both conditions showed similar release kinetics, with a greater burst release occurring at pH 4.5. (mean±SEM, n=3, note: standard error for later time points are obscured by markers)

In Vitro microparticle characterization

The effect of polymer microspheres on macrophage activation state was investigated using cultured RAW 264.7 cells. Size-matched PCADK and PLGA microparticles – without encapsulated inhibitor – were incubated with RAW 264.7 cells for two, four, or six hours and cell lysate collected after treatment. Western blots were run and probed for total- and phospho-p38 MAPK as a marker of activation state. Densitometry was used to quantify the macrophage response to the two different polymer chemistries (**Figure 3.5**). PCADK microparticles did not show a significant increase in p38 MAPK phosphorylation whereas PLGA treated macrophages showed a statistically significant increase in phosphorylation at four and six hours. At these time points, there was a greater than three-fold increase in p38 MAPK activation.

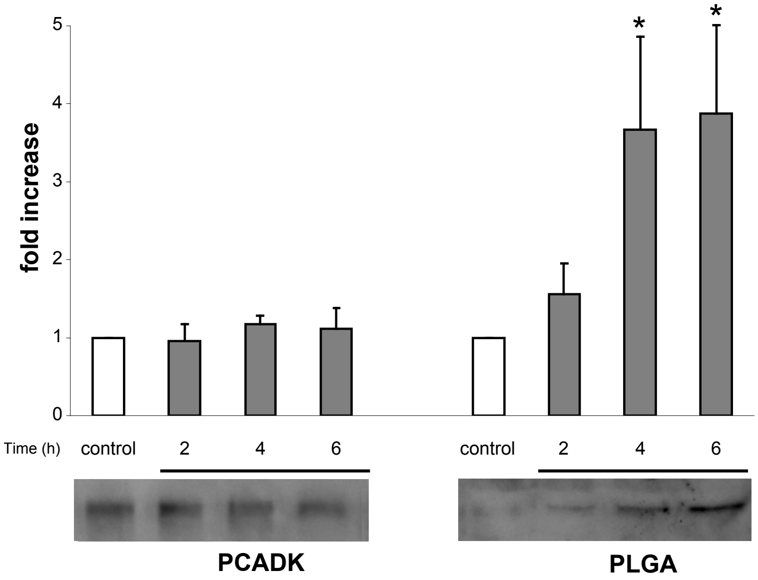

Figure 3.5. Effect of polymer chemistry on macrophage p38 MAPK activation *in vitro*. Empty microparticles were incubated with RAW 264.7 macrophages and cell lysate analyzed for p38 MAPK activation by Western blot. PCADK-treated macrophages showed no increase in p38 MAPK activation, whereas PLGA microparticles increased p38 MAPK phosphorylation over three-fold after four and six hours of incubation. Representative Western blots show relative p-p38 MAPK levels. (mean±SEM, n=3, *p < 0.05 compared to control, Student's t-test)

The bioactivity of encapsulated SB239063 was tested for loaded PCADK microparticles using a similar method. RAW 264.7 macrophages were quiesced and pre-treated with SB239063-loaded polyketal microparticles (PK-p38$_i$) (2 μM SB239063, 0.15 mg microparticles/ml) before being challenged with 10 ng/ml of tumor necrosis factor alpha (TNF-α), an activator of p38 MAPK, for 20 minutes (**Figure 3.6a**). Empty microparticle controls (PK) had no effect on p38 MAPK activation and showed 1.75-2 fold increase in phospho-p38 MAPK. Macrophages treated with PK-p38$_i$ showed a time-dependent response; macrophages treated for two hours did not show any reduction in phospho-p38 MAPK, whereas four hours of treatment reduced phospho-p38 MAPK to unchallenged levels. Six hours of PK-38$_i$ treatment reduced p38 MAPK activation to below basal levels. An inhibition curve was generated in order to determine relative efficacy compared to free inhibitor (**Figure 3.6b**). In this study, PK-p38$_i$ was incubated with cells for six hours before TNF-α stimulation and analyzed for p38 MAPK activation via Western blot. PK-p38$_i$ and free SB239063 showed similar inhibition curves and half maximal inhibition concentrations (IC50) values in the 10^{-7} M range.

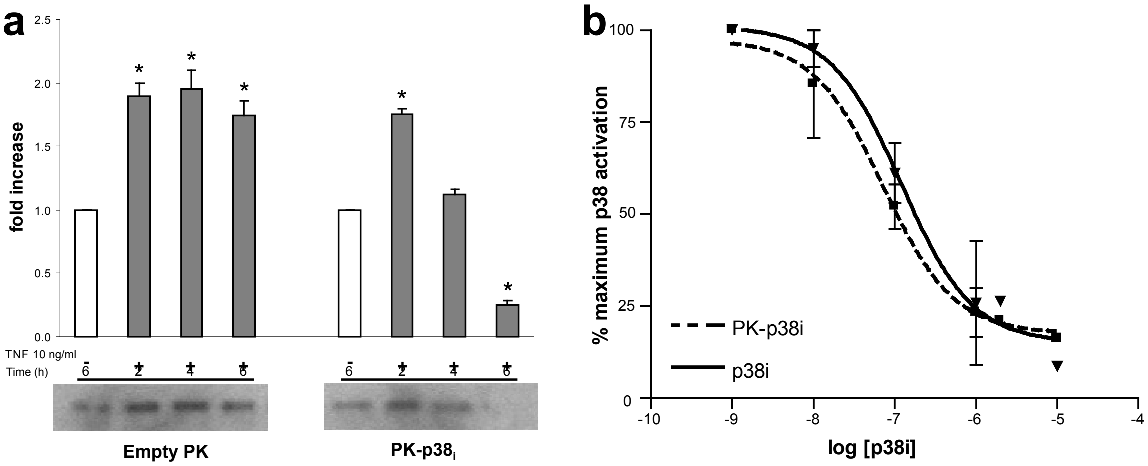

Figure 3.6. *In vitro* bioactivity of encapsulated SB239063. RAW264.7 macrophages were pretreated with microparticles before stimulation with TNF-α, which activates p38 MAPK. Levels of phospho- and total-p38 MAPK were analyzed by Western blot and quantified using densitometry. (a) Empty particles had no effect on levels of p38 MAPK activation. Cells treated with 0.15 mg/ml of PK-P38$_i$ microparticle (2 μM SB239063) showed a time dependent response, suggesting that macrophages needed to engage and release sufficient inhibitor. Representative Western blots show relative levels of phospho-p38 MAPK. (mean±SEM, n=3, *$p < 0.05$ compared to unchallenged cells, Student's t-test) (b) Six hour pretreatment with various concentrations of microparticles showed similar efficacies when compared to free SB239063. IC50 values for both treatments fell in the 10^{-7} M range. (mean±SEM, n=3)

A downstream effect of p38 MAPK activation was additionally assayed using RAW264.7 cells *in vitro*. Superoxide radicals are typically generated by activated inflammatory cells. Cells were pretreated with microparticles, challenged with TNF-α, and then incubated with dihydroethidium (DHE), a probe for superoxide. Results were quantified using high pressure liquid chromatography (HPLC) (**Figure 3.7**). Macrophages that received no treatment (SFM: serum free media) or PK showed significantly higher levels of superoxide after TNF-α stimulation. PK-p38$_i$ treated cells did not show a statistically significant elevation of superoxide. Inset shows representative traces, taken from heart tissue, of DHE-HPLC. The peak at 14 minutes corresponds to 2-hydroxyethidium, the oxidation product of superoxide and DHE.

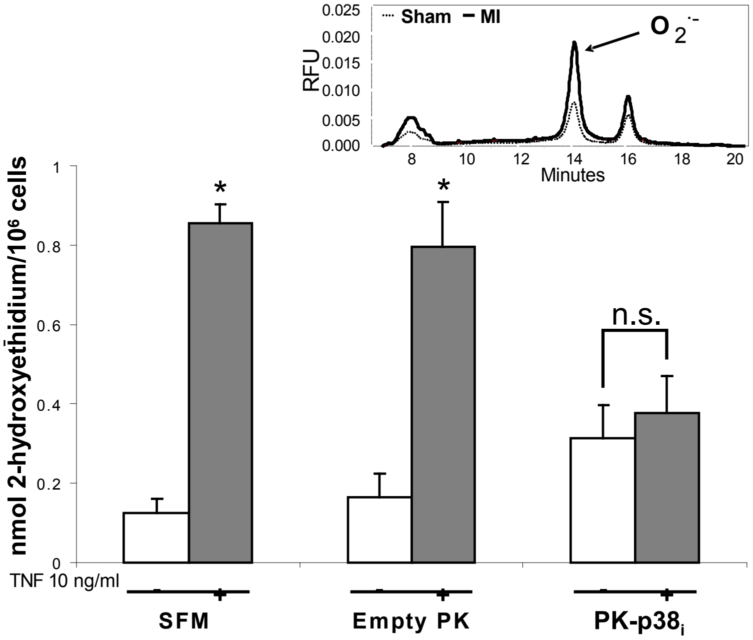

Figure 3.7. DHE-HPLC quantification of superoxide production by RAW264.7 macrophages. Cells were treated with microparticles and stimulated with TNF-α. Downstream activation of p38 MAPK by TNF-α typically increases superoxide production. Cells that received no treatment (SFM) or PK had significantly higher superoxide levels. PK-p38$_i$ treatment reduced the amount of superoxide produced by macrophages in response to TNF-α. Inset: representative HPLC traces observed with DHE-HPLC. The peak corresponding to 2-hydroxyethidium/superoxide elutes at 14 minutes. (mean±SEM, n=3, $*p < 0.05$ compared to unchallenged cells, Student's t-test)

In Vivo Biocompatibility of PCADK Microparticles

Rats were injected with a large dose (five milligrams) of either PLGA or PCADK microparticles in the thigh muscle. The rats were sacrificed 72 hours post injection and muscle examined histologically for signs of inflammation. Sections were stained for

CD45 (green), a cell surface marker for leukocytes, and for DNA with 4',6-diamidino-2-phenylindole dihydrochloride (DAPI, blue) (**Figure 3.8**). Of note, the microparticles were also stained by DAPI; serial sections stained with H&E verified that the sections were at the injection site. PCADK microparticles recruited few CD45 positive cells (a) whereas tissue injected with PLGA microparticles had a large influx of CD45 positive cells.

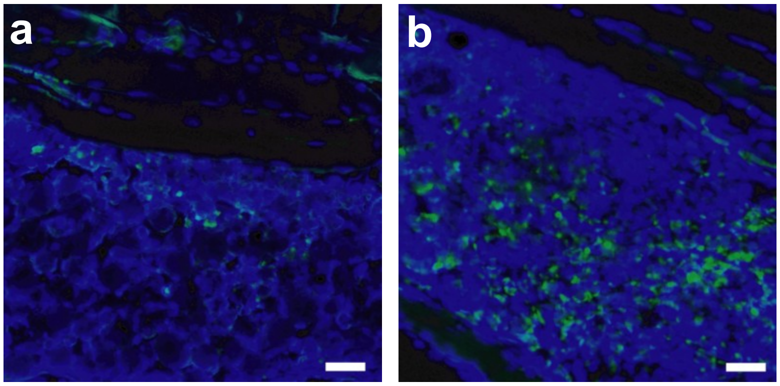

Figure 3.8. Histological analysis of inflammatory cell recruitment of PCADK and PLGA microparticles. Rats were injected with five milligrams of microparticles in the thigh muscle. Three days post-injection, histological sections were stained with DAPI (blue) and anti-CD45 antibody (green). CD45 is a common marker for inflammatory cells. DAPI is typically used to stain DNA, however PLGA and PCADK microparticles also took up the dye. PCADK microparticles (a) recruited fewer CD45 positive cells compared to PLGA microparticles (b). (scale: 100 µm)

In a separate study in mice, a Bioplex assay was used to determine the concentration of a panel of inflammatory cytokines at the injection site. Bioplex assays are multiplexed enzyme linked immunosorbent assays (ELISA) on a bead tests that allow testing of multiple analytes using small sample volumes. Mice were injected with either one milligram of PCADK microparticles or phosphate buffered saline (PBS) and cytokine levels tracked via Bioplex over three weeks. Interleukin-1β (IL-1β) showed the only statistically significant increase of the cytokines tested at one day post injection; saline treated animals had concentrations of 6 pg IL-1β/mg tissue, which was a factor of

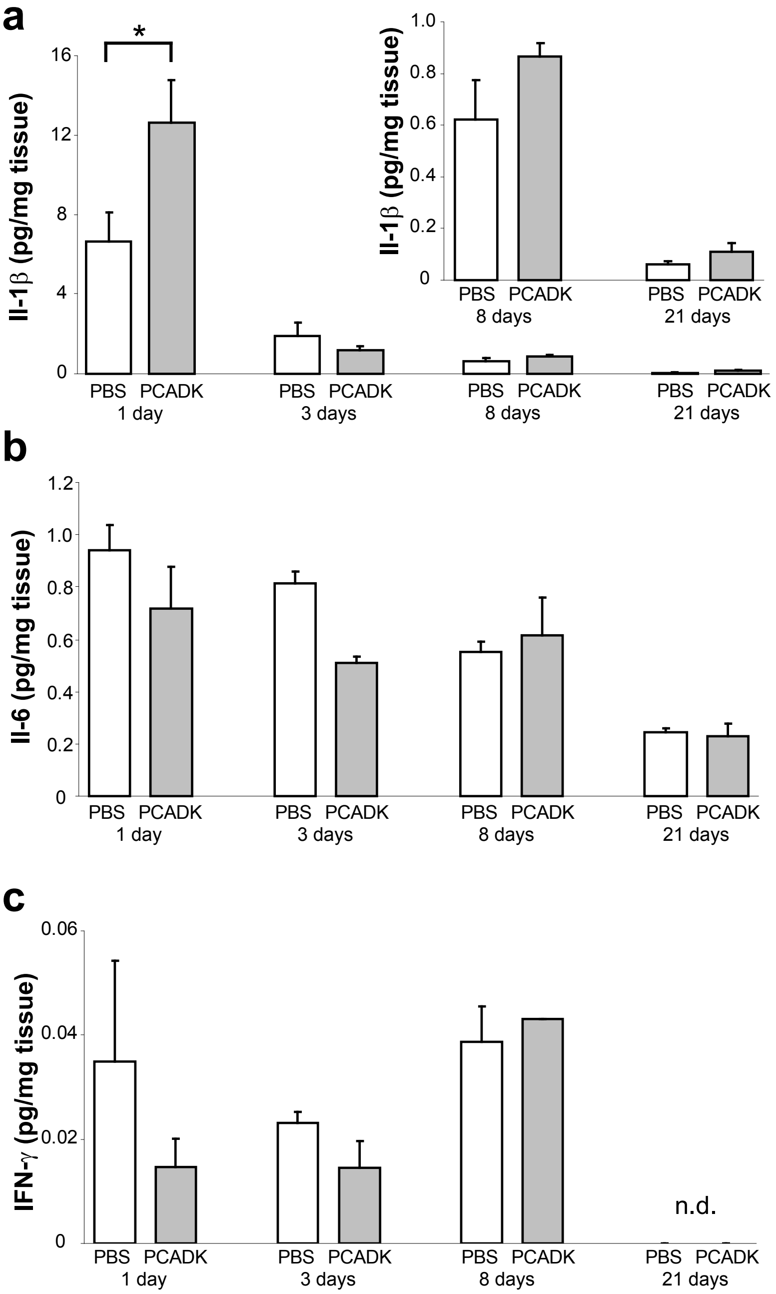

Figure 3.9. Cytokine response to intramuscular injection of microparticles. PCADK microparticles (1 mg) or PBS were injected into the thigh muscle of C57/B6 mice in order to assess cytokine response. Tissue concentrations of a panel of pro-inflammatory cytokines – (a) interleukin-1β, (b) interleukin-6, and (c) interferon-γ – was measured using a Bioplex assay. (inset: zoom of three and 21 day data, n.d. - not detected,(mean±SEM, n=4, *$p < 0.05$ versus PBS control, Student's t-test)

two lower than PCADK treated animals. IL-1β was elevated for both PBS and PCADK one day post injection and quickly returned to low levels at three, 8, and 21 days post injection. The inset is a zoomed view for the later time points. Similar results were seen with interleukin-6 (IL-6) and interferon-γ (IFN-γ); PCADK microparticles did not elevate pro-inflammatory cytokine levels in muscle tissue compared to saline injections at acute and chronic time points. TNF-α and interleukin-12 were also assayed, but were not above the detection limit of this assay (<1 pg/ml, data not shown).

In Vivo p38 MAPK Inhibition

The *in vivo* bioactivity of SB239063 was tested in a rat model of MI. Microparticles were directly injected into the myocardium immediately following LAD ligation. At three and seven days post-MI, tissue was harvested and homogenized with protease and phosphatase inhibitors. Western blots probing for phospho- and total-p38 MAPK were run and quantified via densitometry. Relative p38 MAPK activation was expressed as a ratio of phospho:total p38 MAPK (**Figure 3.10a**). MI operated animals showed a greater than two-fold increase in p38 MAPK activation compared to sham operated animals. Animals treated with free inhibitor ($p38_i$) or PK showed similar levels of phospho-p38 MAPK at three and seven day time points. PK-$p38_i$ treatment was able to significantly reduce the level of p38 MAPK phosphorylation compared to other groups that received MI at both time points. However, PK-p38i was not sufficient to reduce p38 MAPK phosphorylation to sham levels; PK-p38i treatment was 1.4-fold and 2-fold higher than sham at days three and seven, respectively.

Downstream markers of p38 MAPK activation were also measured in infarct tissue. Superoxide production was measured using quantitative DHE-HPLC (**Figure 3.10b**). MI, MI + $p38_i$, and MI + PK groups had between a two- to three-fold increase in 2-hydroxyethidium compared to sham. PK-$p38_i$ treatment significantly reduced the

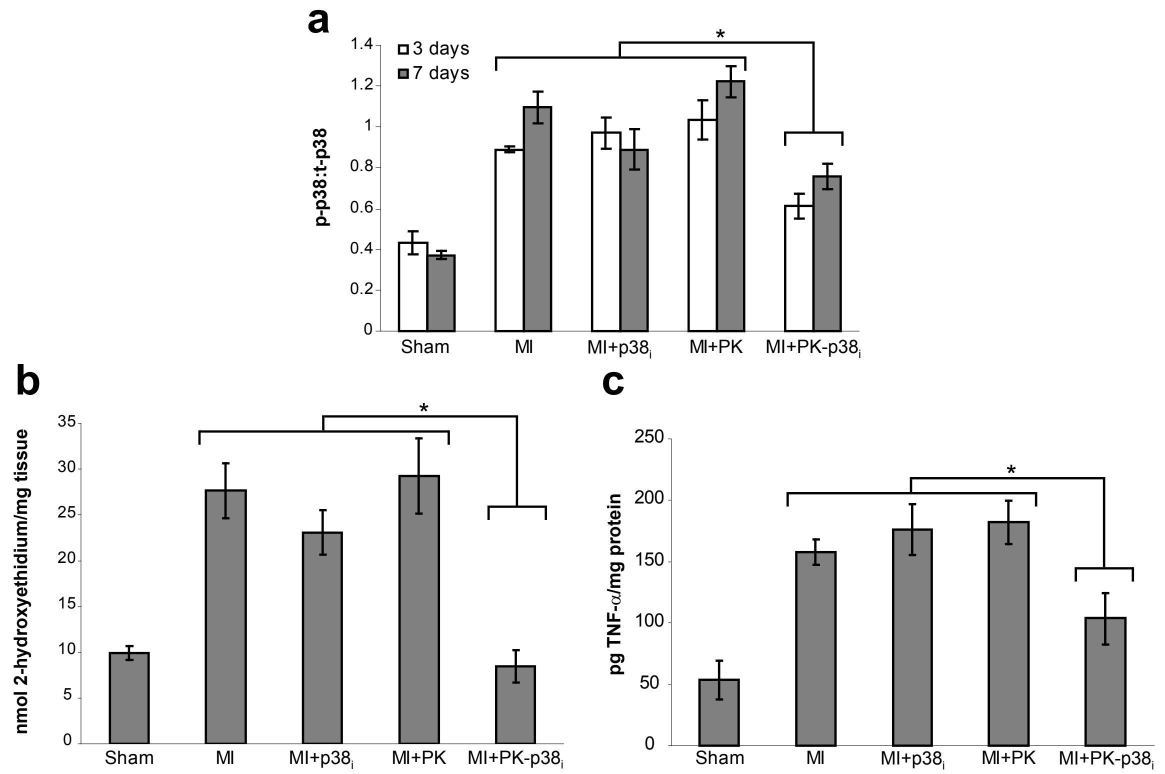

Figure 3.10. *In vivo* inhibition of p38 MAPK and its downstream effects. (a) PK-p38$_i$ treatment inhibited phosphorylation of p38 MAPK at three and seven days in the infarct zone, whereas free inhibitor (p38i) or PK had no effect on phosphorylation at either time point. (mean±SEM, n≥4, * $p < 0.05$ versus other treatment groups, ANOVA followed by Tukey–Kramer post-test) (b) Infarct zone tissue at three days was analyzed for superoxide using DHE-HPLC. MI alone, p38$_i$, and PK had significantly greater superoxide levels compared with sham, whereas PK-p38i decreased the amount of superoxide produced. (mean±SEM, n≥4, * $p < 0.05$ versus other treatment groups, ANOVA followed by Tukey–Kramer post-test) (c) The inflammatory cytokine TNF-α was measured in the infarcted zone by ELISA three days postsurgery. MI alone, free inhibitor, and empty particles had significantly greater amounts of TNF-α, whereas PK-p38i treatment reduced TNF-α levels nearly twofold. (mean±SEM, n≥4, * $p < 0.05$ versus other treatment groups, ANOVA followed by Tukey–Kramer post-test)

amount of superoxide compared to other groups that received MI surgery. Furthermore, 2-hydrodroxyethidium levels were on the order of sham operated animals (9.9 nmol/mg for sham compared to 8.5 nmol/mg for PK-p38$_i$ treated animals).

Concentrations of the pro-inflammatory cytokine TNF-α in the heart were analyzed via ELISA. Results mirrored p38 MAPK activation data with significant elevation of TNF-α levels in animals that received MI, regardless of treatment (**Figure 3.10c**). PK-p38i treatment significantly reduced TNF-α compared to other MI groups (103.6 pg TNF-α/mg protein compared to >150 pg TNF-α/mg protein for other MI groups), but was still two-fold higher than sham operated animals (53.6 pg TNF-α/mg protein).

Cardiac Function

Cardiac function of the rats was monitored at seven and 21 days post-MI using magnetic resonance imaging (MRI). MRI images were used to calculate fractional shortening of the left ventricle and expressed as a percentage (**Figure 3.11**). Sham operated animals maintained healthy heart function with fractional shortening in the 50% range. Animals that received LAD ligation had reduced fractional shortening values in the 35-40% range, regardless of treatment group; neither free inhibitor nor any microparticle treatment was able to prevent loss of function at one week. At three weeks, untreated MI, $p38_i$, PK, PLGA, and PLGA-$p38_i$ treatments all showed further decreases in fractional shortening levels. PK-p38i treatment showed recovery of function between days seven and 21; fractional shortening for PK-p38i treated animals increased from 35% to 45%, representing a ten percent improvement (absolute value). PK-p38i treatment was the only group to have a statistically significant ($p < 0.01$) improvement improvement in fractional shortening between these time points.

Given the late improvement in cardiac function, we examined the levels of fibrosis as a potential explanation. Fibrosis is part of the chronic inflammatory response and typically manifests on the order of weeks post infarction in rats. Hearts were harvested and section for histological analysis. Picrosirius red stain was used to stain collagen (red, compared to surrounding orange tissue) in the sections. Sections were imaged and analyzed digitally in order to quantify the percentage of fibrotic area (**Figure 3.13a**). Sham operated animals, as expected, had very low levels of fibrosis (2%), MI operated animals that received p38$_i$, PK, or no treatment exceeded 30% fibrosis, whereas PK-p38$_i$ treatment had only 15.6% fibrosis. This drop for PK-p38$_i$ treatment represents a significant decrease compared to other MI operated groups, but not quite down to sham levels of fibrosis.

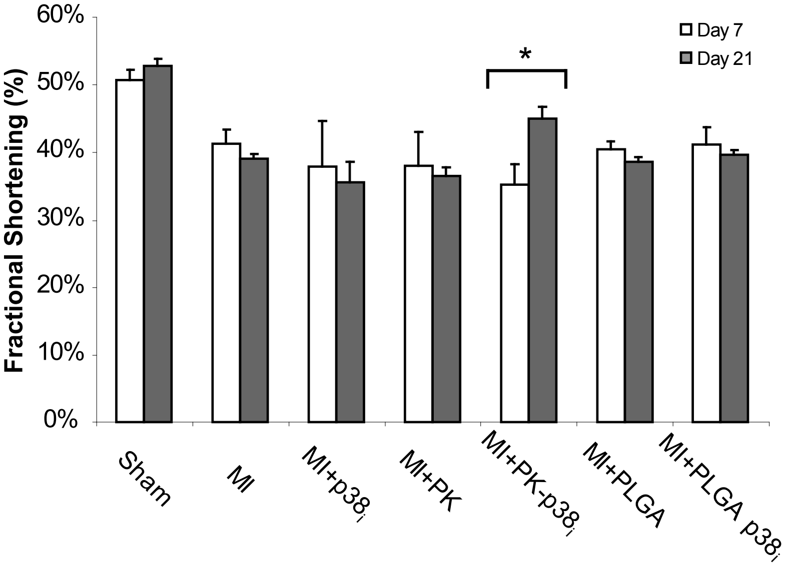

Figure 3.11. PK-p38i treatment resulted in increased cardiac function between days seven and 21. Dimensions of the left ventricle were measured at systole and diastole using MRI at day seven and day 21 post-MI. PK-p38$_i$ showed a statistically significant difference between days seven and 21, whereas all other treatments did not reach significance (mean±SEM, n≥4, * $p < 0.05$, repeated-measures ANOVA). In addition, PK-p38i fractional shortening was significantly higher on day 21 compared with MI alone and all other MI-treatment groups (ANOVA followed by Tukey–Kramer post-test). Of note, PK-p38i treatment showed a significant 10% improvement (absolute value) in cardiac function, whereas PLGA-p38i and soluble SB239063 (p38$_i$) treatments showed a trend towards decreased cardiac output.

In order to compare cardiac function across treatment groups, the change in fractional shortening between days seven and 21 was calculated (**Figure 3.12**). Positive values represent improvement in cardiac function, whereas negative values indicate progression towards cardiac dysfunction. Rats treated with PK-$p38_i$ showed the only statistically significant improvement ($p < 0.01$), with a positive gain of 9.7±1.8 fractional shortening percentage points. Rats that were treated with PLGA-p38i microparticles showed a decrease in fractional shortening (-3.7±1.2%), while free inhibitor ($p38_i$) had a non-statistically significant increase of 3.7±1.1%.

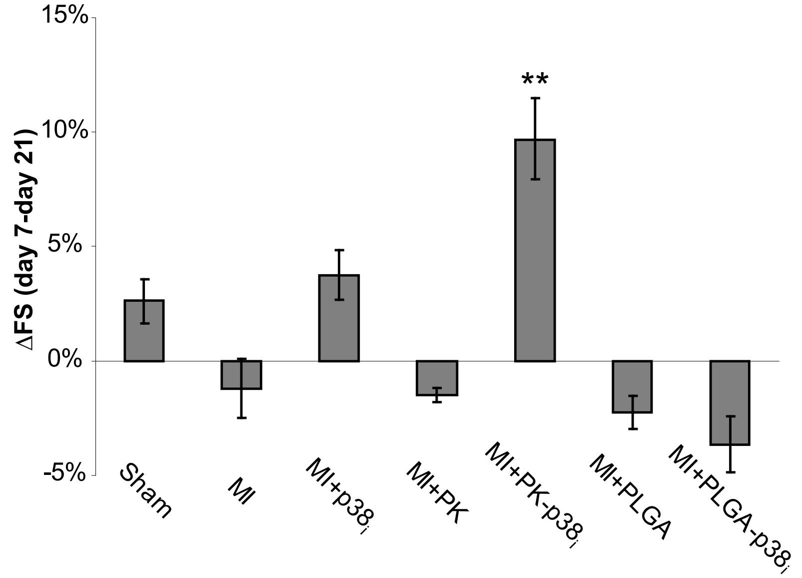

Figure 3.12. Change in fractional shortening between days seven and 21. Fractional shortening was measured and expressed as an absolute percentage difference between days seven and 21. Positive values represent improvement in cardiac function, whereas negative values represent progression towards heart failure. PK-p38i treatment showed a significant 9.7±1.8% improvement (absolute fractional shortening value), while PLGA-p38i treatment showed a decrease (-3.7±1.2%) in fractional shortening. (mean±SEM, $n \geq 4$, $^{**}p < 0.01$ versus all treatment groups)

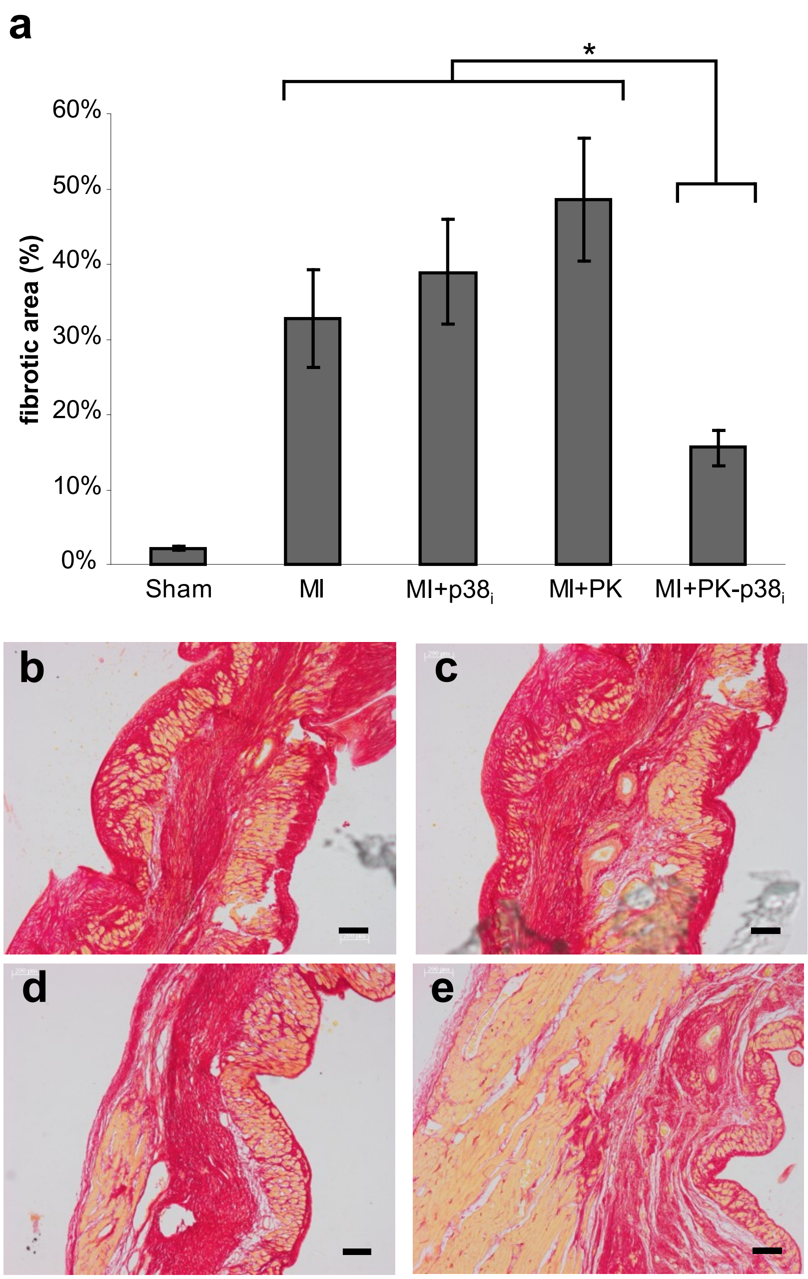

Figure 3.13. PK-p38i therapy reduced fibrotic area in the heart. The left-ventricular free wall was analyzed histologically in at least three serial sections for fibrosis using a collagen-specific Picrosirius Red stain. (a) MI-alone, free-inhibitor and empty-particle treatments had significant increases in fibrosis compared to sham operation. PK-p38i treatment reduced fibrotic area by more than half, though not completely to sham levels. (mean±SEM, $n \geq 4$, * $p < 0.05$ versus other treatment groups, ANOVA followed by Tukey–Kramer post-test) (b-e), Representative Picrosirius Red images of MI (b), MI+free inhibitor (c), MI+PK (d) and MI+PK-p38i (e) treatment are shown (scale bar: 200 μm).

3.3 Discussion

Microspheres formulated from the polymer PCADK can encapsulate the p38 MAPK inhibitor SB239063, can improve the treatment of cardiac dysfunction. PCADK is a recently developed, acid-sensitive polymer that has great potential for treating inflammatory diseases, such as cardiac dysfunction, because it degrades into the neutral, excretable, FDA-approved compounds 1,4-cyclohexane dimethanol (approved by the FDA as an indirect food additive) and acetone (an endogenous compound with potential antioxidant properties) and thus should not exacerbate any existing inflammation [125, 126] (**Figures 3.8** and **3.9**). Furthermore, SB239063 is hydrophobic (logP of 3.5), and therefore microspheres of tailor made sizes can be created from a single emulsion process (**Figure 3.2**). The p38 MAPK pathway is central in activating macrophages and inducing apoptosis in cardiomyocytes, and thus represents a candidate for therapy in the heart [119-124]. We therefore hypothesized that a direct injection of large PCADK microparticles loaded with SB239063 (PK-$p38_i$), 10-20 microns in size, would be retained in the myocardium to slowly release the small molecule inhibitor. This therapeutic strategy leverages PCADK's pH-sensitivity as the microparticles will be stable in the infarct zone, but are capable of being hydrolyzed by macrophages, which are already prevalent in the infarct zone. As macrophages engage the microspheres, small PCADK particles would be exposed to acidic phagosomes, or macrophages may degrade particles, thus increasing the release of an encapsulated drug (**Figure 3.1**).

The degradation products of microparticles frequently cause the activation of inflammatory proteins in macrophages and is a critical issue limiting the use of microparticles for the treatment of inflammatory diseases. We therefore investigated if degradation of PCADK microparticles by macrophages caused the activation of p38 MAPK itself and compared this to the response to PLGA microparticles as a control. Macrophages were incubated with PCADK or PLGA microparticles (15-20 μm diameter) for 2, 4, or 6 hours, harvested and analyzed by Western blotting for p38 phosphorylation. **Figure 3.5** demonstrates that PLGA induced time-dependent increase in p38 MAPK phosphorylation, suggesting elicitation of inflammatory pathways, whereas PCADK did not. These data agree with published reports showing PLGA treatment increases inflammatory cytokine production in cultured cells [7, 8] and also demonstrates that PCADK has potential as a drug delivery vehicle designed to inhibit p38 MAPK activation.

The ability of PCADK microparticles to encapsulate the p38 MAPK inhibitor SB239063, and the bioactivity of these microparticles was investigated using RAW 264.7 macrophages *in vitro*. A single emulsion procedure that was designed to maximally produce microparticles with 10 μg of inhibitor per mg of PCADK; the obtained encapsulation efficiency of SB239063 was 44±7%, and PK-$p38_i$ microparticles had 3-5 μg of inhibitor per mg of PCADK (**Figure 3.3**). To test bioactivity, macrophages were treated with either PK-$p38_i$ or empty PCADK particles (PK) for 2, 4, or 6 hours, washed and stimulated for 20 minutes with TNF-α. As the representative blot and grouped data demonstrate, PK-p38i but not PK, prevented p38 phosphorylation by TNF- α stimulation in a time-dependent manner (**Figure 3.6a**). Additionally, both the free inhibitor and PK-$p38_i$ demonstrated similar dose-response profiles, suggesting little loss of SB239063 activity in PK-$p38_i$ microparticles (**Figure 3.6b**). The release half life of SB239063 from PCADK microparticles is 10 days at pH 7.4 (**Figure 3.4**), and thus on the basis of these release kinetics, only 1.9% of encapsulated inhibitor (or 120 pmol) would be released into the media over the duration of the six hour experiment. These results also suggest that macrophages are playing an active role in inducing the release of SB239063 from PK-$p38_i$ microparticles, either through phagocytosis of the microparticles, leading to intracellular release of the inhibitor, or through fusion of their phagosomes with the microparticles, leading to extracellular release of the inhibitor. In keeping with this, we found no inhibition of TNF-α stimulated p38 MAPK phosphorylation in cultured neonatal cardiac myocytes, suggesting the potential involvement of a cell-mediated mechanism (data not shown).

We also investigated if PK-p38$_i$ microparticle mediated inhibition of p38 MAPK activation also led to a reduction in downstream inflammatory effectors, in particular superoxide. Cultured macrophages were incubated with PK-p38$_i$ microparticles or empty PK microparticles, stimulated with TNF-α and then assayed for extracellular superoxide production. Superoxide production was investigated by measuring accumulation of a superoxide-specific product of DHE, 2-hydroxyethidium by DHE-HPLC [127, 128]. As the data in **Figure 3.7** demonstrate, PK-p38$_i$ pretreatment reduced TNF-α-induced superoxide production while PK had no effect. These data demonstrate that PK-p38$_i$ is active in reducing p38 MAPK phosphorylation, as well as clinically relevant p38 MAPK-dependent second messenger generation.

A key issue involving microparticle drug delivery *in vivo* is the immune response associated with foreign bodies; in general, immune cells are recruited to the area of the microparticles and remain there until the microparticles are metabolized and phagocytosed, thus compromising their function. If the acute inflammatory response cannot remove the foreign body, it is often encapsulated with fibrotic tissue. The foreign body response is particularly severe with particles that have acidic degradation products. In contrast PCADK may minimize the foreign body response because it generates neutral degradation products. In order to compare the tissue biocompatibility of PCADK and PLGA microparticles, rats were subjected to an intramuscular injection of size matched PLGA or PCADK microparticles (100 µl of 50 mg/ml), sacrificed at three days, and histological sections of the injection site were made and stained for CD45, an inflammatory cell marker. **Figure 3.8** demonstrates that PLGA microspheres generated a large influx of CD45-positive cells (**Figure 3.8b**), in agreement with prior studies demonstrating *in vivo* inflammation associated with PLGA delivery [129]. In contrast, PCADK microparticles caused very little recruitment of CD45-positive cells (**Figure 3.8a**). We further investigated the inflammatory response to PCADK microparticles with quantitative cytokine analysis. Mice were subjected to an intramuscular injection of either saline (vehicle) or PCADK microparticles (100 μl of 10 mg/ml) and leg muscles were harvested at acute and chronic time points (1, 3, 8, and 21 days). We found that while PCADK briefly increased levels of interleukin-1β (IL-1β) levels on day one, there was no significant increase subsequently (**Figure 3.9a**). Additionally, there was no significant increase in IL-6 (**Figure 3.9b**) or interferon-gamma (**Figure 3.9c**) at any time point, while levels of TNF-α and IL-12 were below detection limits (data not shown). These data suggest that PCADK microparticles do not induce an inflammatory response, at concentrations far exceeding those needed for drug delivery applications, and can therefore be used as a delivery vehicle for the treatment of inflammatory diseases.

PK-$p38_i$ microparticles were tested in a rat model of MI, as described in the methods. In preliminary experiments, PCADK microparticles with diameters in the 20 μm range remained in the myocardium for several days, most likely because their size precluded them from being carried away in the microcirculation. Following coronary artery ligation, treatments were injected intramyocardially in 100 μl volumes in a randomized and double-blinded fashion. Treatment conditions were vehicle, free inhibitor (2 μM), PK (0.5 mg particle/mL), or PK-$p38_i$ (0.5 mg/mL corresponding to 2 μM SB239063) injected directly into the left ventricular free wall. At three and seven days following ligation, treatment with PK-$p38_i$ significantly inhibited p38 MAPK phosphorylation within the infarct zone, while free inhibitor and PK had no effect (**Figure 3.10a**). These data suggest that PK-$p38_i$ is able to provide sustained p38 MAPK inhibition in the myocardium for at least seven days. Free SB239063 injections were not effective in inhibiting p38 MAPK phosphorylation since the free inhibitor was likely cleared rapidly from the tissue.

Given that *in vitro* data suggest that phagocytosis is important for the release and bioactivity of SB239063 from the microparticles, one of the key questions *in vivo* is how global p38 MAPK inhibition is achieved, especially in non-phagocytic cell types. Since the microparticles injected had a distribution of sizes, there are two likely hypotheses that would explain global p38 MAPK inhibition in the infarct. Smaller particles (<5 μm diameter) were likely phagocytosed by inflammatory cells. The decreased pH of phagolysosomes would likely accelerate PCADK hydrolysis and subsequent SB239063 release. The released inhibitor could then directly inhibit p38 MAPK in the inflammatory cell or diffuse across the cell membrane and act upon surrounding, non-phagocytic cell types (i.e. cardiac myocytes). A second hypothesis involves inflammatory cell interaction with larger microparticles that cannot be phagocytosed. Cannon and Swanson [130] demonstrated that particle phagocytosis was dependent on cell membrane surface area. Beyond a threshhold of 15-20 μm diameters, cells cannot engulf particles based on surface area considerations. Under these cases, inflammatory cells may fuse their phagolysosome with the foreign body, causing surface degradation of the polymer microparticle. This route could release compound directly into the myocardium, thus affecting both phagocytic and non-phagocytic cells.

Because chronic p38 MAPK inhibition has been shown to reduce levels of superoxide during heart failure [131], infarct zone tissue from three day samples was also analyzed for the production of superoxide using DHE-HPLC. As the grouped data in **Figure 3.10b** demonstrate, PK-p38$_i$ treatment significantly reduced superoxide levels while free inhibitor and PK had no effect. Another downstream product of p38 MAPK activation, TNF-α production, was also measured and similarly only PK-p38i treatment was able to significantly reduce this inflammatory cytokine (**Figure 3.10c**).

In addition to *in vivo* biochemical findings supporting the *in vitro* data, the functional outcome of microparticle treatments was measured in separate randomized and double-blinded studies. In these functional experiments, several treatment groups were tested (Sham, MI, PK, PK-p38$_i$) with a separate randomized and blinded study conducted to test PLGA and PLGA microparticles loaded with the p38 MAPK inhibitor SB239063 (PLGA-p38$_i$). We choose to compare the efficacy of PLGA-p38$_i$ microparticles with PK-p38$_i$ microparticles to determine if polymer chemistry had an influence on therapeutic efficacy *in vivo*. The PLGA-p38$_i$ and PK-p38$_i$ microparticles were matched in both size and loading efficiency (**Figure 3.3**). Cardiac function was assessed using MRI and echocardiography seven and 21 days post-infarction and dimensions of the heart were measured in a double blinded manner. While the biochemical data would suggest an immediate effect on function, no significant improvement with any treatment at seven days post-infarction was found (**Figure 3.11**; white bars). At 21 days however, there was a significant improvement in fractional shortening in PK-p38$_i$ treated rats, while no effect was seen with free inhibitor, PK, PLGA, or PLGA-p38i particles (**Figure 3.11**; gray bars). While there was no initial improvement or blunting of loss of cardiac function over the first week, sustained p38 MAPK inhibition slowed the progression of the dysfunction, even demonstrating improvement over time. We believe this can be explained by the fact that significant damage from MI by apoptosis and necrosis is done within the first 24-48 hours [15]. As the release half-life of the particles is seven days and macrophage infiltration takes hours-to-days, it is likely that the inhibitor was not released fast enough to affect this early time point. Thus future studies will examine the effect of generating faster hydrolyzing particles to combat this.

Given that the effect on function was not seen early, we hypothesized that prolonged p38 MAPK inhibition was having an effect on development of fibrosis [132, 133]. Histological sections were made from the rats at 21 days post-infarction and stained for collagen using Picrosirius Red. Digital images of the sections were captured and quantified manually in a blinded manner (**Figure 3.13a**). Untreated MI, free inhibitor, and PK particle treatment had significantly more fibrosis than sham operated animals (**Figures 3.13b-e**). Treatment with PK-p38i resulted in significantly less fibrosis in comparison to other treatment conditions (**Figure 3.13e**). These data, taken together with the functional data, suggest that a single injection of PK-p38$_i$ microparticles reduced fibrosis and progression of cardiac dysfunction following myocardial infarction.

There is a compelling need for development of new biomaterials that can improve the treatment of myocardial infarction. In this chapter, the polyketal PCADK was demonstrated to have the biocompatibility and hydrolysis properties needed for treating inflammatory diseases. PCADK microparticles do not induce an inflammatory response *in vitro* or *in vivo*, and can therefore reside in inflamed tissue and act as a controlled release reservoir for SB239063, having a release half-life of seven days for SB239063 at neutral pH values. We also demonstrate that PCADK microparticles loaded with SB239063 results in prolonged reduction of inflammatory signaling and eventual increased functional outcome from a single injection. In a direct comparison with PLGA, only loaded PCADK microparticles significantly improved function over time. Based on these results, polyketals represent a promising class of materials for treatment of myocardial infarction and other inflammatory diseases.

CHAPTER 4

IMMOBILIZED METAL AFFINITY DRUG DELIVERY SYSTEMS

4.1 Introduction

Microparticle drug delivery systems have been used for over twenty years to deliver a variety of drugs and therapeutics. These systems work well for delivery of small molecule drugs. However, effective microencapsulation of proteins has been limited by low encapsulation efficiencies and high risk of protein denaturation. This chapter describes the adaptation of a widely used immobilized metal affinity protein purification strategy to non-covalently attach proteins to the surface of microparticles for drug delivery purposes.

IMAC was first described by Porath, et al. in 1975 [134], and has made production of purified recombinant proteins possible in large scale with high purities. While several affinity tag systems exist, one of the most common relies on interactions between chelated metal complexes and sequential histidine residues (six histidines are commonly used in a His-tag). Inspired by IMAC chemistry, polyketal microparticles were surface functionalized with NTA in order to non-covalently tether proteins to polyketal microparticle surfaces. Surface modification may allow for dual delivery of therapeutics that prevent cardiac dysfunction on different time scales (i.e. hours versus weeks).

Polyketal microparticles were surface modified with nitrilotriacetic acid-nickel (NTA-Ni) complexes, which have a high affinity for sequential histidine residues (on proteins (**Figure 4.1**). This high affinity interaction can efficiently capture proteins from dilute solutions with little risk of protein denaturation. Proteins that bind to the NTA-Ni complex retain bioactivity and can diffuse away from the microparticles to activate cells from a distance. In addition, this surface modification can also be used for microparticle targeting by tethering cell-specific ligands to the surface of the particles. In this study, protein release kinetics of model His-tagged proteins from the NTA-Ni complex were studied and it was demonstrated that bioactive molecules could be released and act on cells at a distance. Furthermore, targeting specific cell types was attempted by tethering cell surface marker ligands to microparticles. Lastly, potential toxicity issues that could arise due to incorporation of heavy metal ions into the drug delivery vehicle were investigated.

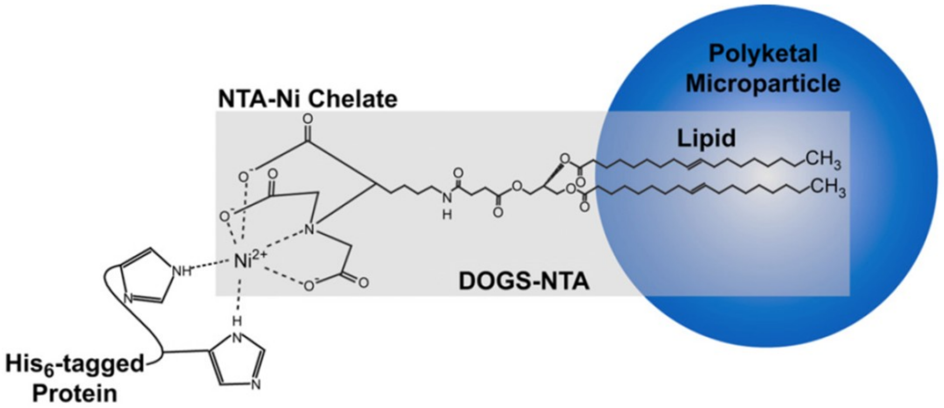

Figure 4.1. Scheme for incorporating NTA-Ni complexes on the surface of microparticles. 1,2-dioleoyl-sn-glycero-3-[(N-(5-amino-1-carboxypentyl)iminodiacetic acid)succinyl] (DOGS-NTA), shown in the shaded box, is an amphiphilic lipid that has the ability to chelate metals. Microparticles can be surface functionalized by simply mixing the lipid in the organic phase of an emulsion. During the drying process, the hydrophilic chelating group migrates to the aqueous interface of the microparticle and is anchored by the hydrophobic lipid tail in the polymer matrix. One the microparticles are fully dry, nickel can be added to the NTA group and His-tagged proteins non-covalently tethered.

4.2 Results

Surface functionalized PCADK microparticles

Polyketal microparticles were functionalized by adding DOGS-NTA (shaded box in **Figure 4.1**) to the organic phase of a single-emulsion polyketal microparticle. The lipid tail serves as an anchor for the more hydrophilic NTA moiety, which migrates to the surface of the microparticle. Microparticles were analyzed using scanning electron microscopy (SEM) (**Figure 4.2a**) and found to have diameters that ranged from 10-20 μm.

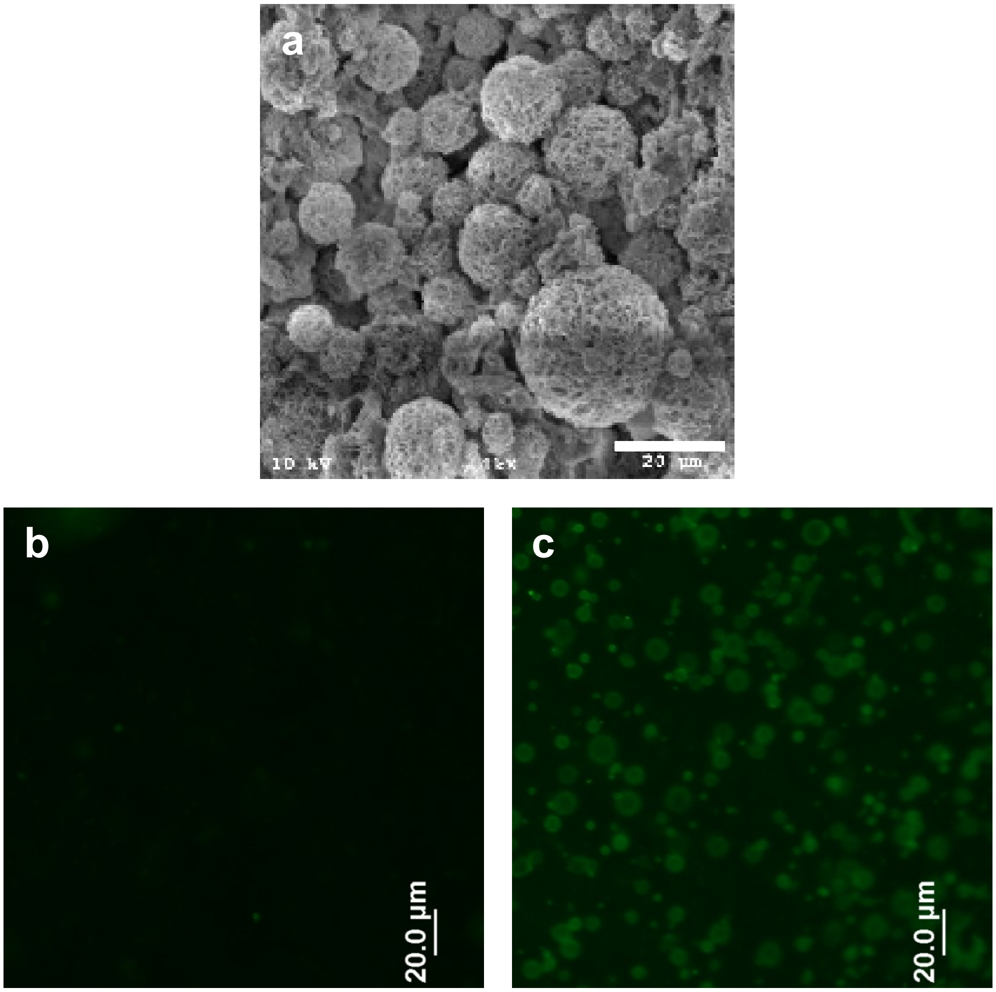

Figure 4.2. Micrographs of NTA functionalized microparticles. (a) Scanning electron micrograph of PCADK microparticles functionalized with 10 wt% NTA. (scale: 20 μm). (b) Microparticles incubated with PBS, which does not contain nickel, and then with His-GFP showed little green fluorescence under epifluorescent microscopy. (c) Microparticles that were incubated in 50 mM $NiCl_2$ solution prior to incubation with His-GFP show strong GFP tethering. (scale: 20 μm)

Proof of protein tethering was assessed using His-tagged green fluorescent protein (His-GFP). Polyketal particles containing NTA that were pretreated with PBS, followed by washing, and exposure to a 100 nM solution of His-GFP showed little fluorescence when examined under fluorescence microscopy (**Figure 4.2b**). In contrast, particles that were pre-incubated in a 0.05M $NiCl_2$ solution prior to incubation with His-GFP exhibited extensive green fluorescence around the microparticles (**Figure 4.2c**).

Quantitative measurement of His-GFP loading

The binding capacity of two formulations of NTA-functionalized microparticles was determined quantitatively using a modified ELISA to determine the amount of GFP on the surface of the microparticles. Both 1 wt% and 10 wt% NTA-Ni microparticles showed similar His-GFP binding properties (**Figure 4.3**). Microparticles that were loaded at concentrations of less than 1 μg His-GFP/ml showed a linear loading profile with a slope corresponding to approximately 40% loading efficiency relative to the total amount GFP in solution. The 1% NTA formulation saturated at a loading concentration of 800 ng His-GFP /ml, while the 10% NTA formulation had a higher saturation point at 1200 ng His-GFP /ml. These loading capacities correspond to a mass dose of 330 ng GFP/mg particle and 440 ng His-GFP /mg particle, respectively.

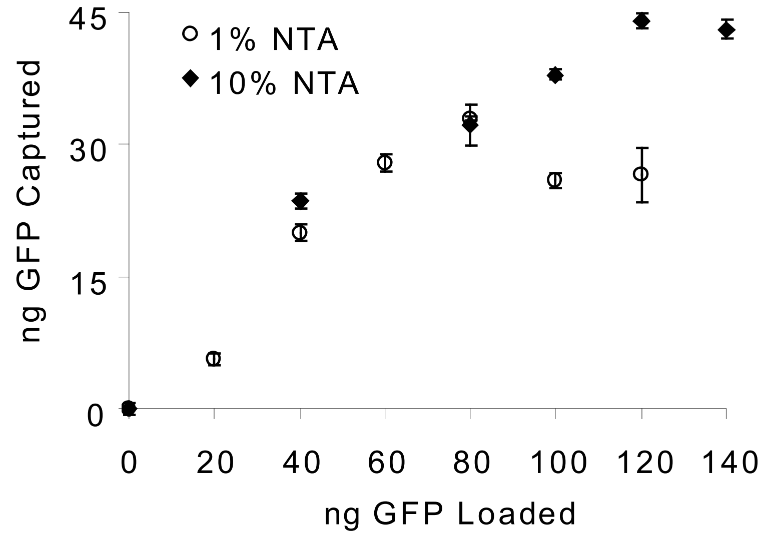

Figure 4.3. Loading capacities for 1% and 10% NTA formulations. Microparticles containing either 1% or 10% NTA were loaded with nickel and incubated in His-GFP solutions ranging from 0-1400 ng/ml. Particles were extensively washed and the amount of bound GFP was determined using a modified ELISA protocol. Both formulations showed similar linear loading capacities, corresponding to 40% loading efficiency. Ten percent formulations saturated at 1200 ng GFP/ml whereas 1% formulations peaked at 800 ng GFP/ml, which corresponded to mass doses of 440 ng GFP/mg particle and 330 ng/mg particle, respectively. (mean±SEM, n=3)

Particle release studies

Release studies were conducted from the surface and core of the particles using two model compounds, His-GFP and rhodamine-B (**Figure 4.4**). The core of the microparticles was loaded with 2 wt% rhodamine-B while the surface was loaded with His-GFP. The release study was conducted under physiological conditions (pH 7.4, 37°C). His-GFP was released with a release half life of 2 h with complete release occurring at 48 h. Rhodamine-B showed an initial burst of approximately 39% released in the first 12 h, with slow release occurring over the next week. A more hydrophobic compound, SB239063, was previously shown to have significantly slower release kinetics, with a release half-life of one week [135].

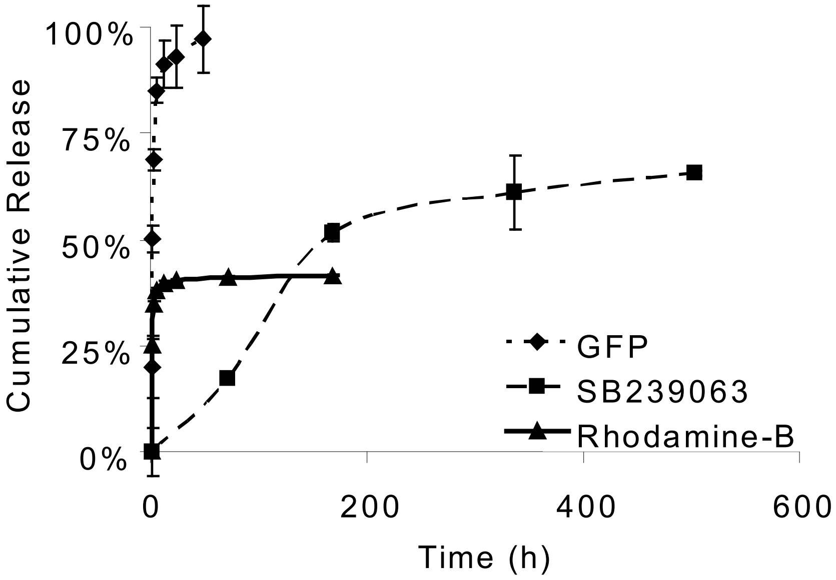

Figure 4.4. Release kinetics for model compounds. Release studies were conducted for a model protein, His-GFP, and two encapsulated compounds, rhodamine-B and SB23063. His-GFP was released relatively rapidly compared to the encapsulated inhibitors. (mean±SEM, n=3)

In vitro metabolic assays

Changes in metabolic activity for two cell lines, neonatal cardiac myocytes (NCM) and RAW264.7 murine macrophages were measured following exposure to microparticles by MTT [3-(4,5-dimethylthiazol-2-yl)-2,5-diphenyl tetrazolium bromide] assay. This assay measures mitochondrial activity of viable cells. NTA-functionalized particles that were pre-incubated with PBS or $NiCl_2$ were tested at doses ranging from 0.25 mg/ml to 2 mg/ml and compared to untreated cells (control) and cells treated with 1 mg/ml of unmodified PCADK microparticles. Neonatal cardiac myocytes treated with NTA microparticles had metabolic activities ranging from 78-92% of control-treated while neonatal cardiac myocytes treated with NTA-Ni microparticles showed no appreciable decrease in metabolic activity compared to control cells (**Figure 4.5a**).

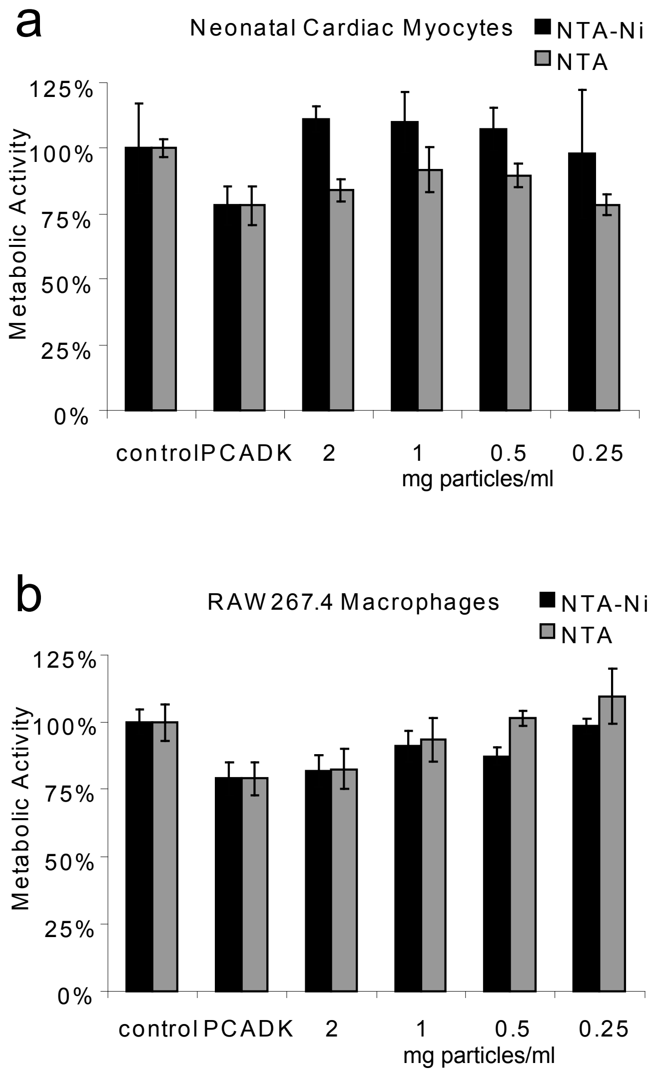

Figure 4.5. Metabolic activity of cells treated with microparticles. MTT assays were used to determine the viability to two different cell types, RAW 264.7 macrophages and neonatal cardiac myocytes, after exposure to microparticles. NTA or NTA-Ni microparticles did not show any appreciable toxicity compared to PCADK microparticles (1 mg/ml) for either cell type after six hours of treatment. In all cases, cell viability was ≤75% compared to untreated cells. Total mass doses given to cells in these experiments were at least two times greater than total mass doses administered to animals in previous studies. (mean±SEM, n=3)

RAW cells treated with 2 mg/ml of either type of modified particle showed similar metabolic activity compared to RAW cells treated with non-modified PCADK microparticles (82-83% metabolic activity). Lower doses of microparticles showed higher metabolic activities, while concentrations of 0.25 mg/ml of NTA and NTA-Ni particles showed similar activity to control-treated cells. No significant difference in metabolic activity between nickel-loaded and nickel-free particles was observed (**Figure 4.5b**).

Delivery of VEGF to HUVEC

In order to determine whether proteins loaded on the surface retain biological activity, human umbilical vein endothelial cells (HUVECs) were treated with microparticles that were surface loaded with NTA-Ni and His-tagged vascular endothelial growth factor (VEGF). All microparticles were previously loaded in a 1 μg/ml solution of His-VEGF before washing and suspension in serum free media. Cells were incubated with doses ranging from 0.01-1 mg microparticles/ml for a period of 20 minutes. The bioactivity of the delivered VEGF was measured by Western blot analysis of cell lysates probed with phospho-VEGF receptor-2 (VEGFR2) and total VEGFR2 antibodies. Densitometric measurements of the blots were made and the ratio of phosphorylated:total VEGFR2 was calculated. Cells that were treated with PK-VEGF showed a dose dependent increase in VEGFR2 phosphorylation, with an 8-fold increase at a 2 mg/ml dose (**Figure 4.6a**) with no effect of lower doses (0.01 mg particles/ml and 0.05 mg particles/ml). HUVECs treated with NTA microparticles incubated with VEGF, but should not contain tethered VEGF due to the lack of nickel, did not show any change in VEGFR2 phosphorylation compared to control cells (**Figure 4.6b**).

In order to demonstrate that the VEGF tethered to the microparticle could be released from the surface over time in its active form, cells were treated with PK-VEGF microparticles using a transwell assay with cells on the bottom of the well, and the particles on the top. Particles were added to the transwell at a concentration of 1 mg microparticles/ml in an equal volume as the amount of media on the cells below the transwell for a final effective concentration of 0.5 mg microparticles/ml. The pore size chosen was 3 µm to ensure that particles with tethered VEGF could not activate the cells directly. HUVECs did not show activation of VEGFR2 after 20 minutes of PK-VEGF treatment across a transwell membrane (data not shown). However, receptor phosphorylation was prevalent after 1, 2, and 3 hours of treatment (**Figure 4.6c**).

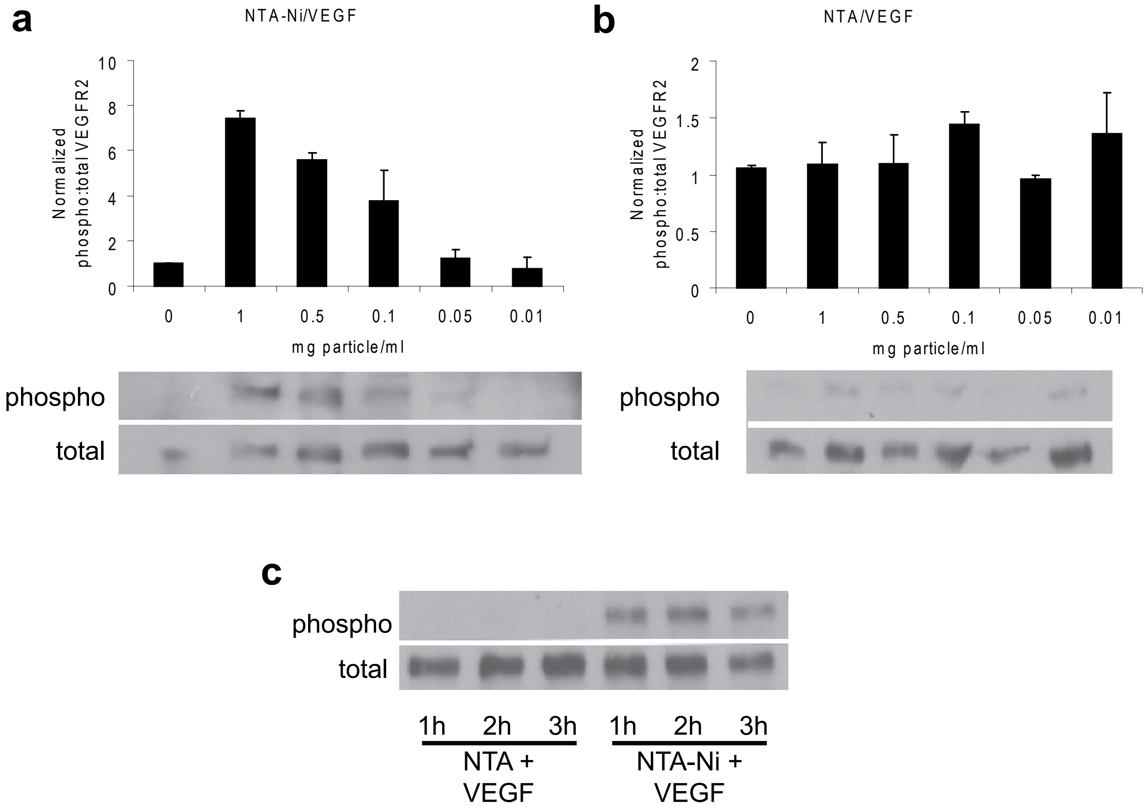

Figure 4.6. Activation of VEGFR2 by VEGF-loaded NTA-Ni Microparticles. HUVEC were treated with microparticles and Western blot analysis was used to determine the extent of VEGFR2 phosphorylation. (a) Microparticles loaded with nickel and then incubated with His-VEGF showed a dose dependent response in VEGFR2 phosphorylation. (b) Microparticles containing only NTA, with no nickel, and incubated with His-VEGF did not show activation of VEGFR2 at any of the doses tested. (c) Microparticles incubated in a 3 µm transwell assay tested the ability of VEGF to diffuse from the microparticle surface and activate cells at a distance. No activation was seen at 20 minutes (data not shown), but sustained VEGFR2 phosphorylation was seen after 1, 2, and 3 hours of incubation.

Cell surface receptor targeting

Small microparticles (1~2 µm) were fabricated containing either 1 wt% coumarin-6 or rhodamine-B and 10% NTA in order to assess the potential of targeting microparticles to specific cell types. Coumarin-6 and rhodamine-B were used a fluorescent tracers for the microparticles. Polyketal microparticles containing NTA-Ni were surface loaded with His-tagged VE-Cadherin, a protein specific to endothelial cells that forms homodimers with high affinity. Two cell lines were tested for targeting, HUVECs (which express VE-Cadherin) and rat neonatal cardiac myocytes (negative control). Cells were incubated with VE-Cadherin loaded microparticles for 3 hours, washed thoroughly, and imaged under fluorescence microscopy. Our data show extensive binding of microparticles functionalized with VE-cadherin to endothelial cells (**Figure 4.7a**) with little binding of non-loaded NTA-Ni microparticles to HUVECs (**Figure 4.7b**). Examination using confocal microscopy suggested that the particles were not internalized by the cells (**Figure 4.8**). Cells that were positive for at least one fluorescent microparticle were counted and expressed as a total percentage of the cells in the field of view (**Figure 4.9**). Three negative control conditions (HUVECs treated with NTA-Ni particles not loaded with VE-Cadherin and NCMs treated with both types of particles) showed that approximately 20% of cells had at least one particle attached. HUVECs treated with VE-Cadherin loaded microparticles had a greater than two-fold enhancement of microparticle targeting with nearly half of the cells being positive for at least one particle.

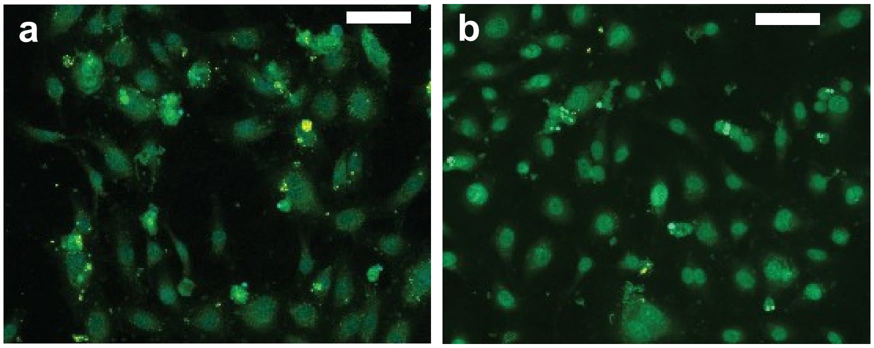

Figure 4.7. Fluorescence micrographs of HUVECs targeted via VE-Cadherin interactions. Microparticles were loaded with coumarin-6 and incubated with cells at a concentration of 0.1 mg/ml for 3h and washed extensively to remove unbound particles. Cells were then fixed and imaged under epifluorescence microscopy in order to count cells (stained green) that were positive for at least one microparticle (yellow) (a) Microparticles loaded with VE-Cadherin were present on nearly half of HUVEC. (b) NTA-Ni particles without VE-cadherin only labeled 20% of cells. (scale: 100 µm)

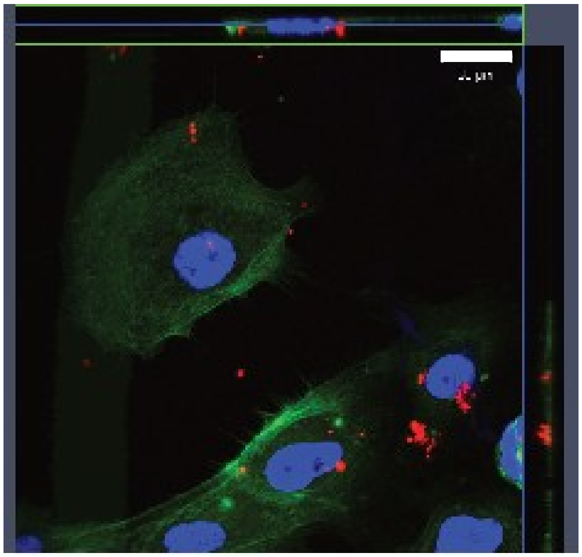

Figure 4.8. Scanning laser confocal micrograph HUVEC with VE-Cadherin loaded microparticle. Orthogonal projection of z-stack suggests that microparticles are not internalized (scale: 20 µm)

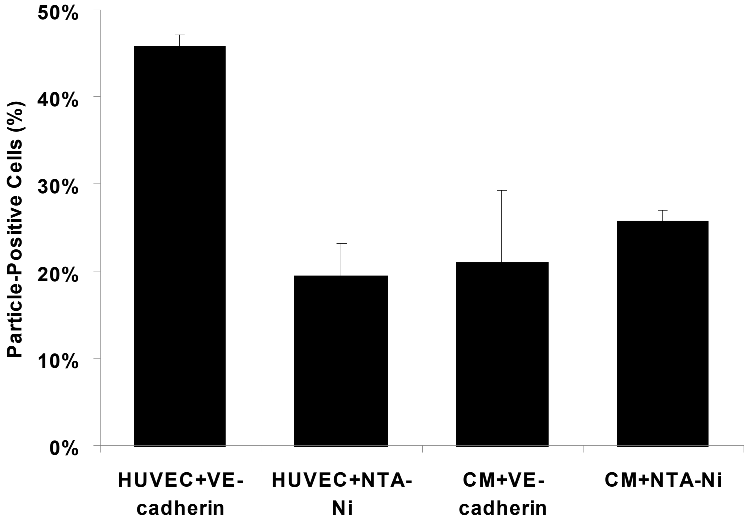

Figure 4.9. Quantification of HUVEC targeting. Negative controls (HUVEC + Ni-NTA, NCM + VE-Cadherin, NCM + Ni-NTA) ranged from 19 to 26% of cells positive for one microparticle. By contrast, HUVECs incubated with VE-Cadherin loaded microparticles had 45.7% of cells labeled by microparticles, which represents a 2.4-fold increase compared to HUVECs treated with non-targeted microparticles (mean±SEM, n=3).

4.3 Discussion

Biological-based therapeutics, such as proteins and nucleic acids, have the potential to treat a variety of diseases due to their great specificity and high potency. However, delivery of biological compounds presents many challenges for drug delivery vehicles due to their sensitive structural properties and hydrophilicity. The data presented in this chapter suggest that metal affinity based systems are a simple, yet effective way to functionalize microparticle carriers in order to obtain microparticle targeting as well as delivery of a protein payload with little risk of denaturation.

Other studies examining the use of NTA-modified surfaces have covalently attached NTA to polystyrene microparticles through a condensation reaction [61] for use in flow cytometry. These techniques require several steps to achieve conjugation and may not be compatible with all polymer chemistries. As an example, polyketals are not readily modified due to the difficulty in incorporating reactive chemical handles onto the polymer backbone. However, surface modification using DOGS-NTA is widely applicable regardless of polymer system. Due to the amphiphilic nature of the DOGS-NTA conjugate, we hypothesized that we could add the lipid to the organic phase of the emulsion and allow the hydrophilic NTA-head groups to migrate to the surface of the microparticle. This one-step procedure does not depend on specific chemical groups and only depends on the emulsion and drying parameters. Thus DOGS-NTA was incorporated without any major alterations in particles size from prior studies.

Our data suggest that protein loading has a weak dependence on NTA incorporation at the concentrations used in this study. Ten percent NTA microparticles had a slightly greater capacity with 440 ng GFP/mg microparticle compared to 330 ng GFP/mg microparticle for the 1% NTA formulation (**Figure 4.3**), though maximal percent loading remained fairly constant. These loading fractions represent physiologically relevant doses for *in vivo* applications; growth factors often have effects at nanomolar concentration, which corresponds to nanograms of protein delivered locally [115]. More importantly, protein loading was achieved in purely aqueous conditions using dilute (<2 μg /ml) solutions of protein; typical double emulsion procedures use protein concentrations in excess of 10 mg/ml [125]. Such high concentrations and protein waste may not be acceptable for expensive proteins that are hard to purify or for scaled-up commercial applications. In addition, protein that does not bind to the surface of the microparticle with the NTA-Ni system is completely recoverable in this loading procedure by centrifuging the particles and recovering the supernatant. This binding was completely reversible as incubation of particles with saturating concentrations (>100 mM) of imidazole-induced immediate release (data not shown). Given the wide popularity of His-tags for purification of recombinant proteins, a large, existing library of proteins can be readily used with the system. Surface functionalization is amenable to screening combinatorial therapies without the need to fabricate a new batch of microparticles for a given protein combination; instead, microparticles can be loaded in a complex, aqueous mixture of therapeutic proteins or targeting ligands. Furthermore, the concept of delivering multiple therapeutics can be taken one step further by the encapsulation of small molecules. As illustrated in **Figure 4.4**, different release kinetics of an encapsulated compound can be achieved due to the physicochemical properties of the drugs or the polymer [136]. Further tuning of the release rates may potentially be achieved by altering the number of NTA groups as well as the length of the His-tag [60]. These techniques may offer ways to modulate the release kinetics of metal affinity systems.

One potential concern for metal-affinity delivery systems is potential toxicity from the metal ions. While heavy metals have been shown to be detrimental, especially in environmental contamination situations, the amount of nickel used in this system is far below toxic concentrations. Ten percent NTA-Ni polyketal formulations maximally contain 5.8 nanograms of nickel per milligram of microparticle. In order to put this into perspective, the average American diet contains 300 micrograms nickel per day [137]. In addition, chelated metals have been shown to have reduced toxicity compared to their free ion counterparts [138]. Our MTT data suggest that NTA-functionalization, with or without nickel, does not add any additional toxicity compared to PCADK microparticles in cardiac myocytes and macrophages. These particular cell types were chosen due to the susceptibility of the heart to nickel poisoning [139] and the phagocytic nature of immune cells, which engage these types of microspheres *in vivo*. Both NTA-functionalized and NTA-Ni-functionalized microparticles showed similar levels of toxicity or better when compared to cells treated by non-modified PCADK microparticles for both cells lines. Previous work in our lab and others has established biocompatibility of PCADK microparticles in a variety of animal models with milligram doses being given to rats and mice [135, 136, 140, 141]. Given that no increase in toxicity associated with the surface functionalization of these microparticles *in vitro*, safe use of these microparticles for *in vivo* applications is anticipated.

After establishing biocompatibility of the NTA-Ni system, we sought to show bioactivity in two potential applications for the non-covalent tethering of proteins. First, we tested the bioactivity of tethered His-tagged VEGF to activate VEGFR2 with the particle directly in contact with cells or separated by a transwell membrane with 3 μm pores. As expected, protein loaded onto the surface of the microparticle showed a dose dependent response when incubated directly on the cells, indicating the protein activity was still intact after complex formation. In this case, VEGF loaded microparticles could have activated its receptor while still bound to the microparticle. In order to separate the effects of tethered protein versus protein that has been released, we tested if VEGF release from microparticles could diffuse across a transwell insert. Our data show that VEGFR2 phosphorylation was seen at 1, 2, and 3 hours but not as early as 20 minutes suggesting that some time was required for VEGF to be released from the surface of the microparticle and diffuse to the cell layer. Furthermore, these data suggest that sustained activation occurs in the transwell system as VEGF signaling with free ligand is rapid [142].

While proteins were released intact from the surface, experiments also demonstrated that targeting could be achieved using cell surface receptors; a greater than two-fold improvement in binding was observed with targeted particles. VE-Cadherin acts as a cell-cell junction protein and is a potential target for endothelial cells due to its selective expression *in vivo*. The targeting system presented here used a His-VE-Cadherin/Fc chimera that greatly increased the size of the protein, thus reducing the density of targeting ligands on the surface of the microparticle. Diffusion of the VE-Cadherin away from the microparticle could have also played a role in the modest targeting. Furthermore, there was a strong potential for microparticles to interact with each other due to the homodimer formation between particles rather than exclusively with cells. Despite these potential confounding variables, significant improvements in targeting were observed and generate enthusiasm for future targeting studies with unique ligands.

Surface modification of polyketal microparticles with IMAC chemistries show potential for improving the delivery of proteins with polymer microspheres. We show here that the NTA-Ni complex is suitable for non-covalent tethering of proteins in their bioactive forms. These proteins can be adapted for use as a therapeutic payload or as targeting ligands for smaller microparticles. Many parameters of the system can potentially be tuned to control features such as release kinetics and warrant further investigation to develop metal affinity delivery systems for future applications.

CHAPTER 5

EXTRACELLULAR DNA AS A PLATFORM FOR TARGETING NECROTIC TISSUE IN THE INFARCT

5.1 Introduction

Traditional approaches to targeting therapeutics or drug delivery vehicles rely on identifying proteins that exist in a higher abundance in a particular organ. Antibodies against these upregulated proteins are then conjugated to drug carriers in order to target delivery. This strategy is potentially difficult for treating cardiac dysfunction due the lack of promising protein candidates that are specifically upregulated in the infarct following MI. In addition, relying on antibodies as targeting ligands precludes drug delivery vehicles from remaining small and able to diffuse large distances due to the inherently large size of antibodies themselves (~150 kDa); the smallest functional unit of an antibody, the variable domain (Fv), is approximately 25 kDa [143]. Conjugation of the Fv fragment would double the size of most therapeutic proteins (e.g. cytokines) and increase the size of a small molecule drug by an order of magnitude or more.

Our approach to targeting infarcted tissue focuses on targeting extracellular DNA released by necrotic cells. Necrotic cells should be abundant in the infarct due to the depletion of ATP downstream of the occlusion and accumulation of metabolic wastes during the ischemic phase of MI. These conditions typically drive necrotic cell death, which comes with loss of cellular membrane integrity. By contrast, controlled cell death (apoptosis) typically proceeds with no loss of membrane integrity and eventual phagocytosis of an apoptotic body without significant extracellular release of DNA. Apoptotic cell death dominates in healthy tissue homeostasis. As a result, each cell that dies through the necrotic pathway should contribute on the order of picograms of DNA per cell. Given that nearly ten million cells show compromised cell membranes in rat models of myocardial infarction [144] (and on the order of billions of necrotic cells in humans suffering from MI), this represents a significant basis for targeting therapeutic molecules.

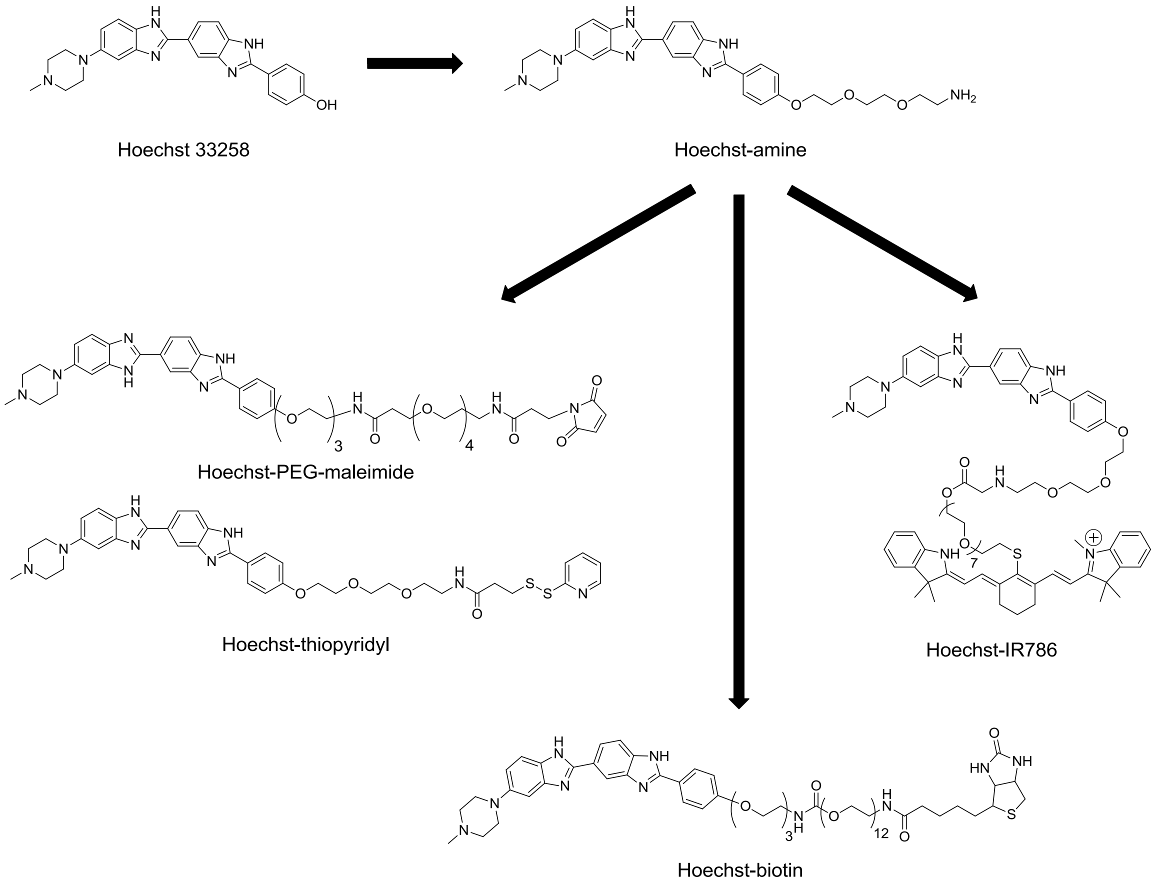

Figure 5.1. A variety of Hoechst conjugates can be synthesized from Hoechst-amine. Hoechst 33258 is available commercially for use as a fluorescent stain for DNA. Using commercial Hoechst as an inspiration, Hoechst with a short PEG linker and primary amine (Hoechst-amine) was synthesized, which allowed for further conjugation. Thiol-reactive Hoechst conjugates (Hoechst-PEG-maleimide and Hoechst-thiopyridiyl) can be used to modify cysteine residues on proteins using either permanent (maleimide/thioether bond) or reversible (thiopyridyl/disulfide bond) covalent linkages. Hoechst-biotin can be used with a variety of streptavidin conjugates and is a highly sensitive probe due to the strong binding affinity between streptavidin and biotin. Hoechst-IR786 is a near-infrared fluorescent dye conjugate that can be used for *in vivo* or whole organ imaging applications.

DNA binding dyes, such as Hoechst, are excellent candidates for small molecule targeting ligands. DNA binding dyes are inherently designed to have a high affinity for DNA, and typically have dissociation constants on the order of many antibody-antigen interactions. Hoechst is also significantly smaller than antibodies with a molecular weight of 534 Da. Furthermore, Hoechst has a history of being used *in vivo* both as a tracer for angiogenesis and as a chemotherapeutic in humans, which suggests that low doses are tolerated by the body.

This chapter will introduce the different Hoechst-conjugates that were synthesized and potential downstream applications. All of the Hoechst conjugates used in these studies were based on Hoechst-amine (**Figure 5.1**). The synthesis of this molecule was describe by Dasari, et al. [145] and served as the foundation for further ligation of Hoechst to other molecules. Furthermore, the use of Hoechst-IR786 for imaging necrosis via near infrared fluorescence imaging will be highlighted. Lastly, attempts to deliver the therapeutic proteins VEGF and SOD to the infarct following MI using Hoechst as a targeting agent will be discussed.

5.2 Results

Synthesis and Characterization of Hoechst-Conjugates

Hoechst-amine was synthesized as reported by Dasari, et al. [145]. A sulfhydryl-reactive Hoechst derivative was synthesized using standard NHS-amine coupling chemistry (**Figure 5.2**). Hoechst-PEG-maleimide was purified using preparative TLC and validated via ^{1}H-NMR and mass spectrometry (**Figure A.4-A.5**, appendix). ^{1}H-NMR was analyzed for the inclusion of vinyl protons, indicative of the maleimide group (singlet, 6.77 ppm). Mass spectrometry was conducted using matrix assisted laser desorption/ionization (MALDI-TOF) and showed a primary ion peak at 954.5, compared to the calculated value of 954.1. UV-absorbance spectra (200-400 nm) of commercially available Hoechst 33258, Hoechst-amine, and Hoechst-PEG-maleimide were collected using 200 μM solutions (**Figure 5.3**). All three species had similar spectra with peaks occurring at 260 and 340 nm.

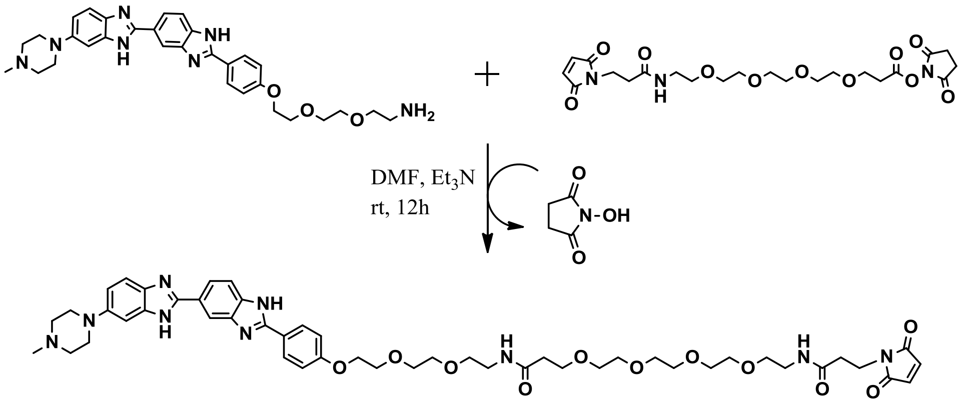

Figure 5.2. Synthesis scheme for Hoechst-maleimide. Hoechst-amine was reacted with N-hydroxylsuccinimide-PEG$_4$-maleimide in dimethlyformamide and triethylamine at room temperature overnight. The reaction mixture was purified using preparative thin layer chromatography in order to isolate Hoechst-PEG-maleimide, which can be used to modify sulfhydryl groups on proteins.

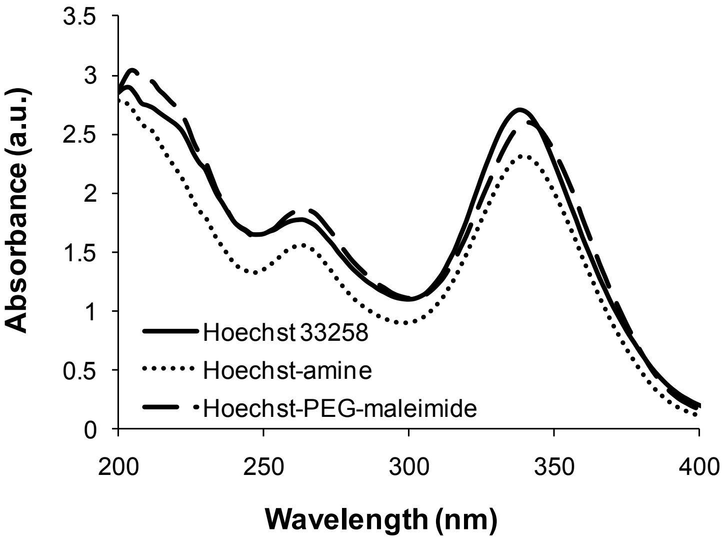

Figure 5.3. UV-Absorbance spectra of Hoechst species. UV spectra were recorded for three Hoechst species, commercially available Hoechst 33258, Hoechst-amine, and Hoechst-PEG-maleimide using a 200 μM solution.

Cell permeability of Hoechst-Conjugates

Primary rat neonatal cardiac myocytes were used to determine the cell permeability of Hoechst species (**Figure 5.4**). Cells were plated in multiwell plates and Hoechst compounds added to the media at a final concentration of 0.1 mg/ml. Fluorescence was measured over 24 hours and used as a measure of permeability as Hoechst compounds significantly increase quantum efficiency (fluorescence intensity) when bound to DNA, the increase in fluorescence can be attributed to compound binding to DNA in the nucleus. Data were normalized to control cells treated with no dye set to unity. Hoechst-amine treated cells showed similar increases in fluorescence when compared to commercial Hoechst (data not shown), with an eight fold increase in fluorescence after six hours. By contrast, Hoechst-biotin did not appear to be cell permeable and had fluorescence intensities equivalent to control cells at 24 hours.

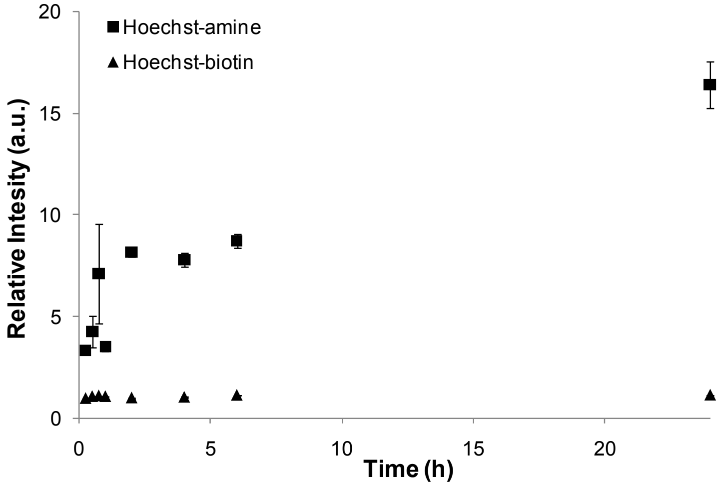

Figure 5.4. Relative cell permeability of Hoechst-amine and Hoechst-biotin. Hoechst conjugates have varying levels of cell permeability. Rat neonatal cardiac myocytes were cultured in multiwell plates and blue fluorescence of the Hoechst was monitored over time. Cells were incubated up to 24 hours with 0.1 mg Hoechst compound/ml in serum free media. Commercially available Hoechst and Hoechst-amine showed similar increases in fluorescence, despite the addition of three ethylene glycol units and a primary amine. Biotinylated Hoechst, which was linked to biotin with a 15-unit PEG chain, showed low levels of fluorescence similar to untreated cells. (mean±SEM, n=3)

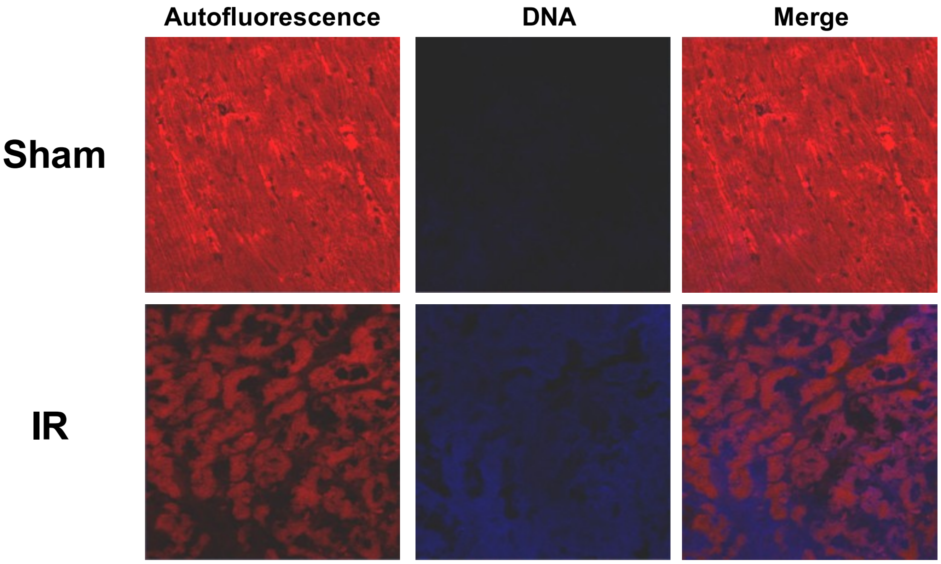

Figure 5.5. ***In vivo*** **testing of Hoechst-biotin in an rat MI model of necrosis.** Rats were subjected to ischemia-reperfusion (IR) surgery in the heart. One day after ischemia-reperfusion surgery, 500 μg of Hoechst-biotin was injected intravenously and allowed to circulate for one hour. Frozen sections of the heart were examined using confocal microscopy. Tissue morphology was examined via red autofluorescence of the tissue. Sham operated animals showed cell membrane integrity in the left ventricle (LV) and little blue fluorescence (Hoechst). IR-operated animals showed necrosis in the LV and diffuse blue staining suggesting release of DNA from necrotic cells.

In vivo permeability was tested in a rat model of myocardial infarction. Rats were subjected to thirty minutes of ischemia followed by reperfusion surgeries (IR surgeries) and allowed to recover for a day. Twenty-four hours post-surgery, 0.5 mg of Hoechst-biotin was administered intravenously via retro orbital injection. The compound was allowed to circulate for one hour before the rat was sacrificed and heart embedded in OCT resin for cryosectioning. Sections were mounted and imaged using confocal microscopy without any additional staining (**Figure 5.5**). Sham operated animals showed very low blue fluorescence indicative of Hoechst-DNA. In particular, no nuclei were stained blue. Autofluorescence was used to examine tissue morphology (red), which indicated that sham operated animals did not have compromised cell membranes. Rats that received IR-surgery, on the other hand, had significant diffuse blue staining, indicating extracellular DNA, and no focal staining of nuclei. Tissue autofluorescence suggested that cell membranes were compromised.

Near Infrared Imaging of Necrosis with Ho-IR786

Near infrared fluorescence imaging is commonly used for imaging live animals or whole organs. The optical properties of most tissues allow good penetration depths, on the order of millimeters to centimeters, of near infrared wavelengths. Hoechst was conjugated to the near infrared fluorescent dye 2-[2-[2-Chloro-3-[(1,3-dihydro-1,3,3-trimethyl-2H-indol-2-ylidene)ethylidene]-1-cyclohexen-1-yl]ethenyl]-1,3,3-

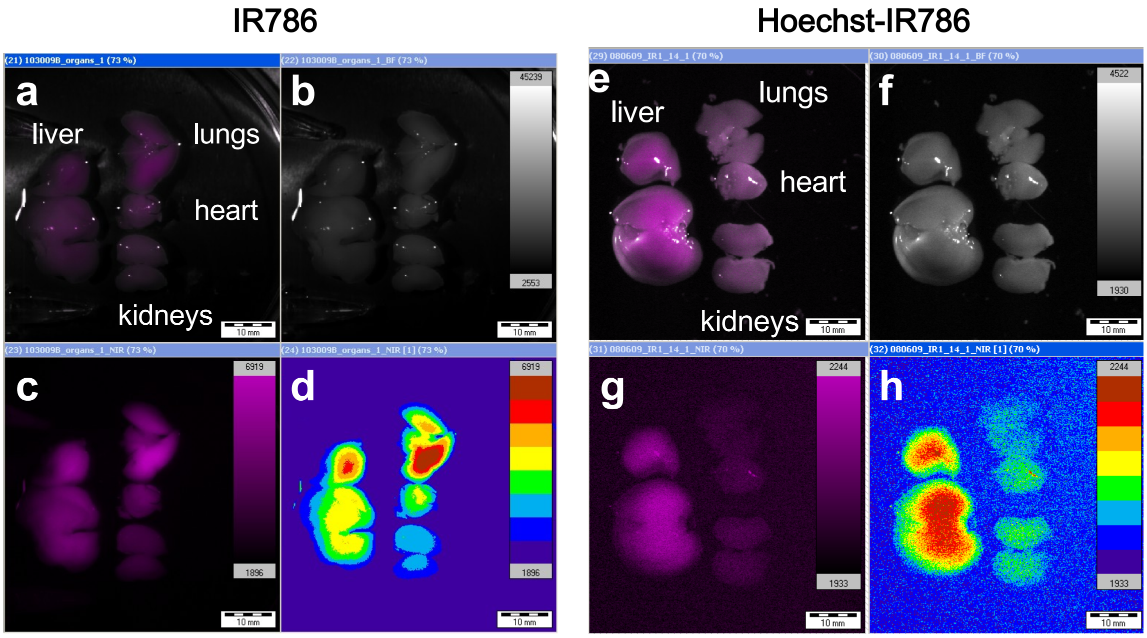

Figure 5.6. Near-infrared fluorescence image of organs from animal injected with IR-786 or Ho-IR786. Mice were subjected to IR-surgery and organs were harvested after administering 10 nanomoles of IR786 (a-d) or Ho-IR786 (e-f) intravenously. IR786 treated animals showed higher fluorescence intensities than Ho-IR786, with peak values reaching 6919 RFU compared to 2244 RFU. Both treatments showed significant accumulation in the liver. (a & e) Brightfield/near infrared merge, (b & f) brightfield, (c & g) near infrared, (d & h) heat map. (scale: 10 mm)

trimethylindolium iodide (IR786) in order to have an extracellular-DNA-specific fluorescent probe to visualize necrosis in the heart.

Mice were subjected to thirty minute IR-surgery and injected with ten nanomoles (100 µl of 100µM dye in 5% ethanol, 5% Cremophor EL, 90% PBS) of dye (either Hoechst-IR786 or IR786) two hours after surgery. Dye was injected intravenously via retro orbital injection. Animals were sacrificed twenty minutes post-injection and perfused with saline to wash out any unbound dye. After three minutes of saline perfusion, tissue was fixed by perfusion of 4% paraformaldehyde in PBS. Animals that were injected with unmodified IR-786 showed significant near-infrared fluorescence in all organs (**Figure 5.6**). Animals that received Hoechst-IR786 showed high levels of dye in the liver. But compared to IR786-treated animals, fluorescence intensity was significantly lower, peaking at 2244 RFU for Hoechst-IR786 compared to 6919 RFU for IR786.

To better quantify fluorescence, hearts were imaged separately at a higher magnification (**Figure 5.7**). Animals that received Hoechst-IR786, regardless of surgery type, showed some elevation in near-infrared fluorescence compared to uninjected control animals. Mean fluorescence intensity for the infarcted area was quantified using ImageJ and normalized to sham operated hearts. Comparison between sham operated and IR-surgery demonstrated significant increase in Hoechst-IR786 fluorescence in the left ventricle when injected two hours post-surgery (n=3, * $p < 0.05$). Animals that were injected 24 hours after surgery showed slight elevation in fluorescence intensity for IR-operated animals compared to sham, but did not reach statistical significance. Additional imaging of animals that received IR-surgery (**Figure 5.7c-d**) showed near-infrared intensity concentrated in the left ventricle free wall. **Figure 5.7c** illustrates that the suture, which was left in the heart and is visualized by the decreased intensity running vertically through the image, is upstream of the highest fluorescence. A planimetry slice

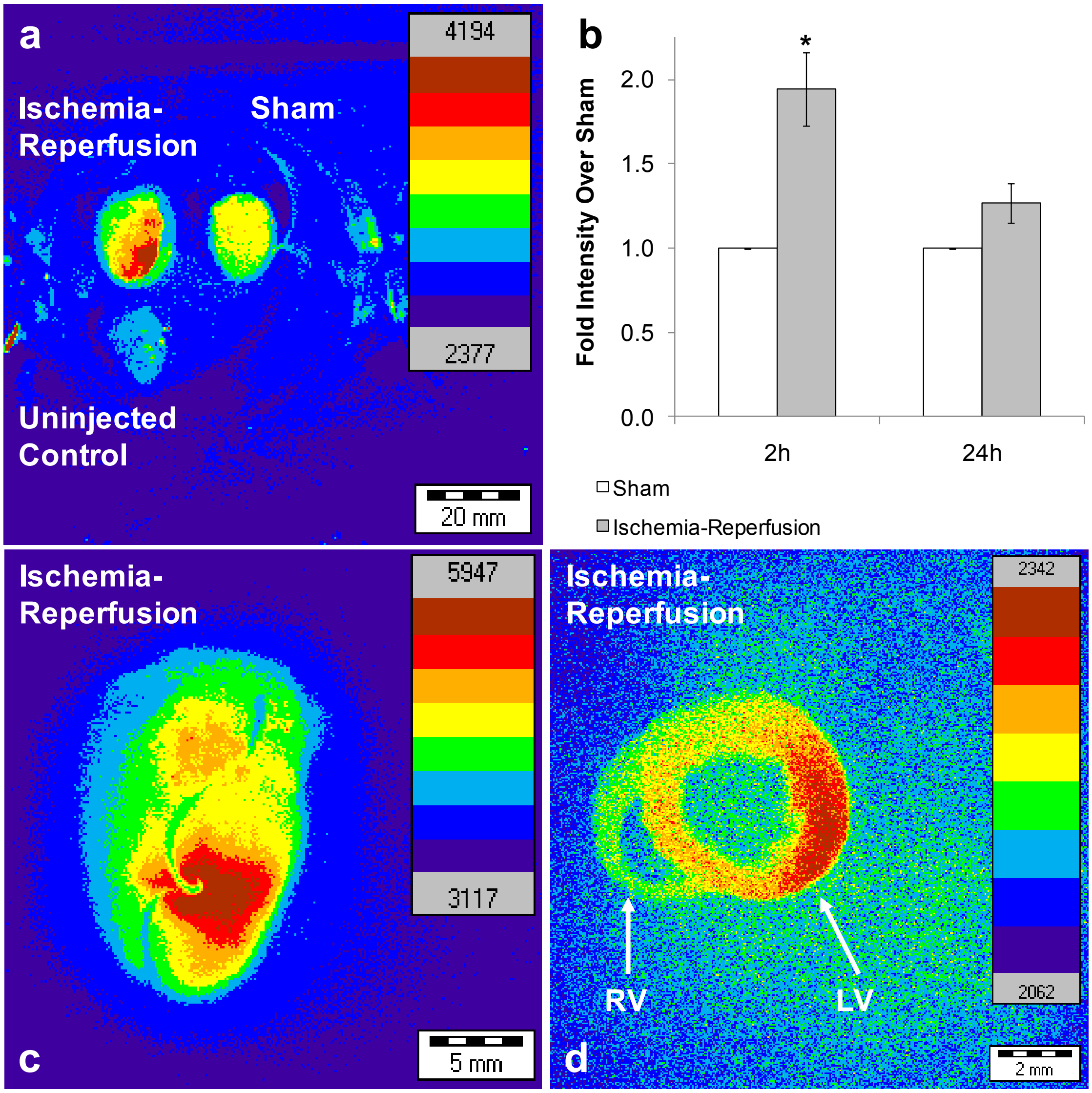

Figure 5.7. Ho-IR786 targets the left ventricle of mice that receive ischemia-reperfusion surgery. (a) Comparison of three hearts, IR-surgery, sham operated, and uninjected control under NIR fluorescence imaging. (b) Mice were subjected to sham or IR-surgery and injected with 10 nmol Hoechst-IR786 at different time points. Animals were sacrificed one hour after injection, perfused, and organs harvest for imaging. Semi-quantitative analysis shows time dependence for NIR intensity. (n=3, * $p < 0.05$ compared to sham, Student's t-test) (c) Zoom of IR-surgery heart that received Hoechst-IR786. Suture remains visible with high NIR fluorescence intensity downstream. (d) Thick section of heart that received IR-surgery and Hoechst-IR786 shows localization of dye in the LV and not in the right ventricle RV.

of an IR-operated heart (**Figure 5.7d**) shows that the fluorescence intensity is greater in the left ventricle compared to the right ventricle.

Hoechst Conjugates of Therapeutic Proteins

VEGF was expressed as previously described [146] and contained unpaired cysteine residues. These residues were targeted for modification using Hoechst-PEG-maleimide and reacted with ten equivalents of the Hoechst compound according to the scheme in **Figure A.6** (appendix). Mice were subjected to IR surgery described above. Two hours following IR-surgery, two micrograms of VEGF or HoVEGF was injected (100 μl injection volume) intravenously via retro orbital injection. The mouse was then sacrificed and perfused for three minutes with normal saline. The heart was dissected into three pieces: left ventricle free wall (LV), right ventricle free wall (RV), and remaining part (termed "heart" in subsequent figures). These pieces were homogenized in RIPA buffer and analyzed for VEGF content via ELISA.

Animals that received either VEGF or HoVEGF injections had higher levels of VEGF compared to uninjected control mice that had received IR-surgery, with the HoVEGF group trending higher (**Figure 5.8**). Animals that received HoVEGF injection had 47±12 pg VEGF/mg protein in the LV and lower amounts in the heart and RV (27±7 pg VEGF/mg protein and 32±8 pg VEGF/mg protein, respectively). VEGF injected animals had less disparity between heart sections with 34±7, 24±5, and 27±7 pg VEGF/mg protein in the LV, heart, and RV, respectively. Injected IR controls had 11±7, 2±1, and 13±9pg VEGF/mg protein in the LV, heart, and RV, respectively. Levels of HoVEGF were significantly higher than IR animals when analyzed using t-test, but did not achieve significance through ANOVA (p=0.06). No other treatments were significant. Amounts of VEGF recovered maximally accounted for less than 1% of the total injected dose.

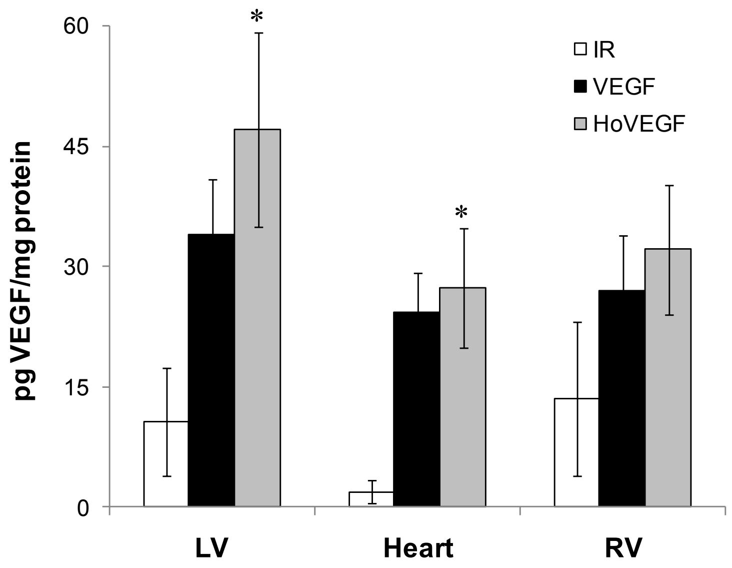

Figure 5.8. Levels of modified and unmodified VEGF in the heart post-IR. Mice were subjected to thirty minutes of ischemia followed by reperfusion. Two hours after surgery, two micrograms of either VEGF or HoVEGF was injected intravenously. The mouse was then sacrificed fifteen minutes after injection and perfused to wash away unbound VEGF. The heart was sectioned into the LV free wall, RV free wall, and the rest of the organ, termed "heart" in these graphs. Tissue pieces were homogenized and tested for VEGF levels via ELISA. (mean±SEM, n≥6, *p < 0.05 compared to IR control, ANOVA followed by Tukey-Kramer post test)

To determine if antioxidant enzymes could be delivered in this manner, SOD protein was modified with Hoechst according to the scheme in **Figure A.7** (appendix). Stock SOD contained no detectable sulfhydryl groups using Ellman's assay and had an activity of 3619 U/mg. Following reaction with 20 equivalents of Traut's reagent (2-iminothiolane, which produces free sulfhydryls upon reacting with amine groups), SOD molecules had an average of 12.5 sulfhydryl groups and activity of 3163 U/mg. Thiolated-SOD was then reacted with Hoechst-PEG-maleimide (two equivalents, with respect to –SH) overnight to produce Hoechst-SOD (HoSOD). No detectable sulfhydryls were present using Ellman's assay and protein activity decreased to 1057 U/mg. The Ellman's assay data suggest that each SOD molecule was functionalized with an average of twelve Hoechst ligands. Mass spectrometry show that protein molecular weight was increased after reacting with Hoechst-PEG-maleimide (**Figure 5.9**).

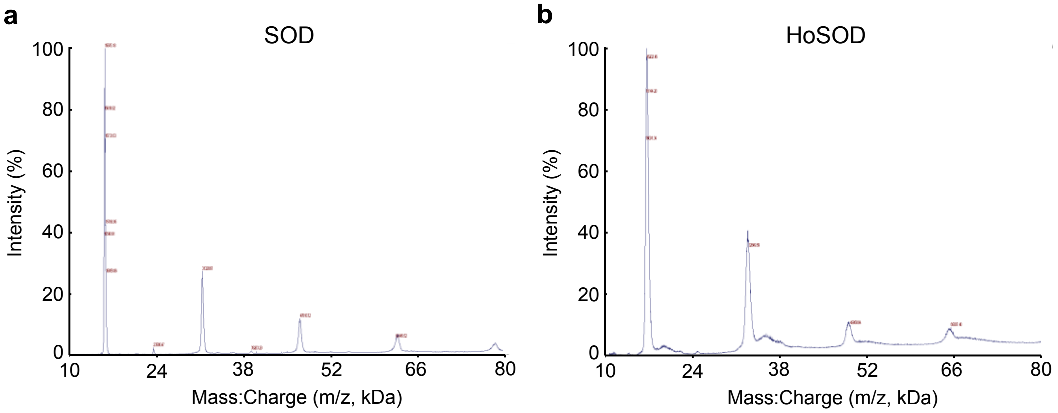

Figure 5.9. Mass spectra for SOD and HoSOD. Mass spectra were collected using MALDI-TOF. (a) Unmodified showed sharp peaks at 15.6 kDa, 31.3 kDa (native protein), 47.0 kDa, and 63.4 kDa. (b) HoSOD, by contrast had heavier peaks, but also peaks that had shoulders with higher molecular weights, suggesting different number of Hoechst ligations. Peaks were found at 16.2 kDa, 32.6, kDa, 50.0 kDa, and 65.0 kDa.

HoSOD was tested in the same mouse model of IR, as described above. These studies were similar to the HoVEGF procedure with a thirty minute ischemic period and injection HoSOD two hours after surgery. Two hundred units of either free SOD or HoSOD were injected intravenously and the animal sacrificed 15 minutes following injection. Animals were perfused with PBS for three minutes before organs harvested and dissected as described previously. Tissue homogenates were analyzed for SOD activity and normalized to protein concentration (**Figure 5.10**). HoSOD was significantly higher than control in all three heart sections, and significantly greater in the septal wall and remain heart piece following free wall dissection compared to SOD treatment ($p<0.05$). SOD injected animals had significantly more activity in the LV, but not in other section of the heart. The amount of HoSOD recovered maximally accounted for 36 U of SOD activity in the LV, after subtracting endogenous SOD activity. This would account for 18% of the initial injected dose.

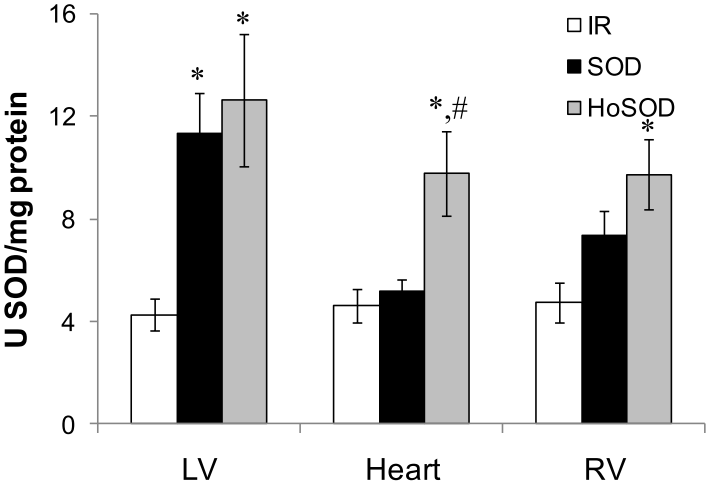

Figure 5.10. SOD activity in the heart fifteen minutes following administration of SOD and HoSOD. Mice were subjected to IR-surgery. Two hours following surgery, 200 U of SOD or HoSOD was injected intravenously. Mice were sacrificed and perfused fifteen minutes post-injection. The heart was dissected and homogenized and analyzed for SOD activity. SOD activity was elevated for both SOD and HoSOD injected animals in all fractions. (mean ± SEM, $n \geq 5$, *$p < 0.05$ compared to IR, # $p > 0.05$ compared to SOD, ANOVA followed by Tukey-Kramer post test)

The study was repeated using a higher dose (400 U) and longer time between injection and sacrifice (one hour). **Figure 5.11** illustrates that all three groups had similar levels of SOD activity (2-3 U/mg protein) under these conditions. Western blot analysis showed no difference in SOD protein levels (data not shown).

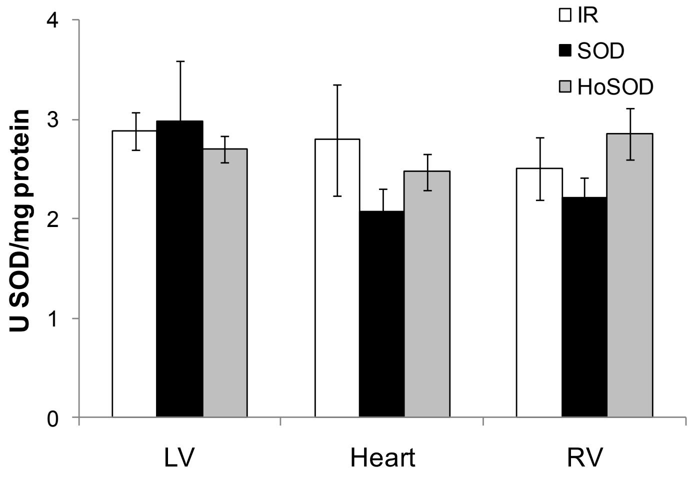

Figure 5.11. SOD activity in the heart one hour following administration of SOD and HoSOD. Mice were subjected to IR-surgery. Two hours following surgery, 400 U of SOD or HoSOD was injected intravenously. Mice were sacrificed and perfused one hour post-injection. The heart was dissected and homogenized and analyzed for SOD activity. SOD activity, regardless of treatment or heart fraction, ranged from 2-3 U/mg protein. (mean ± SEM, n≥3, no statistical significance found)

5.3 Discussion

The overall goal for this aim was to examine the feasibility of using extracellular DNA as a targeting platform for the infarction in the heart following MI. Anoxic conditions during MI generate necrotic lesions in the heart with high concentrations of extracellular DNA. While the necrotic lesion does not represent tissue that can be salvaged, the specific localization of extracellular DNA to the infarct can serve as a targeting platform and reservoir for delivering drugs to the border zone surrounding the infarct core, where cells are still salvageable. Furthermore, this aim is a departure from traditional drug targeting strategies that focus on the use of antibodies and highlight the potential for using small molecules with high binding affinities as targeting ligands. By using small molecule targeting ligands, molecular weights of therapeutics can remain low, especially compared to the 150 kDa that antibody conjugation would add, and thus have increased diffusivity.

Hoechst is widely used in research settings to stain the nuclei of cells in histology and flow cytometry. Commercial Hoechst is cell permeable has a high binding affinity for the minor groove of DNA, particular in regions that are A-T rich. Upon studying the crystal structures of Hoechst-DNA complexes, it became clear that the phenolic hydroxyl was a candidate site for modifying the compound with little risk of negatively affecting binding affinity to DNA. Using Hoechst as a basis, Hoechst-amine was designed to have a short PEG linker with a primary amine at the phenolic hydroxyl site (**Figure 5.1**). The PEG linker was added to modulate cell permeability while the primary amine allowed for further conjugation to other molecules. Unfortunately, direct modification of this phenolic hydroxyl was not possible and Hoechst-amine was synthesized in using the 11-step route shown in **Figures A.1-A.4** (appendix), and verified via mass spectrometry and ^{1}H-NMR (data not shown).

A thiol-reactive version of Hoechst was synthesized using NHS-PEG$_4$-Maleimide, under standard NHS-chemistry linking conditions (dimethyl formamide with triethylamine, overnight at room temperature). The compound was purified using preparative thin layer chromatography and verified using mass spectrometry and ^{1}H-NMR (**Figures A.4-A.5**, appendix). Hoechst-PEG-maleimide allows the site-specific modification of proteins by targeting unpaired cysteine residues. Alternatively, primary amine residues on a protein can be modified using Traut's reagent, which converts amines to sulfhydryls, and subsequently modified using the maleimide conjugate. One beneficial property of using Hoechst is that it has well characterized spectral properties. In order to ensure that optical properties were not adversely affected, absorbance spectra were generated for Hoechst-amine and Hoechst-PEG-maleimide and compared with commercially purchased Hoechst 33258 (**Figure 5.3**). Both pathways were utilized to functionalize therapeutically relevant proteins, and are discussed later in this chapter.

Hoechst-biotin was one of the earlier conjugates synthesized in order to test proof of concept. This compound was designed to be cell impermeable due to its 15-PEG linker and have a high sensitivity mechanism for detection (biotin-streptavidin interaction). *In vitro* cell permeability studies using primary neonatal cardiac myocytes (**Figure 5.4**) and took advantage of the fact that Hoechst compounds are not highly fluorescent unless bound to DNA; by binding in the minor groove of DNA, vibrational and rotational modes are significantly reduced, significantly increasing the fluorescent quantum efficiency of the molecule. It was expected that both Hoechst-amine and Hoechst-biotin would have similar cell permeabilities; Hoechst-amine contains a 3-PEG linker and a very hydrophilic primary amine, whereas Hoechst-biotin had a similarly hydrophilic 12-PEG linker. Hoechst-amine showed similar increases in fluorescence when compared to commercially available Hoechst. Hoechst-biotin, on the other hand, behaved as expected and had fluorescence intensities on par with basal fluorescence of untreated cells.

This result prompted us to test the Hoechst-biotin molecule *in vivo* using a rat model of MI. Under confocal microscopy, extracellular DNA was visualized directly (**Figure 5.5**). The high autofluorescence of cardiac tissue provided a way to visualize cell morphology; sham operated animals had healthy tissue morphology, whereas rats that received IR surgery had increased interstitial spaces between cells. More importantly, sham operated animals had very low levels of blue fluorescence, indicative of low binding of Hoechst-biotin to DNA. In particular, cell nuclei were not labeled blue by the Hoechst-biotin suggesting that the compound was not cell permeable *in vivo*. Furthermore, data provided by the IR operated rats showed significant blue fluorescence in the interstitial spaces between cells. This is consistent with the hypothesis that necrotic cell death generates significant extracellular DNA.

However, an alternative explanation that Hoechst compounds may have some non-specific interactions with cellular components exposed due to necrosis. Hoechst contains three planar, aromatic groups that could interact with hydrophobic pockets of proteins or other molecules. However, these interactions may not increase the fluorescence intensity, as is seen with DNA minor groove binding, and likely occur with very low affinity *in vivo*. Furthermore, preliminary experiments using cells fixed in methanol, which would allow access to all intracellular components, demonstrated that blue fluorescence was only seen in the nuclei. This suggests that the blue signal is specific to DNA binding, but that additional experiments using DNase or other treatments are needed to rule out non-specific Hoechst-binding.

In order to further examine the possibility for targeting extracellular DNA in the infarct, Hoechst-IR786 was synthesized [145]. This molecule consists of a 10-PEG linker and the near-infrared fluorescent dye IR786. Near infrared imaging allows for imaging of live animals and whole organs due to low tissue attenuation of near-infrared wavelengths by tissue. As an initial control, unmodified IR786 was injected intravenously into a mouse and compared to Hoechst-IR786 (**Figures 5.6**). In both cases, the liver showed significant enrichment of the dye. We hypothesize that the dye is likely metabolically cleared from the body through the liver. In addition, there have been reports of IR786 binding to albumin [147], which would also support a hepatic clearance route. In the case of unmodified IR786, high concentrations were also seen in the lungs. This enrichment may be due to a first pass effect; since the dye was injected intravenously, the lungs represent the first capillary bed where it could partition into cell membranes as it passed through the cardiopulmonary circulation. However, the main difference between compounds was the magnitude of fluorescence intensity. While the heat maps in **Figures 5.6** appear similar qualitatively, unmodified IR786 had significantly higher intensities (heat map scale: 1896-6919) compared to Hoechst-IR786 (heat map scale: 1933-2244). This suggests that the increased water solubility and decreased cell permeability resulted in less nonspecific tissue binding of the Hoechst conjugate.

We examined the distribution of Hoechst-IR 786 in the heart tissue following IR. By increasing magnification the differences in the distribution of the compound in the hearts of sham and ischemia-reperfusion operated mice could be compared quantitatively. **Figure 5.7a** demonstrates that there was a basal increase in heart fluorescence due to the Hoechst-IR786, as both sham and ischemia-reperfusion operated animals had higher fluorescence intensities compared to a control heart that did not receive any dye. However, distinct regional differences are seen between sham and ischemia-reperfusion operated animals. Indeed, upon closer examination of ischemia-reperfusion operated hearts, there is a distinct zone that would correspond with the infarcted area. **Figure 5.7c** shows another heart where the suture has been left in place with high fluorescence directly downstream of the ligation. Thick cross-sections of the heart (**Figure 5.7d**) showed localization of the compound in the left ventricle free wall and not the right ventricle. These data are consistent with where one would expect necrotic cell death to occur and correlate with commonly seen triphenyltetrazolium chloride (TTC) staining of infarcted myocardium [148].

Semi-quantitative data generated by measuring fluorescence intensities of the images showed dependence between IR786 enrichment and the time between injection and ischemia-reperfusion (**Figure 5.7b**). Animals that were injected soon after surgery (two hours) had greater differences between ischemia-reperfusion and sham compared to mice that were injected the following day. This finding did not fully agree with previously published literature, as other groups have measured the onset of necrosis at later time points in different animal models of myocardial infarction. A study conducted by Kajstura, et al. injected rats with anti-myosin antibody prior to permanent LAD ligation in order to probe cell membrane integrity post-infarction. This study demonstrated that approximately 100,000 cells were positive for the anti-myosin antibody from 2-4.5 hours post occlusion. The number of cells with compromised membranes increased to three million cells at six hours. These numbers held steady up to 48 hours post infarction, and cells with compromised membranes are nearly absent by seven days. However, the authors acknowledged that the large size of the anti-myosin antibody may have caused an underestimate of the extent of necrosis at early time points [144]. In a similar study validating the use of TTC staining in a permanent occlusion model of MI in rats, Vivaldi, et al. demonstrated irreversible tissue damage after thirty minutes of occlusion (as measured by TTC staining and validated by electron microscopy), but that the infarct matured over the course of six hours after occlusion and persisted for at least two days after injury [149]. Data generated with Hoechst-IR786 are in line with previous studies in that we were able to detected evidence of irreversible cell death two hours after injury. However, previous work using other markers of tissue damage (i.e. staining for myosin components or absence of dehydrogenase enzymes) have observed early irreversible cell death, but suggest that this persists for days post-infarction. Yet, animals injected with Hoechst-IR786 one day post-infarction did not show a significant increase in near infrared fluorescence.

DNA and proteins are cleared and recycled by the body through different mechanisms. This, coupled with differences in surgical models of MI, may have played a role in the differences seen between DNA and protein markers of necrosis. Extracellular DNA is cleared rapidly from the body via endogenous DNase expression. Results from Naperei, et al. demonstrate that application of serum to cells undergoing necrosis *in vitro* clear high molecular weight chromatin DNA by 24 hours [150]. Furthermore, naked DNA injected intravenously into rats has been demonstrated to be cleared from the serum with over 95% cleared in the first five minutes following injection [89]. Given these data, one would expect DNA to be cleared from the infarct rapidly compared to other necrotic markers.

Since the presence of DNA is required for the Hoechst targeting strategy, subsequent studies involving therapeutic proteins focused on the two hour post-surgery time point established by the near infrared imaging studies. Given the limited window of opportunity for targeting the infarct via extracellular DNA, it was important to use therapeutics that could blunt the initial damage following reperfusion. Two candidate proteins were identified: VEGF for neovascularization of the infarct and SOD to blunt the initial surge of oxidative stress that comes with reperfusion of the heart.

As necrotic tissue is not salvageable, it is important that the therapeutic proteins have a mechanism to either have an effect on viable tissue from a distance or be able to be released from the necrotic tissue so that it can be transported to viable cells. The chemical conjugation techniques used for both VEGF and SOD modification generated a stable thioether bond. The rationale behind using this chemistry was that it would allow for better demonstration of targeting compounds to the infarct since clearance from the necrotic tissue would be diminished. However, it is possible to engineer more labile bonds, such as disulfides or ester linkages, which can cleave under physiological conditions (i.e. redox potential, hydrolysis, or enzymatic cleavage). Furthermore, given that necrosis incites significant inflammation and is cleared by leukocytes, it is expected that DNA degradation and clearance play a larger role in the release of Hoechst-conjugated therapeutics. Once liberated from extracellular DNA, Hoechst compounds could then be carried away from necrotic tissue through a combination of diffusive and convective transport. Given that the animal model used in these studies relied on ischemia-reperfusion surgeries, convection was likely the dominant transport factor.

VEGF is a potential therapeutic candidate for this strategy as it is a central regulator of blood vessel growth. During the ischemic period in MI, blood vessels can be lost, along with the cardiac tissue. As a result, even after reestablishment of blood flow in the larger vessels, there may be regions of poor reperfusion. This may be detrimental for stunned myocardium that will eventually die due to insufficient nutrient transport. Neovascularization may be able to maintain or rescue some heart function following MI. VEGF therapy is by no means a curative as vessel growth is slow and requires other factors, such as PDGF, to stabilize growth. However, it is a logical choice for targeting in the acute phase following MI, as it is the first signal that leads to capillary sprouting in tissue and could help in the development of collateral vessels to salvage at risk myocardium. Furthermore, by using the necrotic core as a reservoir, it may be possible to establish a gradient of VEGF in the infarct; as VEGF is liberated from extracellular DNA, it can be transported to the surrounding vasculature via convection and diffusion where it can act on distal endothelial cells. Other groups have established the importance of mitogen gradients and concentrations as they relate to cell polarity and proliferation, respectively [151].

VEGF was expressed with a terminal, unpaired cysteine as previously described [146] allowing for site-specific modification. This is important since many cytokines and growth factors are highly dependent on shape in order to bind and activate their complimentary receptors. The added cysteine residue was modified previously and shown to retain bioactivity. The disadvantage for modifying this route was that a maximum of two Hoechst moieties per active cytokine is possible (VEGF is a native dimer and was expressed such that each subunit contained one unpaired cysteine). Characterization of HoVEGF was difficult since such small amounts of protein at low concentrations were used. These concentrations were not suitable for mass spectrometry analysis or Ellman's assay for free sulfhydryl determination.

Ischemia reperfusion surgeries were conducted in mice in order to test the ability of Hoechst targeting to enrich the growth factor in the infarct. Quantification of VEGF via ELISA showed that there was trend of higher levels of HoVEGF than VEGF in the left ventricle free wall (47 pg VEGF/mg protein compared to 34 pg/mg) (**Figure 5.8**). This trend held for the other sections of the heart analyzed, the right ventricle free wall, and the rest of the ventricle (mostly the septum and parts of the apex, termed "heart" in the figures). However, while there was a trend for more HoVEGF enrichment compared to VEGF, the levels that were recovered from the heart were not significant; the levels of HoVEGF recovered in the left ventricle account for less than one percent of the total injected dose (2 µg). One of the potential issues that may explain this finding is that HoVEGF may be binding elsewhere in the circulation due to the abundance of VEGF receptors throughout the circulation. Given that the binding affinities between VEGF and its receptor and Hoechst and DNA are on the same order of magnitude, there is not a strong likelihood that HoVEGF is enriched in the heart based on the large number of VEGF receptors in the vasculature.

The second candidate protein was selected to avoid the issue of binding to receptors while still having some potential therapeutic benefits. As described earlier, oxidative stress plays a large role in cardiac dysfunction and superoxide radicals are central to the progression of heart failure. Superoxide therapy has shown to be beneficial for cardiac function in other studies if given in high doses acutely following MI. SOD that is immobilized in the necrotic core may have a limited effect on the levels of extracellular ROS in the viable border zone, but given the high reactivity of these radicals, SOD therapy would be optimal directly in the border zone. Furthermore, given that it is not a cytokine, SOD is not expected to have any other competing high-affinity interactions *in vivo*.

From a synthetic point of view, it was also possible to work with larger quantities of SOD, which allowed more thorough characterization of the protein conjugates. Reactions involving SOD were conducted on the milligram scale, rather than the microgram scale, as was done with VEGF. Ellman's reagent was used to track the average number of sulfhydryls per molecule. Ligation of Hoechst moieties was validated through the disappearance of sulfhydryls. The Hoechst-PEG-maleimide conjugate was used over the Hoechst-thiopyridyl conjugate since maleimides react to form thioether bonds, which are not redox-sensitive. The disulfide bond produced by the thiopyridyl coupling can be reduced, liberating the protein from the Hoechst ligand. Modification of SOD was also validated by mass spectrometry (**Figure 5.9**). These data indicate that there was both a shift in the most abundant ion peaks as well as an appearance of a shoulder containing higher m/z species (i.e. higher molecular weights indicative of conjugated the 954 Da Hoechst-PEG-maleimide group).

Results shown in **Figure 5.10** suggest that greater superoxide scavenging activity is seen with animals injected with HoSOD in all three heart sections. While this is promising, the fact that unmodified SOD also elevated superoxide scavenging activity in the tissue suggests that fifteen minutes may not be sufficient time to wash away non-specifically bound protein. This was surprising given that each mouse was perfused immediately following sacrifice in order to remove any HoSOD or SOD that remained in the blood. Moreover, no strong LV versus RV localization suggests a DNA-independent binding mechanism. The amount SOD activity in the left ventricle maximally amounted to 10% of the initial injected dose and did not appear to be specific to the areas where necrosis was expected; SOD activity was elevated in all sections of the heart compared to non-injected control animals that received IR-surgery.

The experiment was repeated with twice the dose (400 U) and longer time between injection and sacrifice (one hour). In this case, there were no differences between the treatment groups in all heart sections (**Figure 5.11**). This suggests that most of the injected protein was cleared from the tissue within the hour following injection. It is possible that the DNA is concurrently cleared from the necrotic tissue by DNases, reducing the amount of extracellular DNA available for targeting.

The studies involving therapeutic proteins had several limitations stemming from the surgical conditions used in the animal models. Previous studies examining the time course of necrosis post-MI typically utilized permanent exclusion models of MI. Ischemia-reperfusion surgeries do not achieve the same levels of anoxia and may not produce similar levels of tissue necrosis. However, IR-surgeries were used in these studies since they are more clinically relevant models of MI. In addition, there was some concern that permanent occlusion models may not provide enough access to the necrotic core for Hoechst compounds; permanent occlusion models would rely on diffusion from collateral circulation or transmural diffusion. It is possible that a thirty minute of ischemia was not ideal for creating a significant region of necrosis; work by DeBoer, et al. using a canine model of MI suggest 120 minutes of total occlusion are required to obtain greater that 95% necrosis in the infarct [152].

Another key factor that needs to be explored is the issue of timing after MI. Given the differences in techniques used to monitor necrosis post-MI, there was no significant body of literature describing extracellular DNA in the heart after injury. It is possible that both the timing of the injections and animal sacrifice post injection may not have been ideal. The studies using therapeutic Hoechst-conjugates were designed based on the results from the Hoechst-IR786 study, which suggested that extracellular DNA was present at two hours but diminished at 24 hours. A more intermediate time, such as six hours, would be an interesting time point to study as previously cited work by other groups indicate maturation of the necrotic lesion at this time point. The amount of time between injection and animal sacrifice also plays a significant role in detecting infarct-specific targeting. Acute (fifteen minutes) time points were used in this work in order to minimize the amount of protein lost to natural clearance mechanisms. As demonstrated by the SOD data, waiting an hour after injection returned SOD activity levels to basal levels. This suggests that SOD may have been degraded or inactivated by other pathways in the heart. Significant work by others has examined strategies such as PEGylation in order to improve circulation half life of proteins, which may play a role in designing targeted protein therapeutics.

These data demonstrate that Hoechst-conjugates with a variety of functionality can be synthesized. By tailoring the PEG-linker length, Hoechst-conjugates can be rendered impermeable to cell membranes. This factor is critical in avoiding potential side effects, such as Hoechst inhibiting DNA helicase in healthy cells. Near infrared imaging showed that Hoechst-based imaging probes show some promise for labeling extracellular DNA in necrotic tissue. Other imaging modalities may benefit from Hoechst probes. The data using therapeutic proteins were disappointing, but raised several considerations for Hoechst-therapeutics. Delivering proteins with high affinity interactions with other targets *in vivo* may pose some issues due to off target binding. Given that VEGF-VEGFR2 binding affinity is in the nanomolar range [153], HoVEGF likely bound to VEGF receptors in the circulation rather than enriching in the infarct. Furthermore, small molecules may enrich in the infarct to a higher degree due to increased diffusivity. Future work may focus on developing therapeutic small molecule conjugates and will be discussed further the subsequent chapter.

CHAPTER 6

SUMMARY AND FUTURE DIRECTIONS

The work included in this dissertation demonstrates three different drug delivery strategies that are uniquely tailored to overcome the obstacles of cardiac drug delivery.

6.1 Polyketal Microsphere Formulations

Chapter 3 describes how changing polymer chemistry of microparticle drug delivery formulations can lead to a positive outcome in a permanent occlusion model of MI in rats. In this aim, the p38 MAPK was inhibited using a small molecule drug for at least a week *in vivo* through a single intramyocardial injection of a sustained release microparticle formulation. Other studies conducted with similar inhibitors required multiple daily doses to achieve comparable effects [112-114]. This approach can potentially be dangerous due to off-target side effects or lack of patient compliance, and more costly in terms of the amount of drug delivered. The PCADK microparticle formulation was able to successfully improve cardiac function with a single injection whereas the current state of the art, PLGA microparticles, did not have a positive effect. The study demonstrated that PCADK microspheres showed decreased collagen deposition three weeks post-infarction. The inhibition of fibrosis translated to an improvement in cardiac function between days seven and 21.

Several factors may have played a role in this finding. Release kinetics *in vivo* may have played a role as endogenous esterases may accelerate PLGA release profiles. Degradation products also likely played a role; PCADK degrades into acetone and 1,4-cyclohexane dimethanol. Both products are non-toxic and lack acid moieties that could lower the pH and inflame the local microenvironment. This is a significant advantage that is unique to polyketals amongst other degradable polymer systems. Since the publication of the p38 MAPK inhibitor study in *Nature Materials* in 2008 [135], the Davis and Murthy groups and others have shown similar results with various therapeutics and disease models.

Seshadri, et al. delivered the antioxidant protein superoxide dismutase (SOD) to an ischemia-reperfusion model of MI using PCADK microspheres [141]. Delivering SOD to the myocardium using PCADK microparticles had the advantage of sustained release as well as the ability to scavenge both intra- and extra-cellular superoxide. Parenteral delivery of SOD does not cross the cell membrane and is limited to scavenging extracellular superoxide. Microparticle formulations were internalized by inflammatory cells, the key generator of radical oxidants, and scavenge superoxide before it is released into the tissue. This contributed to a four-fold reduction in cardiac myocyte apoptosis compared to IR-surgeries alone, which was comparable to sham levels of apoptosis. As a result, at three days post-infarction, animals treated with SOD-loaded polyketal microparticles (PK-SOD) had significantly better fractional shortening values compared to untreated animals. However, at 21-days post-infarction, this initial improvement in cardiac function was lost and there was no statistical significance between IR-surgery alone and PK-SOD groups despite a 30% difference in the change in fractional shortening from baseline. However, using a second therapy to target chronic inflammation (PK-p38$_i$ microparticles) had some additive effects as animals that were treated with both PK-SOD and PK-p38$_i$ did achieve statistically significant improved cardiac function compared to untreated animals, suggesting that SOD therapy is not a "magic bullet" and that multiple therapies delivered in concert are needed to prevent cardiac dysfunction.

Polyketals have been used to treat animal models of liver and lung inflammations. In both example a faster hydrolyzing copolymer of 1,4-cyclohexane dimethanol and 1,5-pentanediol (PK3) were used in microparticle formulations. Yang, et al. delivered the anti-inflammatory drug imatinib (Gleevec, Novartis) encapsulated in PK3 microspheres in an acute liver failure model [136]. The PK3 microsphere formulation with the drug to significantly reduce serum levels of alanine aminotransaminase, a clinical marker of liver failure, through intravenous injection of PK3 microparticles. Lee, et al. also demonstrated improved liver function in a mouse model of liver inflammation by delivering anti-TNF-α siRNA encapsulated in polyketal microparticles *in vivo* [140]. Finally, Fiore, et al. showed that PK3 microparticles were biocompatible for pulmonary drug delivery and that formulations could deliver SOD to prevent lung fibrosis in response to bleomycin challenge [154].

Numerous projects could be initiated using polyketals microparticles for various inflammatory diseases with different drugs, as is highlighted above. In the cardiovascular space, ongoing work in the Davis laboratory is investigating using polyketal microparticles to deliver other therapeutics to the heart. In one project, siRNA is being encapsulated using an ion-pairing method to reduce levels of enzymatic proteins that produce ROS. This work will hopefully show beneficial effects of blunting the levels of ROS in the heart for the first time using siRNA-polymer therapy for cardiac dysfunction. There is also continuing work with SB239063 microparticles to better understand the pharmacokinetics and mechanism of action *in vivo*. Collaborations are ongoing with other laboratories to investigate the potential for using polyketal microparticles to reprogram adult somatic cells into induced pluripotent stem cells by delivering transcription factors via polyketal nanoparticles.

While different permutations of treating inflammatory diseases with different therapeutics can be generated, polyketal technology would greatly be advanced by a systematic study investigating the effects of reaction conditions on polymer molecular weight. One of the key issues with polyketal technology today is low molecular weight. Increased molecular weight can improve encapsulation efficiencies, particularly for proteins, and produce structures with improved mechanical properties, such as macroscale implants. Current polymerization protocols can routinely yield polymers on the order of 5 kDa. The addition of reprecipitation steps reduces the yield but can increase molecular weight up to 10-12 kDa, but these molecular weights are still not comparable to degradable polyesters, which can be produced in commercial scale with molecular weights exceeding 100 kDa. By increasing the molecular weight would allow for the use of polyketals as structural elements. A potential project could consist of characterizing mechanical properties of polyketals and engineering different molecular architecture, such as branching, in order to improve molecular weight. One important aspect of this project will be focusing on polymer solubility. As polyketals increase in molecular weight, they may tend to become insoluble in common organic solvents. One collaborative project that was attempted, but ultimately did not progress focused on electrospinning polyketals into nanoscale fibers that could be used for tissue engineering applications. Electrospinning requires highly viscous and entangled solutions of polymers, which generally requires high molecular weight. Even attempting to use an emulsion to electrospin, which has be previously shown to improve the electrospinning of low molecular weight polymers [155], did not yield fibrous structures. Increased molecular weight polyketals or branched polyketals could be used to fabricate scaffolds to deliver cells and other bioactive factors to the heart as has been reported by other groups in the electrospinning literature [156].

6.2 Metal-Affinity Drug Delivery Systems

Chapter 4 describes a simple, yet effective, technique that can be used to functionalize the surface of polymer microparticles with NTA-Ni. This functionality allows for the non-covalent tethering of any His-tag bearing protein, which can serve as a therapeutic payload or targeting ligand. The primary benefit conferred by this technique is that proteins can be loaded without exposure to organic solvent, a potential denaturation risk, and without any complicated chemical modifications, both of which could reduce protein bioactivity. An added benefit is that any protein not tethered to the particle can be recovered by centrifuging the microparticles and collecting the supernatant. This is particularly useful when working with expensive or difficult to express proteins. Once tethered to the particle, bioactive protein can release from the particle and the non-covalent linkage is strong enough to achieve modest targeting to cell surface proteins *in vitro*.

While the paper published in *Biomaterials* [157] showed proof of principle for the concept, the NTA-Ni drug delivery system has yet to be applied to a MI model. Given the rapid release kinetics seen *in vitro*, this system is suited for delivering a “one-two-punch” consisting of a fast acting protein drug followed by sustained delivery of a longer acting small molecule. To that end, mechanisms that mitigate the inflammatory response are being investigated. One project involves modulating macrophage response by co-delivering interleukin-4 (IL-4) and a small molecule anti-inflammatory (such as SB239063) in order to drive macrophages towards a less inflammatory M2 phenotype. The initial milieu of cytokines in a tissue can drive macrophages towards resolving or increasing inflammation in tissue [158]. Exogenous IL-4 has been shown to reduce the inflammatory response in myocarditis and improve cardiac function [159], and may have beneficial effects for treating cardiac dysfunction following MI.

One of the hurdles that this project may face is the lack of control of the release kinetics His-tagged protein. The release half life of His-tagged GFP *in vitro* was 12 hours, which may be too short for some therapeutic proteins. The foundation for another project could lie in modulating the kinetics of protein release from NTA-Ni systems. As mentioned in Chapter 2, the NTA-Ni/Histidine interaction can be modulated using a variety of factors. One of the common ways to do this in the chromatography field is by changing the divalent metal ion; cobalt is routinely substituted for nickel and has higher affinity. While this is feasible, cobalt is more toxic and could lead to additional problems. A more likely solution would be to synthesize a multivalent NTA moiety [160]. While the metal-histidine interaction strength would be the same, the apparently affinity would be stronger due to increased avidity. Over the course of the project, two potential avenues for achieving this were identified. The first involved synthesizing a trivalent NTA-lipid molecule, similar to the DOGS-NTA lipid described in Chapter 4. The second involved direct modification of poly(vinyl alcohol) (PVA). PVA is routinely used as a surfactant to stabilize emulsions used to form microparticles. Previous studies have shown that up to five weight percent of PVA is retained in the dry microparticle [161]. The PVA is arranged in a tennis-ball-fuzz-like morphology, with parts of a PVA chain embedding into the polymer core and other parts of the chain interacting with the water interface. These pendant hydroxyl groups could be modified to contain NTA-Ni. In both cases, a His-tagged protein would have the same off rate from the NTA-Ni, but it would hop between metal complexes, increasing its residence time on the microparticle. An additional level of control could also be achieved by modulating the number of Histidine residues on the recombinant protein [58].

While the data show that nickel loaded microparticles did not have any adverse effects on neonatal cardiac myocytes or RAW 264.7 macrophages, the general concern for nickel hypersensitivity, which has been hypothesized to underlie some adverse reactions to metal implants, may ultimately preclude NTA-Ni systems from being used in humans. However, there is growing data in the chromatography literature examining binding affinities of less toxic ions, such as Zn(II) [162, 163], that may be better suited for drug delivery applications.

6.3 Hoechst-Based Targeting of Extracellular DNA

Chapter 5 demonstrates that a variety of Hoechst-inspired compounds could be synthesized for the purpose of targeting extracellular DNA in necrotic tissue. These conjugates showed differential cell permeability in order to prevent binding to DNA in cell nuclei as well as different functionality for conjugation to other molecules. Proof of principle for targeting necrotic extracellular DNA in the heart was demonstrated using a near infrared-Hoechst conjugate. This compound was able to highlight the infarcted region of the heart from the surrounding tissue. However, subsequent studies using Hoechst-conjugated VEGF did not show any enrichment in the left ventricle free wall as measured by ELISA. Hoechst-conjugated SOD also failed to show enrichment in the infarcted area following intravenous injections, even at high doses, as measured through highly sensitive SOD activity assays. While these attempts were unsuccessful, Hoechst-conjugated molecules may still play a role in the cardiac field as a probe for necrosis in imaging as well as a targeting ligand for other disease models.

We are currently investigating the possibility of using Hoechst-diethylene triamine pentaacetic acid (Ho-DTPA) as a contrast agent for positron emission tomography (PET) or MRI. Ho-DTPA can chelate metals such as gadolinium or copper-64, which are commonly used in MRI and PET, respectively. Late contrast gadolinium imaging is currently used today to determine the extent of necrosis following MI. While this has been shown to be effective, the necrotic signal is highly dependent factors such as time after gadolinium administration and extent of occlusion in experimental models [164]. Development of necrosis-specific probes that are not dependent on hemodynamic properties of necrotic tissue may be more suitable for these purposes and for imaging silent infarctions or non-ST elevated MI.

Before these contrast agents can be used for these purposes, the kinetics of extracellular DNA in the heart must first be determined. Previous studies relied on protein-based measures of necrosis; Kajstura, et al. and others have previously used a circulating antibody for myosin as a surrogate marker for necrosis [144, 148]. However, different components generated by necrotic cell death are likely cleared at different rates;

DNA clearance is expected to be much faster than protein components and thus would have a shorter window of opportunity to target extracellular DNA. Commercially available DNA assays are not appropriate for measuring extracellular DNA as most of these dyes are cell permeable. Radiolabeled Hoechst compounds could provide us with the kinetic data for DNA clearance and was proposed. However, proper clearance to synthesize and use radioactive compounds was not obtained over the course of this project. A more thorough understanding of how fast DNA is cleared from the infarct would allow for better assessment of the feasibility of using Hoechst-targeted therapeutics or contrast agents. Ultimately, the future directions discussed hinge on a suitable window of opportunity for targeting the extracellular DNA.

One of the obvious applications for Hoechst-conjugates is in treating tumors. Tumor masses contain a necrotic core which persists due to insufficient vascularization. The Murthy laboratory has applied Hoechst technology to the chemotherapeutic gemcitabine. This strategy has an advantage in that it is autocatalytic; small amounts of the Hoechst-gemcitabine localizing in the tumor will actually generate more extracellular DNA. Subsequent doses of the chemotherapeutic then have a larger platform to target, which in turn kills additional cells. Early results for this therapy are promising and manuscripts have been submitted for review.

However, in the cardiovascular arena, the greatest chance for success with Hoechst-targeted therapeutics likely lies in small molecule conjugates. Given that diffusivity is proportional to the mass of a given species, small molecule conjugates have a greater chance of escaping the capillary beds and diffusing deep into to the necrotic tissue were it can bind to extracellular DNA. This effect would be significantly more pronounced in large animal models of MI compared to rodents. Potential projects could focus on the synthesis and testing of Hoechst-TEMPOL or Hoechst-ebselen, commonly used small molecule mimetics of SOD and catalase, respectively. Alternatively, cleavable linkers could be used to deliver small molecule inhibitors.

Another strategy that may prove successful for Hoechst-based targeting is to decorate the surface of a delivery vehicle with the ligand. This would have the beneficial effect of increasing the avidity and improve binding properties. This strategy has been frequently used with liposomal formulations and antibody targeting ligands. However, the size of the delivery vehicle will likely play a large role, as a balance must be found between the binding force between Hoechst and DNA and the convective drag force between the delivery vehicle and blood/lymphatic flow.

6.4 Perspective

Materials development is still in the process of catching up to the biological demands of *in vivo* applications. Most of the materials used in medicine today were selected on the basis of availability and mechanical suitability based on what clinicians had on hand. A famous example highlights the fact that researchers at the NIH were inspired by the elasticity and durability of a woman's girdle, which eventually led to the use of the same material, poly(ether urethane), in the first artificial heart [165]. While these approaches have produced large advancements in the field of medicine, the need for specifically designed chemistries for biological applications is becoming increasingly evident. However, this type of research requires a multidisciplinary approach that requires teams to start with rational design of molecules, progress to synthesis, and eventually test these compounds *in vivo*. This dissertation was an attempt to achieve this goal of interdisciplinary biomaterials and drug delivery development.

APPENDIX A

EXPERIMENTAL METHODS

A.1 Polyketal synthesis

Poly(cyclohexane-1,4-diyl acetone dimethylene ketal) (PCADK) was synthesized as described in Lee, et al (2007) [125]. Briefly, 1,4-cyclohexanedimethanol was reacted with 2,2-dimethoxypropane in an acetal exchange reaction. First, 1,4-cyclohexane dimethanol was dissolved in benzene and brought to 100°C with constant stirring. A solution of p-toluenesulfonic acid in ethyl acetate was added to the reaction flask in order to catalyze the reaction. The ethyl acetate was allowed to boil off, and distilled 2,2-dimethoxypropane was added to the benzene solution in an equimolar ratio to 1,4-cyclohexanedimethanol, initiating the polymerization reaction. Additional doses of 2,2-dimethoxypropane and benzene were subsequently added to the reaction dropwise to the reaction flask via a metering funnel to compensate for the 2,2-dimethoxypropane and benzene that had been distilled off. After 8 hours, the reaction was stopped by addition of 500 μL of triethylamine. The polymer was isolated by precipitation in cold hexane (stored at -20°C) followed by vacuum filtration. The molecular weight of the resulting polymer was approximately 6 kDa with a mean polydispersity of 1.923. All reagents were purchased from Sigma-Aldrich. 2,2-dimethoxypropane and benzene were distilled prior to use. p-Toluenesulfonic acid was recrystallized prior to use. All other reagents were used as received.

A.2 Microparticle formulation

SB239063-loaded microparticles

Polyketal particles loaded with SB239063 (Axxora) (PK-p38i) were generated using an emulsion-solvent evaporation technique. Five-hundred micrograms of inhibitor and 50 mg of PCADK were dissolved in 500 µl of dichloromethane. The polymer solution was then added to 5 mL of 4% poly(vinyl alcohol) (PVA) and homogenized at a low speed for 60s. The resulting emulsion was transferred to 30 mL of 1% PVA and stirred at approximately 100 rpm for 4h to allow for evaporation of dichloromethane and solidification of microparticles. The particles were then centrifuged and washed in deionized water three times to remove residual PVA. The suspension was then frozen in liquid nitrogen and lyophilized to produce a free flowing powder.

PLGA (Resomer RG 503 H, 48:52 lactide:glycolide, 0.32-0.44 i.v., Boehringer Ingelheim) was used as received. Microparticles containing SB239063 were made with the same protocol for PCADK particles.

NTA modified PCADK microparticles

PCADK was synthesized as described above. NTA-bearing microparticles were made in 100 mg batches via a single emulsion procedure. 1,2-dioleoyl-sn-glycero-3-[(N-(5-amino-1-carboxypentyl)iminodiacetic acid)succinyl] (DOGS-NTA, Avanti Polar Lipids) was dissolved in dichloromethane at 10 mg/ml. The following procedure was used to produce 10 wt% NTA microparticles; other concentrations were obtained by varying the amount of DOGS-NTA stock solution and neat dichloromethane. Ninety milligrams of PCADK was added to 1 ml of DOGS-NTA stock solution and gently heated to dissolve the polymer. Five milliliters of 4% PVA in water was added to the polymer solution and the mixture was homogenized using a Powergen 500 (ThermoFisher) homogenizer for 60 seconds. The resulting emulsion was transferred to

30 ml of 1% PVA and stirred for 4-6 h to evaporate the dichloromethane. Particles were then centrifuged and washed with deionized water before being frozen in liquid nitrogen and lyophilized to produce a free flowing powder. Microparticles were subsequently loaded with Ni^{+2} by incubating overnight in a 0.05 M $NiCl_2$ solution at a concentration of 1 mg particles/ml.

A.3 Synthesis of Hoechst compounds

Hoechst-amine and Ho-IR786 synthesis

Hoechst amine was synthesized according to the schemes in **Figures A.1-A.3**. Detailed experimental procedures and characterization of Hoechst-amine and Hoechst-IR786 were described by Dasari, et al [145].

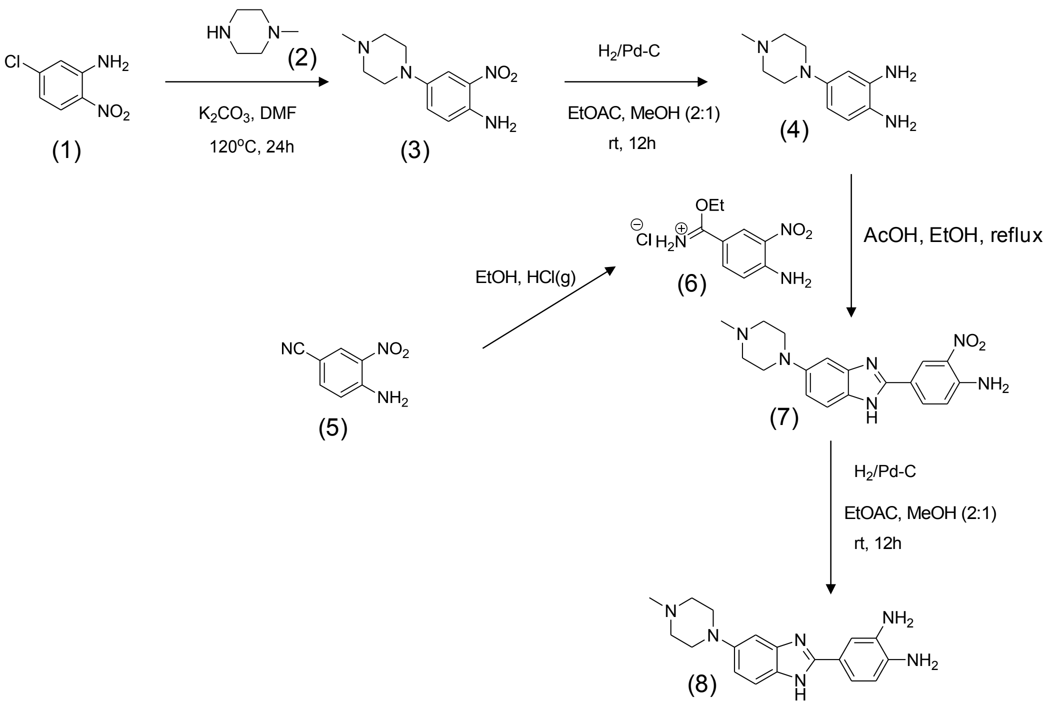

Figure A.1. Synthetic scheme for 4-(5-(4-methylpiperazin-1-yl)-1H-benzo[d]imidazol-2-yl)benzene-1,2-diamine (8).

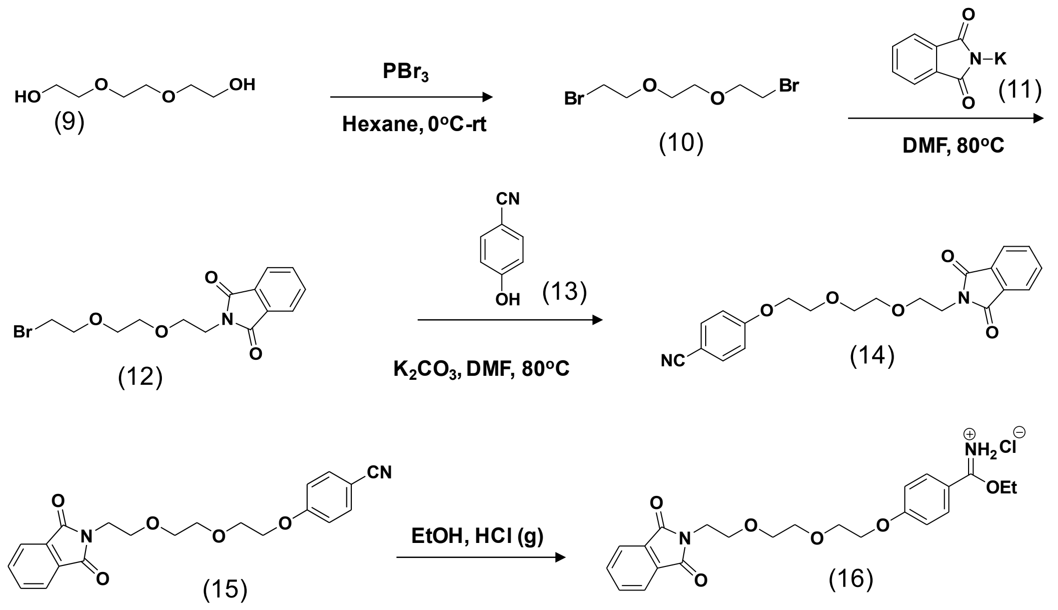

Figure A.2. Synthetic scheme for ethyl 4-(2-(2-(2-(1,3-dioxoisoindolin-2-yl)ethoxy)ethoxy)ethoxy) benziminium salt (16).

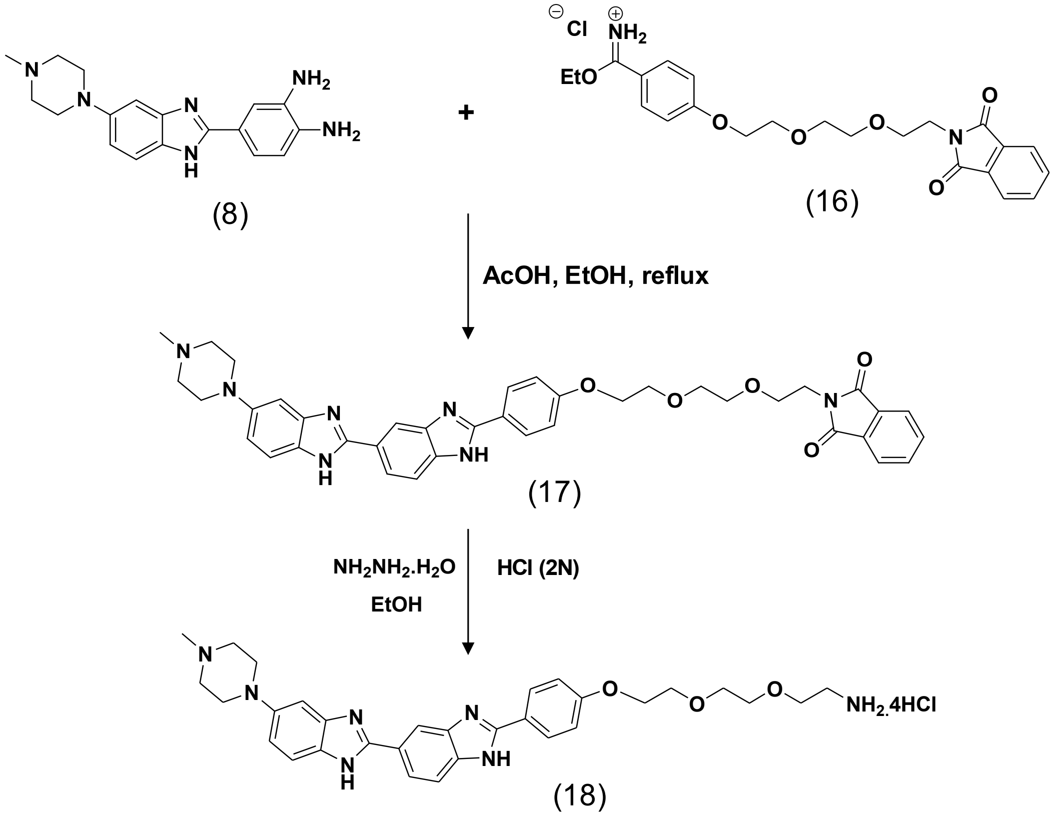

Figure A.3. Synthesis scheme for Hoechst-pthalimide coupling and Hoechst-amine deprotection.

Hoechst-biotin& Hoechst-maleimide

Hoechst-biotin and Hoechst-maleimide were synthesized from Hoechst-amine using NHS-coupling chemistry. EZ-link NHS-PEG12-Biotin and NHS-PEG4-Maleimide were purchased form Thermo/Pierce. Twenty-five milligrams of Hoechst-amine was dissolved in 5 ml of anhydrous dimethy formamide (DMF) with 20 equivalents of triethyl amine under nitrogen). One equivalent of NHS-PEG compound was added to the reaction mixture and stirred overnight. Progress was monitored using TLC (MeOH:DCM). Upon completion of the reaction, DMF was removed under reduced pressure and the reaction mixture dissolved in 20% MeOH in DCM with 0.5% triethylamine. This mixture was streaked on preparative TLC plates and developed using 10% MeOH in DCM with 0.5% triethylamine. The product band was scraped off and MeOH:DCM used to extract the product.

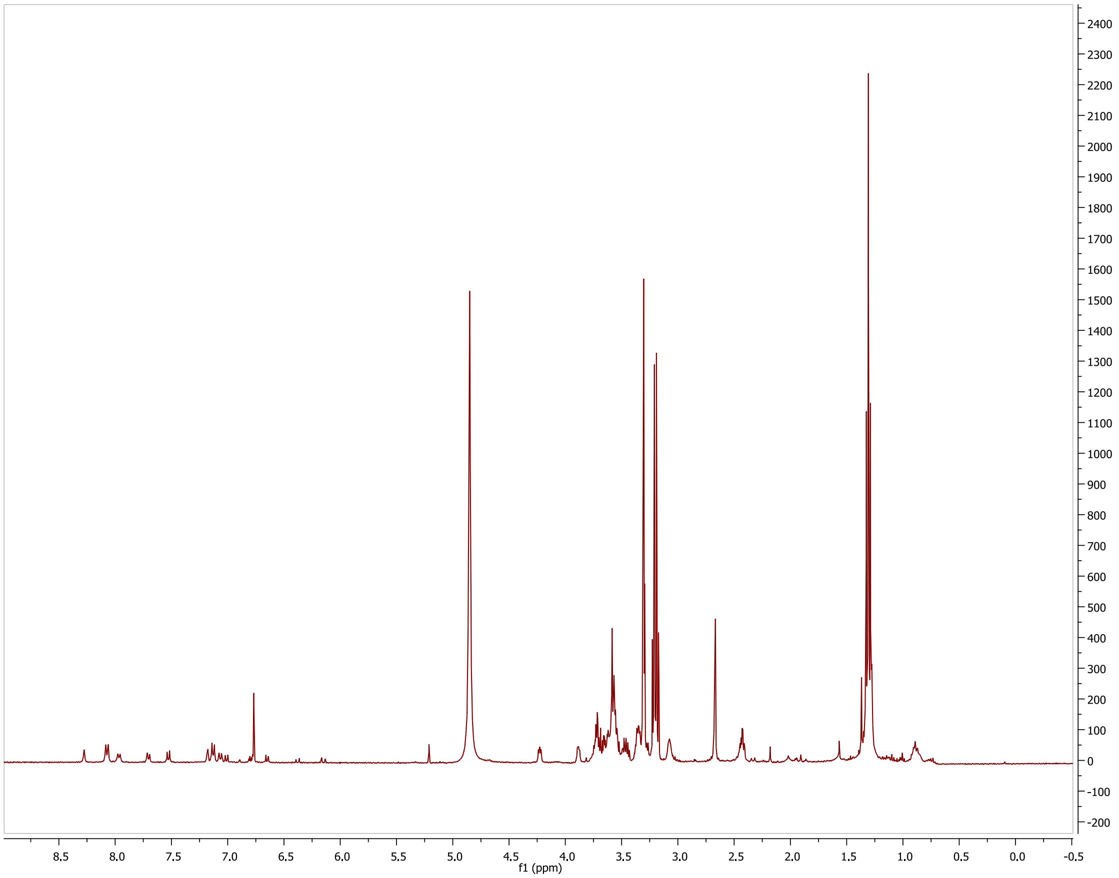

Figure A.4. Hoechst-maleimide ^{1}H-NMR spectrum.

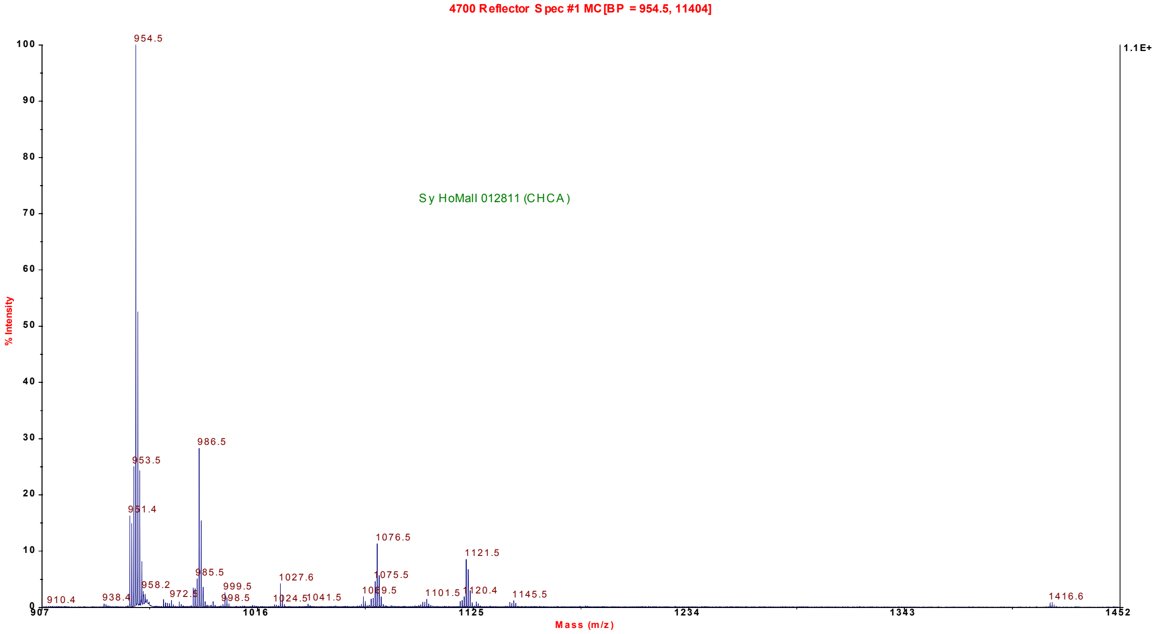

Figure A.5. Hoechst-maleimide mass spectrum.

Protein Conjugation

VEGF was expressed with unpaired cysteine residues as described by Phelps, et al [146]. Protein was provided at 140-280 µg/ml and were dialyzed against PBS (adjusted to pH 8 with 2 mM EDTA) for 24 hours at 4°C. Ten equivalents of Hoechst-maleimide were added to the VEGF and reacted overnight at 4°C. The reaction mixture was then dialyzed (MWCO 3500 Da) against PBS overnight at 4°C to remove any unreacted Hoechst-maleimide. Aliquots of the protein were made and stored at -20°C.

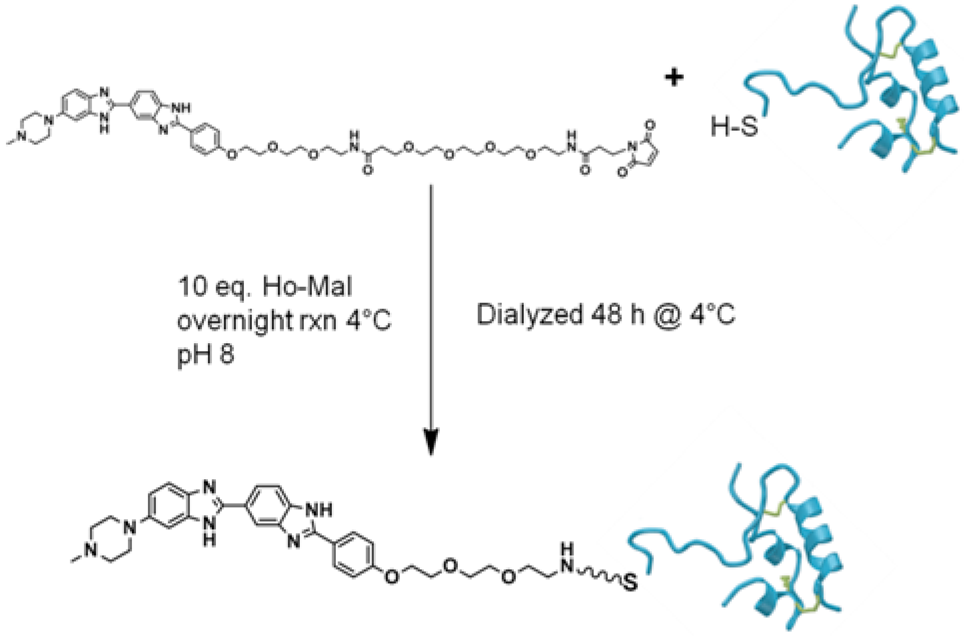

Figure A.6. Synthesis scheme for HoVEGF.

Superoxide dismutase (from Bovine erythrocytes, ≥3000 U/mg, Sigma-Aldrich) was dissolved at 10 mg/ml in PBS adjusted to pH 8 with 2 mM EDTA. SOD was assumed to have 20 primary amines, subsequent equivalents were calculated based on this assumption. Traut's reagent (Sigma-Aldrich) was added in a 20 equivalent excess and allowed to react for one hour at room temperature. Unreacted Traut's reagent was separated from thiolated-SOD (SOD-SH) using a polyacrylamide desalting column (MWCO 6000 Da, Thermo/Pierce) run with PBS adjusted to pH 8 with 2 mM EDTA. Two-hundred microliter fractions were collected in a UV 96-well plate and UV spectra taken for each well to determine fractions that contained SOD. Protein concentration (μBCA assay, Thermo/Pierce), SOD activity (SOD Activity Kit – WST, Dojindo Molecular Technologies), and sulfhydryl content (Ellman's Assay, Thermo/Pierce) of the pooled SOD-SH fractions were assessed according to manufacturers' protocols. SOD-SH was then reacted with Hoechst-Maleimide (2 equivalents with respect to –SH). The reaction mixture was again purified using a polyacrylamide size exclusion column as described above. Modified protein was validated using MALDI-TOF as described previously. Protein concentration was increased using centrifuge-based Pierce Protein Concentrators (9MWCO 9000 Da, Thermo/Pierce) as needed.

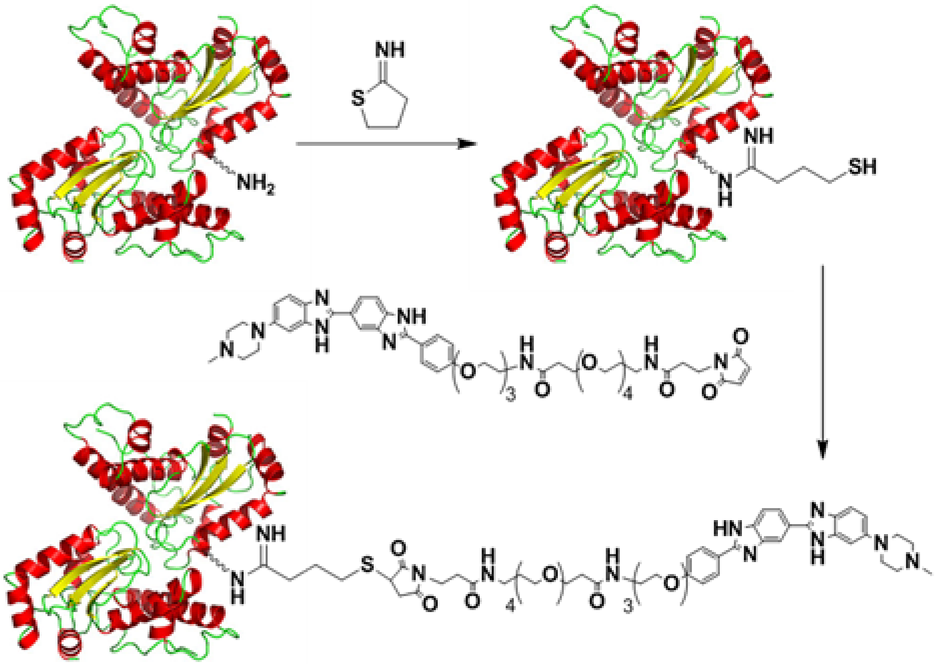

Figure A.7. Synthetic scheme for HoSOD.

A.4 Cell culture

RAW264.7 macrophages were maintained in DMEM (Fisher) supplemented with 10% fetal bovine serum (Hyclone), l-glutamine, and penicillin/streptomycin (Invitrogen). For experiments involving TNF-α stimulation, cells were plated at confluence 18 hours prior to experiments in serum free media (SFM, DMEM supplemented with l-glutamine and penicillin/streptomycin). Media was then aspirated and replaced with treatment media containing either SB239063 dissolved in DMSO, neat DMSO as a control, or polyketal microparticles. Cells were preincubated with the treatment for the indicated time and washed with fresh SFM media before being exposed to 10 ng/mL TNF-α (Sigma).

Human umbilical vein endothelial cells (HUVEC) were maintained in M199 media (Hyclone) supplemented with 20% fetal bovine serum (FBS, Hyclone), penicillin/streptomycin/l-glutamine (Gibco), heparin (20 U/ml, BD biosciences), and endothelial cell growth supplement (BD Biosciences). Cells were passaged with trypsin/EDTA at 80-90% confluence. Tissue culture flasks were coated with a 1 mg/ml solution of gelatin for 20 min at room temperature before plating cells.

Rat neonatal cardiac myocytes were obtained from 1-2 day old Sprague-Dawley pups (Charles River Labs). Pups were sacrificed and ventricles isolated and minced. The tissue was minced and suspended in a 1 mg/ml solution of collagenase (Worthington) in Hank's buffered saline solution (HBSS) for 4-6 h at 4°C. The suspension was filtered through a 70 μm screen and centrifuged 10 min at 500g. The supernatant was discarded and pellet resuspended and washed in Hanks' buffered saline solution (HBSS) three times before being plated in DMEM supplemented with 10% FBS. Tissue culture flasks were treated with a 1 μg/ml solution of fibronectin before cells were plated.

Prior to all experiments, cells were quiesced overnight in serum-free media. All cells were incubated at 37°C with 5% CO2 and 100% humidity.

A.5 Bioplex cytokine analysis and inflammation studies

C57BL6 adult mice (Charles River) were anesthetized under isofluorane (1-3%, Charles River). Thighs were shaved and skin was incised to expose the muscle. For cytokine measurements, muscle was injected with 1 mg of polymer (100 µl of 10 mg/mL solution in sterile saline). The contralateral leg was injected with saline as a control. For immunohistochemical analysis 5 mg (100 µl of 10 mg/mL solution in sterile saline) was injected into the muscle. At the designated intervals, mice were sacrificed by CO2 and the leg muscles exposed. Approximately 50 mg of muscle was removed at the injection site and processed.

For cytokine analysis, tissue was frozen in liquid nitrogen and homogenized in Cell Lysis Buffer (Bio-Rad) according to manufacturer's instructions. Briefly, tissue was homogenized in 0.5 mL of lysis buffer and sonicated to ensure full disruption of tissue. The homogenate was centrifuged and supernatant incubated with X-Plex multiplex beads (Bio-Rad) according to manufacturer's instructions and analyzed on a Bio-Rad Bioplex system.

A.5 Histological analysis

For immunohistochemical analysis, tissue was fixed in 4% paraformaldehyde (Sigma) and embedded in paraffin. Histological sections were made and stained with anti-CD-45 antibody using standard immunohistochemical techniques. DAPI was used to visualize nuclei in the sections. Slides were imaged under fluorescence microscopy and digital images of the sections saved.

Collagen deposition was determined by Picrosirius Red (Sigma) staining as previously described [166].

A.6 Western blot analysis

p38 MAPK Western Blots

Cell (250 μg) or tissue (500 μg) protein homogenates were incubated with an antibody against total p38 (Cell Signaling) overnight at 4°C, prior to 2 hour incubation with Protein-A agarose beads (Sigma). Beads were washed and boiled in sample buffer prior to loading on a 12% polyacrylamide-SDS gel. Proteins were transferred to a PVDF membrane (Bio-Rad) and blots probed with an antibody for phospho-specific p38 (Cell Signaling). Films were scanned and quantified using Image J software.

A.7 Quantification of superoxide via DHE-HPLC

To determine levels of superoxide in cells and tissues, a novel method described recently was used. Dihydroethidium (DHE) is a commonly used immunohistochemical marker to measure superoxide in tissues. However, when DHE is oxidized by superoxide, it becomes impermeable to cells. Therefore, any DHE oxidized in the extracellular space will remain in the incubation medium. This oxidation product, 2-hydroxyethidium, has a different retention that ethidium and can be quantified by high performance liquid chromatography (HPLC) with fluorescence detection [167].

To detect tissue superoxide following myocardial infarction in rats, the left ventricular free wall was harvested at the indicated time point and equal sized pieces were incubated at 37°C in 1 mL of Krebs/Hepes buffer (KHB; pH= 7.35) containing 50 μM dihydroethidium (Invitrogen) for 30 minutes. Following incubation, buffer was syringe filtered and 100 μL placed in a tube containing 300 μL methanol. The sample was loaded on a C18 column for reverse-phase HPLC anaylsis using an acetonitrile gradient and data were normalized to wet tissue weight.

For cell culture experiments, macrophages were incubated with polyketals for the indicated time period. Following polyketal pre-treatment, cells were incubated with 10 ng/mL TNF-α for 5 minutes in KHB at 37°C, prior to addition of 25 µM dihydroethidium for 20 minutes. Buffer was collected and analyzed in a manner similar to tissue studies. TNF-α measurement. Protein homogenates were evaluated for TNF-α levels by ELISA (eBiosciences) according to manufacturer's protocol and normalized to protein levels determined by Bradford assay.

A.8 NTA-Ni microparticle characterization

GFP quantification

Green fluorescent protein (GFP) bearing a His-tag was obtained from Millipore. Microparticles were loaded with GFP by incubating them in GFP solutions made with phosphate buffered saline (PBS) at a concentration of 1 mg particles/ml overnight at 4°C. Particles were centrifuged and washed three times with PBS. Following washing, microparticles were incubated with a horseradish peroxidase-conjugated antibody against GFP (1:5000 dilution in PBS-T with 1% goat serum, Rockland) for 2 h at 4°C. Particles were again washed with PBS three times and resuspended in PBS at a concentration of 1 mg particles/ml. Five microliters of the particle suspension were aliquotted into wells of a 96-well plate and amounts of GFP quantified colorimetrically via tetramentylbenzidine (1-Step Slow TMB, Pierce) conversion in a plate reader (Biotek Synergy 2). Kinetic reads were compared to standard curves and supernatants that have been immobilized on HisGrab 96-well plates (Pierce).

Release studies

Microparticles containing 2 wt% rhodamine-B (TCI Chemicals) and 10 wt% NTA were made using a modification to the above procedure. Microparticles were loaded in a

1 μg/ml solution of GFP overnight at 4°C. After washing, microparticles were suspended at 1 mg/ml in PBS and aliquotted into separate samples. The release study was conducted at 37°C. At specified time points, particles were centrifuged, supernatant collected for analysis, and fresh buffer used to resuspend the particles. GFP was quantified via ELISA and rhodamine-B via fluorescence measurements. Total rhodamine-B was measured by hydrolyzing the particles in 1 N HCl and measuring fluorescence. SB239063 release data was obtained from Sy et al. (35)

MTT assay

Cells were plated at confluence in 6 well plates and quiesced with serum-free media overnight. Cells were then washed with PBS and treated with microparticles suspended in serum free media (1 ml per well) for 6 h. 3-[4,5-dimethylthiazol-2-yl]-2,5-diphenyl tetrazolium bromide (MTT) was dissolved in phenol red-free DMEM at a concentration of 0.5 mg/ml. Following microparticle treatment, cells were washed three times with PBS to remove microparticles and incubated with MTT media for 2h. Cells were then washed three times with PBS and 0.5 ml of MTT solvent (0.1 N HCl in isopropanol) was added to each well to dissolve formazan crystals. This solution was centrifuged to pellet cell debris and measured spectrophotometrically at 570 nm.

VEGF studies and Western Blotting

His-tagged VEGF (His-VEGF) was expressed as described in (36). HUVECs were plated on gelatin coated 6 well plates at confluence and quiesced overnight in serum-free media. Ten percent NTA microparticles were loaded with nickel as described above, washed, and incubated with a solution of 1 μg His-VEGF/ml in PBS overnight at 4°C. The microparticles were then washed three times with PBS and resuspended in a serum-free media at various concentrations. One milliliter of media with microparticles was added to each well and incubated at 37°C for 20 minutes. Controls of NTA-Ni microparticles (no His-VEGF) and free VEGF (0-100 ng/ml) were also tested. Following incubation, cells were washed three times with ice cold PBS with phosphatase inhibitors (Sigma). Protein was harvested in 75 μl of ice cold RIPA buffer with protease and phosphatase inhibitors (Sigma). Lysates were centrifuged to pellet cell debris and microBCA assays (Pierce) were used to determine protein concentrations for each sample. Protein lysates were run under denaturing conditions (Laemmli Buffer system) on 7% polyacrylamide gels and transferred to PVDF membranes. Membranes were blocked and probed for phospho- and total- VEGFR2 antibodies (Cell Signaling) using manufacturer protocols. Band intensities were determined by exposing films using a HRP-ECL (Amersham) system.

Cell targeting studies

HUVECs were plated on gelatin-coated coverslips at 30% confluence and quiesced overnight in serum-free media. Ten percent NTA-microparticles with 1% coumarin-6 or rhodamine-B were loaded with nickel as described above, washed three times and incubated with a 100 nM solution of rhVE-Cadherin (R&D Systems) and 2 mM CaCl2 overnight. Particles were then washed and suspended in serum-free media at a concentration of 0.1 mg microparticle/ml. Cells were washed once with PBS and incubated with microparticles for 3h at 37°C. Following incubation, media was aspirated and washed once with PBS, followed by a 30-min incubation with 4% paraformaldehyde in PBS at room temperature. Cells were then rinsed three times with PBS+0.1% BSA before coverslips were mounted on glass slides and imaged using fluorescent microscopy.

A.9 Animal studies

Rat Myocardial Infarction Model

Adult male Sprague-Dawley rats (obtained from Charles River) weighing 250 grams were subjected to myocardial infarction/injection surgeries in a randomized and double-blinded manner. Briefly, the animals were anesthetized (1-3% isoflurane (Webster Veterinary) and, following tracheal intubation, the heart was exposed by separation of the ribs. Myocardial infarction was performed by ligation of the left anterior descending coronary artery. For PK injection or cell therapy studies, immediately after coronary artery ligation, polyketals (50 µL) were injected into the infarct zone through a 30-gauge needle while the heart was beating. Following injection, the chests were closed and animals allowed to recover on a heating pad. At the indicated time points, magnetic resonance imaging (MRI) was performed and data analyzed in a blinded manner. For immunohistological evaluation, hearts were harvested and fixed in 4% paraformaldehyde. Following dehydration, hearts were embedded in paraffin and 5 µm sections were made.

Mouse Ischemia-Reperfusion Surgery

C57/Bl6 mice, 8-12 weeks old, were anesthetized (1-3% isoflurane) and intubuated. The heart was exposed by separation of the ribs and the LAD ligated for thirty minutes. Following thirty minutes of occlusion, the suture was release and chest sutured.

In Vivo Imaging of Myocardial Infarction

IR-surgery was performed as described above. After 2 h, 10 nmol of Hoechst-IR in 0.1 mL saline, supplemented with 5% ethanol and 5% cremophor EL (PEG-functionalized castor oil), was injected intravenously via retro-orbital injection. The compound was allowed to circulate for 1 h before the animals were sacrificed and perfused for 5 min with saline and 5 min with 4% paraformaldehyde in PBS buffer. Organs were then harvested and imaged in an *in vivo* imager (Olympus OV100).

REFERENCES

1. Lloyd-Jones, D., et al., *Heart disease and stroke statistics--2010 update: a report from the American Heart Association.* Circulation, 2010. **121**(7): p. e46-e215.

2. Anversa, P., et al., *Stem Cells, Myocardial Regeneration and Methodological Artifacts.* Stem Cells, 2006.

3. Beltrami, A.P., et al., *Adult cardiac stem cells are multipotent and support myocardial regeneration.* Cell, 2003. **114**(6): p. 763-76.

4. Korf-Klingebiel, M., et al., *Bone marrow cells are a rich source of growth factors and cytokines: implications for cell therapy trials after myocardial infarction.* Eur Heart J, 2008. **29**(23): p. 2851-8.

5. Wollert, K.C., *Cell therapy for acute myocardial infarction.* Curr Opin Pharmacol, 2008. **8**(2): p. 202-10.

6. Uhrich, K.E., et al., *Polymeric systems for controlled drug release.* Chem Rev, 1999. **99**(11): p. 3181-98.

7. Ding, T., J. Sun, and P. Zhang, *Immune evaluation of biomaterials in TNF-alpha and IL-1beta at mRNA level.* J Mater Sci Mater Med, 2007. **18**(11): p. 2233-6.

8. Iwasaki, Y., et al., *Reduction of surface-induced inflammatory reaction on PLGA/MPC polymer blend.* Biomaterials, 2002. **23**(18): p. 3897-903.

9. Yellon, D.M. and D.J. Hausenloy, *Myocardial reperfusion injury.* N Engl J Med, 2007. **357**(11): p. 1121-35.

10. Bolli, R., *Oxygen-derived free radicals and myocardial reperfusion injury: an overview.* Cardiovasc Drugs Ther, 1991. **5 Suppl 2**: p. 249-68.

11. Bolli, R., *Causative role of oxyradicals in myocardial stunning: a proven hypothesis. A brief review of the evidence demonstrating a major role of reactive oxygen species in several forms of postischemic dysfunction.* Basic Res Cardiol, 1998. **93**(3): p. 156-62.

12. Dorweiler, B., et al., *Ischemia-reperfusion injury - Pathophysiology and clinical implications.* European Journal of Trauma and Emergency Surgery, 2007. **33**(6): p. 600-612.

13. Sun, J.Z., et al., *Evidence for an essential role of reactive oxygen species in the genesis of late preconditioning against myocardial stunning in conscious pigs.* J Clin Invest, 1996. **97**(2): p. 562-76.

14. Tang, X.L., et al., *Oxidant species trigger late preconditioning against myocardial stunning in conscious rabbits.* Am J Physiol Heart Circ Physiol, 2002. **282**(1): p. H281-91.

15. Zhao, Z.Q. and J. Vinten-Johansen, *Myocardial apoptosis and ischemic preconditioning.* Cardiovasc Res, 2002. **55**(3): p. 438-55.

16. Ertl, G. and S. Frantz, *Wound model of myocardial infarction.* Am J Physiol Heart Circ Physiol, 2005. **288**(3): p. H981-3.

17. Frangogiannis, N.G., *The mechanistic basis of infarct healing.* Antioxid Redox Signal, 2006. **8**(11-12): p. 1907-39.

18. Hill, J.H. and P.A. Ward, *The phlogistic role of C3 leukotactic fragments in myocardial infarcts of rats.* J Exp Med, 1971. **133**(4): p. 885-900.

19. Kaur, K., A.K. Sharma, and P.K. Singal, *Significance of changes in TNF-alpha and IL-10 levels in the progression of heart failure subsequent to myocardial infarction.* Am J Physiol Heart Circ Physiol, 2006. **291**(1): p. H106-13.

20. Cai, D., et al., *Age-associated impairment in TNF-alpha cardioprotection from myocardial infarction.* Am J Physiol Heart Circ Physiol, 2003. **285**(2): p. H463-9.

21. Heba, G., et al., *Relation between expression of TNF alpha, iNOS, VEGF mRNA and development of heart failure after experimental myocardial infarction in rats.* J Physiol Pharmacol, 2001. **52**(1): p. 39-52.

22. Halawa, B., et al., *[Levels of tumor necrosis factor (TNF-alpha) and interleukin 6 (IL-6) in serum of patients with acute myocardial infarction].* Pol Arch Med Wewn, 1999. **101**(3): p. 197-203.

23. Frangogiannis, N.G., et al., *Resident cardiac mast cells degranulate and release preformed TNF-alpha, initiating the cytokine cascade in experimental canine myocardial ischemia/reperfusion.* Circulation, 1998. **98**(7): p. 699-710.

24. Sorescu, D. and K.K. Griendling, *Reactive oxygen species, mitochondria, and NAD(P)H oxidases in the development and progression of heart failure.* Congest Heart Fail, 2002. **8**(3): p. 132-40.

25. Vandervelde, S., et al., *Signaling factors in stem cell-mediated repair of infarcted myocardium.* J Mol Cell Cardiol, 2005. **39**(2): p. 363-76.

26. Ertl, G. and S. Frantz, *Healing after myocardial infarction.* Cardiovasc Res, 2005. **66**(1): p. 22-32.

27. Khaper, N., et al., *Antioxidant enzyme gene expression in congestive heart failure following myocardial infarction.* Mol Cell Biochem, 2003. **251**(1-2): p. 9-15.

28. Li, Q., et al., *Gene therapy with extracellular superoxide dismutase protects conscious rabbits against myocardial infarction.* Circulation, 2001. **103**(14): p. 1893-8.

29. Wang, P., et al., *Overexpression of human copper, zinc-superoxide dismutase (SOD1) prevents postischemic injury.* Proc Natl Acad Sci U S A, 1998. **95**(8): p. 4556-60.

30. Hallewell, R.A., et al., *Genetically engineered polymers of human CuZn superoxide dismutase. Biochemistry and serum half-lives.* J Biol Chem, 1989. **264**(9): p. 5260-8.

31. Mani, K., *Programmed cell death in cardiac myocytes: strategies to maximize post-ischemic salvage.* Heart Failure Reviews, 2008. **13**(2): p. 193-209.

32. Burke, A.P. and R. Virmani, *Pathophysiology of acute myocardial infarction.* Med Clin North Am, 2007. **91**(4): p. 553-72; ix.

33. Perin, E.C. and J. Lopez, *Methods of stem cell delivery in cardiac diseases.* Nat Clin Pract Cardiovasc Med, 2006. **3 Suppl 1**: p. S110-3.

34. Langer, R., *Drug delivery and targeting.* Nature, 1998. **392**(6679): p. 5-10.

35. Panyam, J. and V. Labhasetwar, *Biodegradable nanoparticles for drug and gene delivery to cells and tissue.* Advanced Drug Delivery Reviews, 2003. **55**(3): p. 329-347.

36. Uhrich, K.E., et al., *Polymeric systems for controlled drug release.* Chemical Reviews, 1999. **99**(11): p. 3181-3198.

37. Bilati, U., E. Allemann, and E. Doelker, *Poly(D,L-lactide-co-glycolide) protein-loaded nanoparticles prepared by the double emulsion method--processing and formulation issues for enhanced entrapment efficiency.* J Microencapsul, 2005. **22**(2): p. 205-14.

38. Cohen, S., et al., *Controlled delivery systems for proteins based on poly(lactic/glycolic acid) microspheres.* Pharm Res, 1991. **8**(6): p. 713-20.

39. Morlock, M., et al., *Microencapsulation of rh-erythropoietin, using biodegradable poly(D,L-lactide-co-glycolide): Protein stability and the effects of stabilizing excipients.* European Journal of Pharmaceutics and Biopharmaceutics, 1997. **43**(1): p. 29-36.

40. Nihant, N., et al., *POLYLACTIDE MICROPARTICLES PREPARED BY DOUBLE EMULSION/EVAPORATION TECHNIQUE .1. EFFECT OF PRIMARY EMULSION STABILITY.* Pharmaceutical Research, 1994. **11**(10): p. 1479-1484.

41. Morita, T., et al., *Protein encapsulation into biodegradable microspheres by a novel S/O/W emulsion method using poly(ethylene glycol) as a protein micronization adjuvant.* J Control Release, 2000. **69**(3): p. 435-44.

42. Carrasquillo, K.G., et al., *Non-aqueous encapsulation of excipient-stabilized spray-freeze dried BSA into poly(lactide-co-glycolide) microspheres results in release of native protein.* Journal of Controlled Release, 2001. **76**(3): p. 199-208.

43. Lin, C.C. and A.T. Metters, *Enhanced protein delivery from photopolymerized hydrogels using a pseudospecific metal chelating ligand.* Pharmaceutical Research, 2006. **23**(3): p. 614-622.

44. Zhang, G., et al., *Controlled release of stromal cell-derived factor-1 alpha in situ increases c-kit+ cell homing to the infarcted heart.* Tissue Eng, 2007. **13**(8): p. 2063-71.

45. Lin, X., et al., *Controlled release of matrix metalloproteinase-1 plasmid DNA prevents left ventricular remodeling in chronic myocardial infarction of rats.* Circ J, 2009. **73**(12): p. 2315-21.

46. Liu, L.S., et al., *Hyaluronate-heparin conjugate gels for the delivery of basic fibroblast growth factor (FGF-2).* J Biomed Mater Res, 2002. **62**(1): p. 128-35.

47. Wei, H.J., et al., *Gelatin microspheres encapsulated with a nonpeptide angiogenic agent, ginsenoside Rg1, for intramyocardial injection in a rat model with infarcted myocardium.* J Control Release, 2007. **120**(1-2): p. 27-34.

48. Spinale, F.G., *Myocardial matrix remodeling and the matrix metalloproteinases: influence on cardiac form and function.* Physiol Rev, 2007. **87**(4): p. 1285-342.

49. Chang, C.J., *Effects of nerve growth factor from genipin-crosslinked gelatin in polycaprolactone conduit on peripheral nerve regeneration--in vitro and in vivo.* J Biomed Mater Res A, 2009. **91**(2): p. 586-96.

50. Liang, H.C., et al., *Genipin-crosslinked gelatin microspheres as a drug carrier for intramuscular administration: in vitro and in vivo studies.* J Biomed Mater Res A, 2003. **65**(2): p. 271-82.

51. Vandelli, M.A., et al., *Gelatin microspheres crosslinked with D,L-glyceraldehyde as a potential drug delivery system: preparation, characterisation, in vitro and in vivo studies.* Int J Pharm, 2001. **215**(1-2): p. 175-84.

52. Gu, F., B. Amsden, and R. Neufeld, *Sustained delivery of vascular endothelial growth factor with alginate beads.* Journal of Controlled Release, 2004. **96**(3): p. 463-472.

53. Bhattarai, N., et al., *PEG-grafted chitosan as an injectable thermosensitive hydrogel for sustained protein release.* Journal of Controlled Release, 2005. **103**(3): p. 609-624.

54. Porath, J., et al., *Metal chelate affinity chromatography, a new approach to protein fractionation.* Nature, 1975. **258**(5536): p. 598-9.

55. Hochuli, E., H. Dobeli, and A. Schacher, *New metal chelate adsorbent selective for proteins and peptides containing neighbouring histidine residues.* J Chromatogr, 1987. **411**: p. 177-84.

56. Verbelen, C., H.J. Gruber, and Y.F. Dufrene, *The NTA-His6 bond is strong enough for AFM single-molecular recognition studies.* J Mol Recognit, 2007. **20**(6): p. 490-4.

57. Kim, J.S., et al., *Highly-efficient purification of native polyhistidine-tagged proteins by multivalent NTA-modified magnetic nanoparticles.* Bioconjugate Chemistry, 2007. **18**(2): p. 333-341.

58. Tsai, S.Y., et al., *Effect of number of poly(His) tags on the adsorption of engineered proteins on immobilized metal affinity chromatography adsorbents.* Process Biochemistry, 2006. **41**(9): p. 2058-2067.

59. Lata, S. and J. Piehler, *Stable and functional immobilization of histidine-tagged proteins via multivalent chelator headgroups on a molecular poly(ethylene glycol) brush.* Anal Chem, 2005. **77**(4): p. 1096-105.

60. Lata, S., et al., *High-affinity adaptors for switchable recognition of histidine-tagged proteins.* J Am Chem Soc, 2005. **127**(29): p. 10205-15.

61. Lauer, S.A. and J.P. Nolan, *Development and characterization of Ni-NTA-bearing microspheres.* Cytometry, 2002. **48**(3): p. 136-145.

62. Bischler, N., et al., *Specific interaction and two-dimensional crystallization of histidine tagged yeast RNA polymerase I on nickel-chelating lipids.* Biophys J, 1998. **74**(3): p. 1522-32.

63. Kubalek, E.W., S.F. Le Grice, and P.O. Brown, *Two-dimensional crystallization of histidine-tagged, HIV-1 reverse transcriptase promoted by a novel nickel-chelating lipid.* J Struct Biol, 1994. **113**(2): p. 117-23.

64. Venien-Bryan, C., et al., *Characterization of the growth of 2D protein crystals on a lipid monolayer by ellipsometry and rigidity measurements coupled to electron microscopy.* Biophysical Journal, 1998. **74**(5): p. 2649-2657.

65. Ruger, R., et al., *Generation of immunoliposomes using recombinant single-chain Fv fragments bound to Ni-NTA-liposomes.* J Drug Target, 2005. **13**(7): p. 399-406.

66. Huang, Z.H., et al., *Facile synthesis of multivalent nitrilotriacetic acid (NTA) and NTA conjugates for analytical and drug delivery applications.* Bioconjugate Chemistry, 2006. **17**(6): p. 1592-1600.

67. Chikh, G.G., et al., *Attaching histidine-tagged peptides and proteins to lipid-based carriers through use of metal-ion-chelating lipids.* Biochim Biophys Acta, 2002. **1567**(1-2): p. 204-12.

68. Patel, J.D., et al., *Preparation and characterization of nickel nanoparticles for binding to his-tag proteins and antigens.* Pharmaceutical Research, 2007. **24**(2): p. 343-352.

69. Lin, C.C. and A.T. Metters, *Metal-chelating affinity hydrogels for sustained protein release.* Journal of Biomedical Materials Research Part A, 2007. **83A**(4): p. 954-964.

70. Lin, C.C. and A.T. Metters, *Bifunctional monolithic affinity hydrogels for dual-protein delivery.* Biomacromolecules, 2008. **9**(3): p. 789-795.

71. Zamora, P.O., et al., *Local delivery of basic fibroblast growth factor (bFGF) using adsorbed silyl-heparin, benzyl-bis(dimethylsilylmethyl)oxycarbamoyl-heparin.* Bioconjug Chem, 2002. **13**(5): p. 920-6.

72. Govender, T., et al., *Polymeric nanoparticles for enhancing antiretroviral drug therapy.* Drug Deliv, 2008. **15**(8): p. 493-501.

73. Byrne, J.D., T. Betancourt, and L. Brannon-Peppas, *Active targeting schemes for nanoparticle systems in cancer therapeutics.* Adv Drug Deliv Rev, 2008. **60**(15): p. 1615-26.

74. Park, J.W., et al., *Tumor targeting using anti-her2 immunoliposomes.* J Control Release, 2001. **74**(1-3): p. 95-113.

75. Muzykantov, V.R., *Targeting of superoxide dismutase and catalase to vascular endothelium.* J Control Release, 2001. **71**(1): p. 1-21.

76. Lee, R.J., et al., *Antibody targeting of stem cells to infarcted myocardium.* Stem Cells, 2007. **25**(3): p. 712-7.

77. Lum, L.G., et al., *Targeting of Lin-Sca+ hematopoietic stem cells with bispecific antibodies to injured myocardium.* Blood Cells Mol Dis, 2004. **32**(1): p. 82-7.

78. Muro, S. and V.R. Muzykantov, *Targeting of antioxidant and anti-thrombotic drugs to endothelial cell adhesion molecules.* Curr Pharm Des, 2005. **11**(18): p. 2383-401.

79. Lukyanov, A.N., W.C. Hartner, and V.P. Torchilin, *Increased accumulation of PEG-PE micelles in the area of experimental myocardial infarction in rabbits.* J Control Release, 2004. **94**(1): p. 187-93.

80. Ulrich, A.S., *Biophysical aspects of using liposomes as delivery vehicles.* Biosci Rep, 2002. **22**(2): p. 129-50.

81. Khaw, B.A., et al., *Plug and seal: prevention of hypoxic cardiocyte death by sealing membrane lesions with antimyosin-liposomes.* Nat Med, 1995. **1**(11): p. 1195-8.

82. Verma, D.D., et al., *ATP-loaded liposomes effectively protect the myocardium in rabbits with an acute experimental myocardial infarction.* Pharm Res, 2005. **22**(12): p. 2115-20.

83. Zhigang, W., et al., *Ultrasound-mediated microbubble destruction enhances VEGF gene delivery to the infarcted myocardium in rats.* Clin Imaging, 2004. **28**(6): p. 395-8.

84. Verma, D.D., et al., *Protective effect of coenzyme Q10-loaded liposomes on the myocardium in rabbits with an acute experimental myocardial infarction.* Pharm Res, 2007. **24**(11): p. 2131-7.

85. Hartner, W.C., et al., *ATP-loaded liposomes for treatment of myocardial ischemia.* Wiley Interdiscip Rev Nanomed Nanobiotechnol, 2009. **1**(5): p. 530-9.

86. Takahama, H., et al., *Prolonged targeting of ischemic/reperfused myocardium by liposomal adenosine augments cardioprotection in rats.* J Am Coll Cardiol, 2009. **53**(8): p. 709-17.

87. Stroun, M., et al., *The origin and mechanism of circulating DNA.* Ann N Y Acad Sci, 2000. **906**: p. 161-8.

88. Vlassov, V.V., P.P. Laktionov, and E.Y. Rykova, *Extracellular nucleic acids.* Bioessays, 2007. **29**(7): p. 654-67.

89. Hisazumi, J., et al., *Significant role of liver sinusoidal endothelial cells in hepatic uptake and degradation of naked plasmid DNA after intravenous injection.* Pharm Res, 2004. **21**(7): p. 1223-8.

90. Leon, S.A., et al., *Free DNA in the serum of cancer patients and the effect of therapy.* Cancer Res, 1977. **37**(3): p. 646-50.

91. Lo, Y.M., et al., *Plasma DNA as a prognostic marker in trauma patients.* Clin Chem, 2000. **46**(3): p. 319-23.

92. Shak, S., *Aerosolized recombinant human DNase I for the treatment of cystic fibrosis.* Chest, 1995. **107**(2 Suppl): p. 65S-70S.

93. Tan, E.M., et al., *Deoxybonucleic acid (DNA) and antibodies to DNA in the serum of patients with systemic lupus erythematosus.* J Clin Invest, 1966. **45**(11): p. 1732-40.

94. Costerton, J.W., P.S. Stewart, and E.P. Greenberg, *Bacterial biofilms: a common cause of persistent infections.* Science, 1999. **284**(5418): p. 1318-22.

95. Birch, L., et al., *Accurate and robust quantification of circulating fetal and total DNA in maternal plasma from 5 to 41 weeks of gestation.* Clin Chem, 2005. **51**(2): p. 312-20.

96. Jensen, R.H., R.G. Langlois, and B.H. Mayall, *Strategies for choosing a deoxyribonucleic acid stain for flow cytometry of metaphase chromosomes.* J Histochem Cytochem, 1977. **25**(8): p. 954-64.

97. Latt, S.A., *Microfluorometric detection of deoxyribonucleic acid replication in human metaphase chromosomes.* Proc Natl Acad Sci U S A, 1973. **70**(12): p. 3395-9.

98. Weisblum, B. and E. Haenssler, *Fluorometric properties of the bibenzimidazole derivative Hoechst 33258, a fluorescent probe specific for AT concentration in chromosomal DNA.* Chromosoma, 1974. **46**(3): p. 255-60.

99. Vega, M.C., et al., *Three-dimensional crystal structure of the A-tract DNA dodecamer d(CGCAAATTTGCG) complexed with the minor-groove-binding drug Hoechst 33258.* Eur J Biochem, 1994. **222**(3): p. 721-6.

100. Vega, M.C., M. Coll, and C. Aleman, *Intrinsic conformational preferences of the Hoechst dye family and their influence of DNA binding.* Eur J Biochem, 1996. **239**(2): p. 376-83.

101. Baraldi, P.G., et al., *DNA minor groove binders as potential antitumor and antimicrobial agents.* Med Res Rev, 2004. **24**(4): p. 475-528.

102. Kraut, E.H., et al., *Phase II study of pibenzimol in pancreatic cancer. A Southwest Oncology Group study.* Invest New Drugs, 1991. **9**(1): p. 95-6.

103. Patel, S.R., et al., *Phase I-II study of pibenzimol hydrochloride (NSC 322921) in advanced pancreatic carcinoma.* Invest New Drugs, 1991. **9**(1): p. 53-7.

104. Cullis, E.R., et al., *Tumour overexpression of inducible nitric oxide synthase (iNOS) increases angiogenesis and may modulate the anti-tumour effects of the vascular disrupting agent ZD6126.* Microvasc Res, 2006. **71**(2): p. 76-84.

105. Machalinski, B., et al., *In vivo and in vitro studies on the toxicity of Hoechst 33342 (Ho342). Implications for employing Ho342 for the isolation of haematopoietic stem cells.* Ann Transplant, 1998. **3**(3): p. 5-13.

106. Omar, A.I. and B. Hu, *Detection of early tissue injury in vivo using fluorescent cell death markers in rat dentate gyrus.* Neurosci Lett, 2003. **348**(3): p. 143-6.

107. Paku, S. and K. Lapis, *Morphological Aspects of Angiogenesis in Experimental Liver Metastases.* American Journal of Pathology, 1993. **143**(3): p. 926-936.

108. Ding, A.G. and S.P. Schwendeman, *Acidic microclimate pH distribution in PLGA microspheres monitored by confocal laser scanning microscopy.* Pharm Res, 2008. **25**(9): p. 2041-52.

109. Anversa, P., *Myocyte death in the pathological heart.* Circ Res, 2000. **86**(2): p. 121-4.

110. Anversa, P., A. Leri, and J. Kajstura, *Cardiac regeneration.* J Am Coll Cardiol, 2006. **47**(9): p. 1769-76.

111. Bolli, R., et al., *Direct evidence that oxygen-derived free radicals contribute to postischemic myocardial dysfunction in the intact dog.* Proc Natl Acad Sci U S A, 1989. **86**(12): p. 4695-9.

112. Kumar, S., J. Boehm, and J.C. Lee, *p38 MAP kinases: key signalling molecules as therapeutic targets for inflammatory diseases.* Nat Rev Drug Discov, 2003. **2**(9): p. 717-26.

113. Lee, J.C., et al., *Inhibition of p38 MAP kinase as a therapeutic strategy.* Immunopharmacology, 2000. **47**(2-3): p. 185-201.

114. Peifer, C., G. Wagner, and S. Laufer, *New approaches to the treatment of inflammatory disorders small molecule inhibitors of p38 MAP kinase.* Curr Top Med Chem, 2006. **6**(2): p. 113-49.

115. Davis, M.E., et al., *Local myocardial insulin-like growth factor 1 (IGF-1) delivery with biotinylated peptide nanofibers improves cell therapy for myocardial infarction.* Proc Natl Acad Sci U S A, 2006. **103**(21): p. 8155-60.

116. Christman, K.L. and R.J. Lee, *Biomaterials for the treatment of myocardial infarction.* J Am Coll Cardiol, 2006. **48**(5): p. 907-13.

117. Sy, J.C. and M.E. Davis, *Delivering regenerative cues to the heart: cardiac drug delivery by microspheres and peptide nanofibers.* J Cardiovasc Transl Res, 2010. **3**(5): p. 461-8.

118. Cavalier, M., J.P. Benoit, and C. Thies, *The formation and characterization of hydrocortisone-loaded poly((+/-)-lactide) microspheres.* J Pharm Pharmacol, 1986. **38**(4): p. 249-53.

119. Li, Z., et al., *Selective inhibition of p38alpha MAPK improves cardiac function and reduces myocardial apoptosis in rat model of myocardial injury.* Am J Physiol Heart Circ Physiol, 2006. **291**(4): p. H1972-7.

120. Liu, Y.H., et al., *Inhibition of p38 mitogen-activated protein kinase protects the heart against cardiac remodeling in mice with heart failure resulting from myocardial infarction.* J Card Fail, 2005. **11**(1): p. 74-81.

121. Minamino, T., et al., *MEKK1 suppresses oxidative stress-induced apoptosis of embryonic stem cell-derived cardiac myocytes.* Proc Natl Acad Sci U S A, 1999. **96**(26): p. 15127-32.

122. Porras, A., et al., *P38 alpha mitogen-activated protein kinase sensitizes cells to apoptosis induced by different stimuli.* Mol Biol Cell, 2004. **15**(2): p. 922-33.

123. Ren, J., et al., *Role of p38alpha MAPK in cardiac apoptosis and remodeling after myocardial infarction.* J Mol Cell Cardiol, 2005. **38**(4): p. 617-23.

124. See, F., et al., *p38 mitogen-activated protein kinase inhibition improves cardiac function and attenuates left ventricular remodeling following myocardial infarction in the rat.* J Am Coll Cardiol, 2004. **44**(8): p. 1679-89.

125. Lee, S., et al., *Polyketal microparticles: a new delivery vehicle for superoxide dismutase.* Bioconjug Chem, 2007. **18**(1): p. 4-7.

126. Heffernan, M.J. and N. Murthy, *Polyketal nanoparticles: a new pH-sensitive biodegradable drug delivery vehicle.* Bioconjug Chem, 2005. **16**(6): p. 1340-2.

127. Fernandes, D.C., et al., *Analysis of dihydroethidium-derived oxidation products by HPLC in the assessment of superoxide production and NADPH oxidase activity in vascular systems.* Am J Physiol Cell Physiol, 2006.

128. Gongora, M.C., et al., *Role of extracellular superoxide dismutase in hypertension.* Hypertension, 2006. **48**(3): p. 473-81.

129. Kim, M.S., et al., *An in vivo study of the host tissue response to subcutaneous implantation of PLGA- and/or porcine small intestinal submucosa-based scaffolds.* Biomaterials, 2007. **28**(34): p. 5137-43.

130. Cannon, G. and J. Swanson, *The macrophage capacity for phagocytosis.* J Cell Sci, 1992. **101**(4): p. 907-913.

131. Widder, J., et al., *Vascular endothelial dysfunction and superoxide anion production in heart failure are p38 MAP kinase-dependent.* Cardiovasc Res, 2004. **63**(1): p. 161-7.

132. Clerk, A. and P.H. Sugden, *Inflame my heart (by p38-MAPK).* Circ Res, 2006. **99**(5): p. 455-8.

133. Sugden, P.H. and A. Clerk, *Oxidative stress and growth-regulating intracellular signaling pathways in cardiac myocytes.* Antioxid Redox Signal, 2006. **8**(11-12): p. 2111-24.

134. Porath, J., et al., *Metal Chelate Affinity Chromatography, a New Approach to Protein Fractionation.* Nature, 1975. **258**(5536): p. 598-599.

135. Sy, J.C., et al., *Sustained release of a p38 inhibitor from non-inflammatory microspheres inhibits cardiac dysfunction.* Nat Mater, 2008. **7**(11): p. 863-8.

136. Yang, S.C., et al., *Polyketal copolymers: a new acid-sensitive delivery vehicle for treating acute inflammatory diseases.* Bioconjug Chem, 2008. **19**(6): p. 1164-9.

137. Barceloux, D.G., *Nickel.* J Toxicol Clin Toxicol, 1999. **37**(2): p. 239-58.

138. Borenfreund, E. and J.A. Puerner, *Cytotoxicity of metals, metal-metal and metal-chelator combinations assayed in vitro.* Toxicology, 1986. **39**(2): p. 121-34.

139. Novelli, E.L.B., et al., *Toxic effects of nickel exposure on heart and liver of rats.* Toxic Substance Mechanisms, 1997. **16**(3): p. 251-258.

140. Lee, S., et al., *Solid polymeric microparticles enhance the delivery of siRNA to macrophages in vivo.* Nucleic Acids Res, 2009. **37**(22): p. e145.

141. Seshadri, G., et al., *The delivery of superoxide dismutase encapsulated in polyketal microparticles to rat myocardium and protection from myocardial ischemia-reperfusion injury.* Biomaterials, 2009. **31**(6): p. 1372-9.

142. Labrecque, L., et al., *Regulation of vascular endothelial growth factor receptor-2 activity by caveolin-1 and plasma membrane cholesterol.* Molecular Biology of the Cell, 2003. **14**(1): p. 334-347.

143. Riechmann, L., J. Foote, and G. Winter, *Expression of an antibody Fv fragment in myeloma cells.* Journal of Molecular Biology, 1988. **203**(3): p. 825-828.

144. Kajstura, J., et al., *Apoptotic and necrotic myocyte cell deaths are independent contributing variables of infarct size in rats.* Lab Invest, 1996. **74**(1): p. 86-107.

145. Dasari, M., et al., *Hoechst-IR: An Imaging Agent That Detects Necrotic Tissue in Vivo by Binding Extracellular DNA.* Organic Letters, 2010. **12**(15): p. 3300-3303.

146. Phelps, E.A., et al., *Bioartificial matrices for therapeutic vascularization.* Proc Natl Acad Sci U S A, 2010. **107**(8): p. 3323-8.

147. Berezin, M.Y., et al., *Ratiometric analysis of fluorescence lifetime for probing binding sites in albumin with near-infrared fluorescent molecular probes.* Photochem Photobiol, 2007. **83**(6): p. 1371-8.

148. Khaw, B., et al., *Specificity of localization of myosin-specific antibody fragments in experimental myocardial infarction. Histologic, histochemical, autoradiographic and scintigraphic studies.* Circulation, 1979. **60**(7): p. 1527-1531.

149. Vivaldi, M.T., R.A. Kloner, and F.J. Schoen, *Triphenyltetrazolium staining of irreversible ischemic injury following coronary artery occlusion in rats.* Am J Pathol, 1985. **121**(3): p. 522-30.

150. Napirei, M., S. Wulf, and H.G. Mannherz, *Chromatin breakdown during necrosis by serum Dnase1 and the plasminogen system.* Arthritis & Rheumatism, 2004. **50**(6): p. 1873-1883.

151. Gerhardt, H., et al., *VEGF guides angiogenic sprouting utilizing endothelial tip cell filopodia.* The Journal of Cell Biology, 2003. **161**(6): p. 1163-1177.

152. DeBoer, L.W., et al., *A flow- and time-dependent index of ischemic injury after experimental coronary occlusion and reperfusion.* Proceedings of the National Academy of Sciences, 1983. **80**(18): p. 5784-5788.

153. Millauer, B., et al., *High affinity VEGF binding and developmental expression suggest Flk-1 as a major regulator of vasculogenesis and angiogenesis.* Cell, 1993. **72**(6): p. 835-46.

154. Fiore, V.F., et al., *Polyketal microparticles for therapeutic delivery to the lung.* Biomaterials, 2010. **31**(5): p. 810-7.

155. Sy, J.C., A.S. Klemm, and V.P. Shastri, *Emulsion as a Means of Controlling Electrospinning of Polymers.* Advanced Materials, 2009. **21**(18): p. 1814-+.

156. Zong, X., et al., *Electrospun fine-textured scaffolds for heart tissue constructs.* Biomaterials, 2005. **26**(26): p. 5330-8.

157. Sy, J.C., et al., *Surface functionalization of polyketal microparticles with nitrilotriacetic acid-nickel complexes for efficient protein capture and delivery.* Biomaterials, 2010. **31**(18): p. 4987-94.

158. Gordon, S. and F.O. Martinez, *Alternative activation of macrophages: mechanism and functions.* Immunity, 2010. **32**(5): p. 593-604.

159. Li, J., et al., *Immunomodulation by interleukin-4 suppresses matrix metalloproteinases and improves cardiac function in murine myocarditis.* Eur J Pharmacol, 2007. **554**(1): p. 60-8.

160. Lata, S. and J. Piehler, *Synthesis of a multivalent chelator lipid for stably tethering histidine-tagged proteins onto membranes.* Nat Protoc, 2006. **1**(4): p. 2104-9.

161. Sahoo, S.K., et al., *Residual polyvinyl alcohol associated with poly (D,L-lactide-co-glycolide) nanoparticles affects their physical properties and cellular uptake.* J Control Release, 2002. **82**(1): p. 105-14.

162. Sidenius, U., et al., *Comparison of different transition metal ions for immobilized metal affinity chromatography of selenoprotein P from human plasma.* J Chromatogr B Biomed Sci Appl, 1999. **735**(1): p. 85-91.

163. Bresolin, I.T., et al., *Evaluation of immobilized metal-ion affinity chromatography (IMAC) as a technique for IgG(1) monoclonal antibodies purification: the effect of chelating ligand and support.* Appl Biochem Biotechnol, 2010. **160**(7): p. 2148-65.

164. Oshinski, J.N., et al., *Imaging time after Gd-DTPA injection is critical in using delayed enhancement to determine infarct size accurately with magnetic resonance imaging.* Circulation, 2001. **104**(23): p. 2838-42.

165. Langer, R., *Biomaterials for Drug Delivery and Tissue Engineering.* MRS Bulletin, 2006. **31**(06): p. 477-485.

166. Sanada, S., et al., *IL-33 and ST2 comprise a critical biomechanically induced and cardioprotective signaling system.* J Clin Invest, 2007. **117**(6): p. 1538-49.

167. Fink, B., et al., *Detection of intracellular superoxide formation in endothelial cells and intact tissues using dihydroethidium and an HPLC-based assay.* Am J Physiol Cell Physiol, 2004. **287**(4): p. C895-902.

VITA

JAY CHRISTOPHER SY

Jay was born in Dhahran, Saudi Arabia and grew up in the nearby city of Ras Tanura where he attended schools run by Saudi ARAMCO. His family moved to Michigan in 1994 where he attended Cranbrook-Kingswood Middle School and eventually went on to Phillips Exeter Academy in New Hampshire. Jay earned his Bachelor of Science in Engineering in Bioengineering from the University of Pennsylvania in 2005. After spending a year conducting research at Vanderbilt University, Jay joined the Biomedical Engineering joint Ph.D. program at Georgia Tech and Emory University in 2006. Jay was active in the Biomedical Engineering community and served on the Recruiting Task Force, BME Student Advisor Committee, and participated in the Leadership Development Program. Outside of lab, he filled his time playing on IBB intramural sports teams, being a "foodie" by finding and cooking new and interesting food, and by spending time with the two ladies who kept him sane over the course of his dissertation: his girlfriend, Rachel, and their dog, Emma.